NRL Memorandum Report 3005

ARPA-NRL Laser Program
Semiannual Technical Report to Defense Advanced Research Projects Agency 1 January 1974 - 30 June 1974

Laser Physics Branch
Optical Sciences Division

April 1975

NAVAL RESEARCH LABORATORY
Washington, D.C.

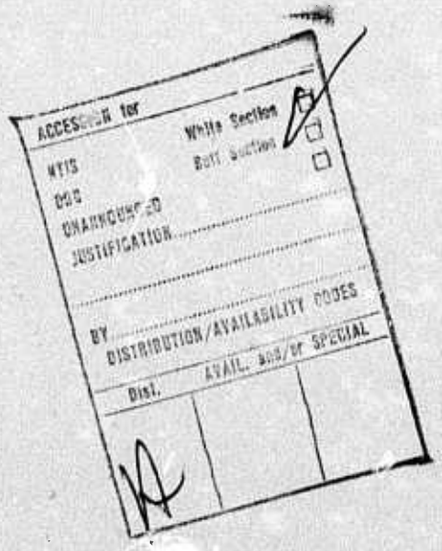
ACCESSION for
White Section
NTIS
Buff Section
DDC
UNANNOUNCED
JUSTIFICATION
BY
DISTRIBUTION/AVAILABILITY CODES
Dist. AVAIL. and/or SPECIAL

SECURITY CLASSIFICATION OF THIS PAGE (When Data Entered)

REPORT DOCUMENTATION PAGE

READ INSTRUCTIONS BEFORE COMPLETING FORM

1. REPORT NUMBER: NRL Memorandum Report 3005
2. GOVT ACCESSION NO.
3. RECIPIENT'S CATALOG NUMBER
4. TITLE (and Subtitle): ARPA-NRL LASER PROGRAM — SEMIANNUAL TECHNICAL REPORT TO DEFENSE ADVANCED RESEARCH PROJECTS AGENCY, 1 January 1974 — 30 June 1974.
5. TYPE OF REPORT & PERIOD COVERED: A semiannual technical report; work continuing.
6. PERFORMING ORG. REPORT NUMBER
7. AUTHOR(s): Laser Physics Branch
8. CONTRACT OR GRANT NUMBER(s): NRL-MR-3005; 156 p.
9. PERFORMING ORGANIZATION NAME AND ADDRESS: Naval Research Laboratory, Washington, D.C. 20375
10. PROGRAM ELEMENT, PROJECT, TASK AREA & WORK UNIT NUMBERS: NRL Problem N01-48, 49, K03-53; ARPA Order-2062, Proj. No. 2E20
11. CONTROLLING OFFICE NAME AND ADDRESS: Defense Advanced Research Projects Agency, Arlington, Virginia 22209
12. REPORT DATE: April 1975
13. NUMBER OF PAGES: 155
14. MONITORING AGENCY NAME & ADDRESS (if different from Controlling Office): NRL-N01-48, NRL-K03-53
15. SECURITY CLASS. (of this report)
15a. DECLASSIFICATION/DOWNGRADING SCHEDULE
16. DISTRIBUTION STATEMENT (of this Report)

Approved for public release; distribution unlimited.

J. R. Airey, L. Champagne, N. Djeu, J. K. Hancock, Neville Harris

DDC RECEIVED AUG 11 1975 D

17. DISTRIBUTION STATEMENT (of the abstract entered in Block 20, if different from Report)
18. SUPPLEMENTARY NOTES
19. KEY WORDS (Continue on reverse side if necessary and identify by block number)

Lasers
Electrical lasers
Chemical lasers
Electronic state lasers
Chemical kinetics
Energy transfer

20. ABSTRACT (Continue on reverse side if necessary and identify by block number)

The ARPA-NRL Laser Program is concerned with the development of laser technology in three project areas: Chemical Infrared Lasers, Electrical Infrared Lasers and Electronic State Lasers.

The Chemical Infrared Laser Program is focussed on DF-CO_2 supersonic transfer laser experiments designed to evaluate chemical augmentation of gas dynamic lasers. Augmentation has been observed but is limited by deactivation processes. The temperature dependence of energy transfer processes in CO, CO_2 and N_2O has been measured

(Abstract Continues)

DD FORM 1 JAN 73 1473 EDITION OF 1 NOV 65 IS OBSOLETE S/N 0102-014-6601

251 950

SECURITY CLASSIFICATION OF THIS PAGE (When Data Entered)

20. Abstract (Continued)

The Electrical Infrared Laser Program has two primary projects, short-pulse CO_2 laser technology and electric-discharge gas dynamic lasers (EDGDL). The short pulse laser project has successfully been completed culminating in reliable 70 J single-pulse operation. A compact high-pressure e-beam-controlled CO_2 laser has been developed for the generation of picosecond laser pulses. Infrared fluorescence from HCl generated by energy transfer from vibrationally excited D_2 has been measured. Experiments to produce a $D_2^* \rightarrow HCl$ EDGDL are continuing.

In electronic state laser development, a number of experimental approaches are being studied. These include direct electron excitation, optical pumping and chemiexcitation schemes. The discovery of an optically pumped Hg laser at 5461 Å is described as well as the details and progress of the other approaches.

TABLE OF CONTENTS

FOREWORD

The Laser Physics Branch of the Optical Sciences Division, Naval Research Laboratory, Washington, D. C., prepared this semiannual report on work sponsored by the Advanced Research Projects Agency, ARPA Order 2062. Co-authors of the report were J.R. Airey, L. Champagne, N. Djeu, J. K. Hancock, Neville Harris, George A. Hart, M. C. Lin, Thomas J. Manuccia, F J. O'Neill, S. K. Searles, D. F. Starr, J. A. Stregack, W. S. Watt, B. Wexler, W. Whitney.

SEMIANNUAL TECHNICAL REPORT

Reporting Period

1 January 1974 - 30 June 1974

1.	DARPA Order	2062
2.	Program Code Number	2E20
3.	Name of Contractor	Naval Research Laboratory
4.	Effective Date of Contract	1 July 1972
5.	Contract Expiration Date	30 June 1975
6.	Amount of Contract	$590,000 (FY-74)
7.	Contract Number	63201D
8.	Principal Investigator	J.R. Airey
9.	Telephone Number	(202) 767-3217
10.	Project Scientist	W. S. Watt
11.	Telephone Number	(202) 767-2074
12.	Title of Work	High Power Lasers

Sponsored by

DEFENSE ADVANCED RESEARCH PROJECTS AGENCY

DARPA Order No. 2062

CHEMICAL INFRARED LASER PROGRAM

1. DF-CO_2 SUPERSONIC TRANSFER CHEMICAL LASER (TCL)

The DF-CO_2 laser operates in the 10 μ CO_2 band as a result of vibrational energy transfer from DF (which is vibrationally excited during its chemical formation) to the asymmetric stretching mode of CO_2. The DF-CO_2 supersonic TCL is capable of operation at high enough cavity pressures that atmospheric pressure recovery can be attained. Thus the DF-CO_2 TCL is of interest both as a chemical laser operating without pumps and as a means of upgrading gas-dynamic CO_2 lasers by the use of chemical energy to further increase the population inversion in the CO_2.

The principle of the NRL DF-CO_2 supersonic TCL, the apparatus acquisition and modification, and the mode of operation both as a chemical laser and gasdynamic laser have been described in previous reports[1-5].

During the last reporting period chemical augmentation was clearly demonstrated although limited by deactivation by HF formed in the combustor. Despite these encouraging results, other data indicated that the nozzle design with injection of the D_2 in the subsonic throat region was unlikely to lead to significant chemical pumping of a CO_2 GDL.

Note: Manuscript submitted February 7, 1975.

(1-5) ARPA-NRL Laser Program Semiannual Technical Reports, 1 July 1971 - 30 December 1973, NRL Memo Report Nos. 2483, 2529, 2654, 2767, 2846.

Since then, fixed position and scanning gain experiments have been made and preliminary measurements with a new nozzle have been carried out. This nozzle, which was built, in collaboration with Bell Aerospace Company, allows D_2 injection at the tips of the nozzle blades and is shown in Figure 1. Whereas with the injection in the subsonic region there was strong evidence of substantial chemical reaction occurring before the gas entered the laser cavity, this phenomenon is avoided with the new nozzle. This injection procedure also allows measured and predicted gain profiles to be compared directly.

The apparatus used for both single position and scanning gain measurements is shown schematically in Figure 2. Briefly, the mirror system sweeps the output of a stabilized CO_2 laser through the active medium while maintaining its direction perpendicular to the flow axis. The He-Ne laser and the chopper are used for alignment and calibration purposes. With this arrangement, gain measurements of approximately 5 cm segments of the gas-flow could be made in a single scan through the 30 cm deep active medium. The minimum gain that could be accurately measured was estimated to be 0.3% cm^{-1}. However in practice, vibration of the machine, degradation of the optical windows during the tests and fluid dynamic disturbances in the cavity coupled with the low gain environ-

ment being probed limited the amount of useful data acquired. This data did confirm, however, that the gain was not significantly increased during the "chemistry-on" cycle from that of the GDL which is in accord with the earlier laser oscillator studies.

During these tests power measurements were also carried out and provided the first clear evidence of an enhancement over the GDL power during the chemistry-on period. This data is shown in Figure 3. Here the power during the chemistry cycle #3, is seen to be above that in the GDL cycle #1, (the effect of a momentary unstarting of the diffuser is indicated at position A).

Although a wide variation of the gas flows and hence the combustor temperature and pressure conditions were examined, the power during the chemistry-on cycle was never substantially more than in the GDL cycle. This fact was particularly puzzling in light of modelling calculations which predicted significant chemical augmentation even when allowing for the large HF deactivation. During these tests however, it was observed that, under conditions where large excesses of D_2 were injected into the gas flow, the combustor temperature and pressure were increased. The most likely explanation is that under these conditions significant pre-reaction is taking place in the subsonic region. The

deuterium is injected at a slight angle against the flow and is expected to be entrained in the boundary layer. However with the higher delivery pressure used to achieve excess injection the D_2 may well penetrate through the boundary layer resulting in the observed phenomena.

In summary then, the experiments with the original GDL nozzle modified to allow injection of deuterium into the subsonic portion of the accelerating flow are as follows. Chemical pumping by DF has been demonstrated but is offset by the large deactivating effect of HF produced in the combustor. Gain measurements tend to confirm the power measurements and there are strong indications that pre-reaction is a limiting feature.

Following completion of these tests, the Bell nozzle was installed and the combustor conditions required to start the diffuser were examined. The Bell nozzle has approximately 20% less throat area and further contraction of the original diffuser was anticipated in order to swallow the starting shock wave. However even with the increased contraction, a 25% higher combustor pressure was needed to start the diffuser. This, combined with the non-parallel mixing produced by the truncated nozzles produces an approximately 50% higher cavity pressure ($\geq$ 90 torr). The supersonic mixing and the resulting reaction of the D_2 and F_2 produce larger flow

disturbances than in the first nozzle configuration which further limit the usefulness of the scanning gain technique.

Preliminary experiments were also performed using a laser cavity. These experiments were performed with low fluorine concentrations and while chemical pumping of the CO_2 was observed, no significant increase over GDL power was observed. It should be noted that for the combustor to operate properly with the Bell nozzle, a 20% increase in pilot fuel (CH_4) was required. This results in an increase in HF formation in the combustor which has a pronounced deleterious effect on laser performance. Further laser tests using the Bell nozzle will be undertaken to characterize laser performance during the next reporting period.

Figure 1

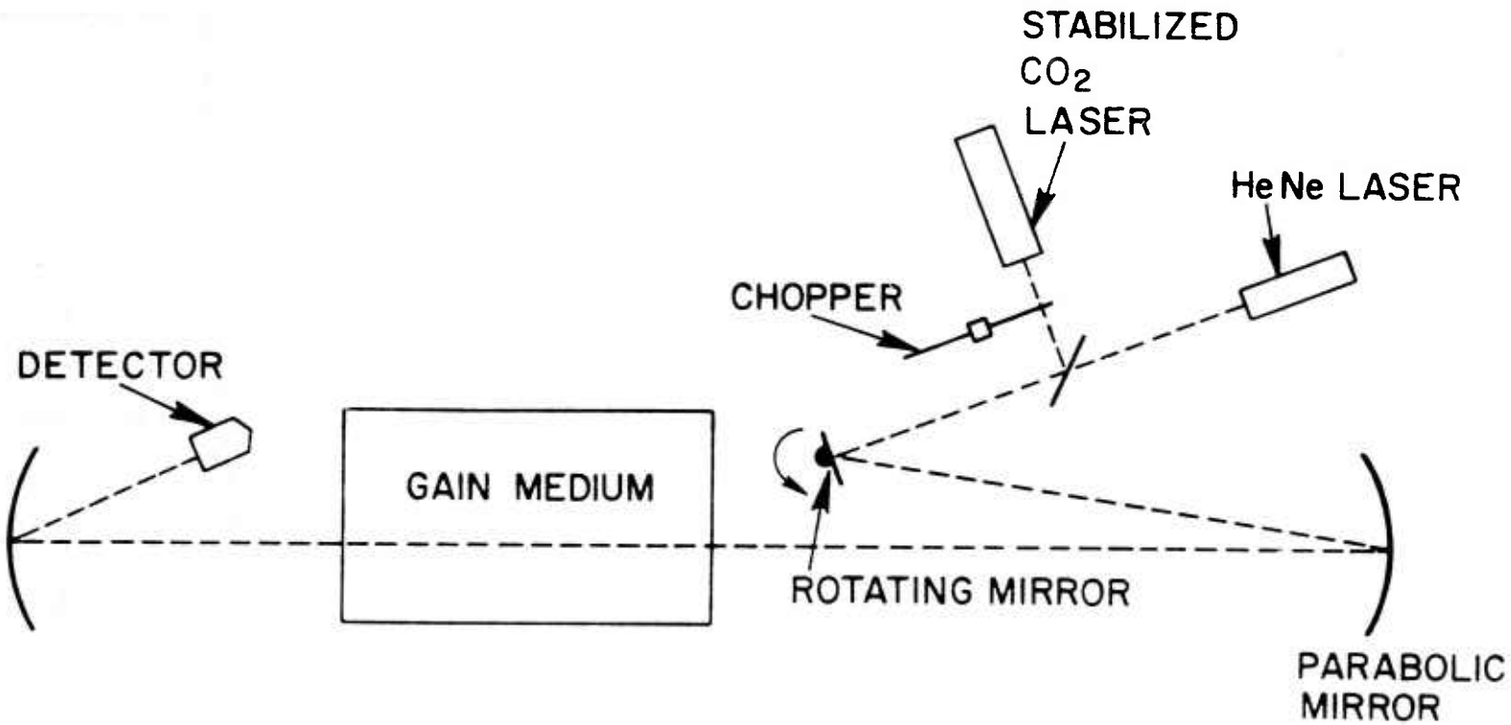

Fig. 2 — Scanning gain apparatus

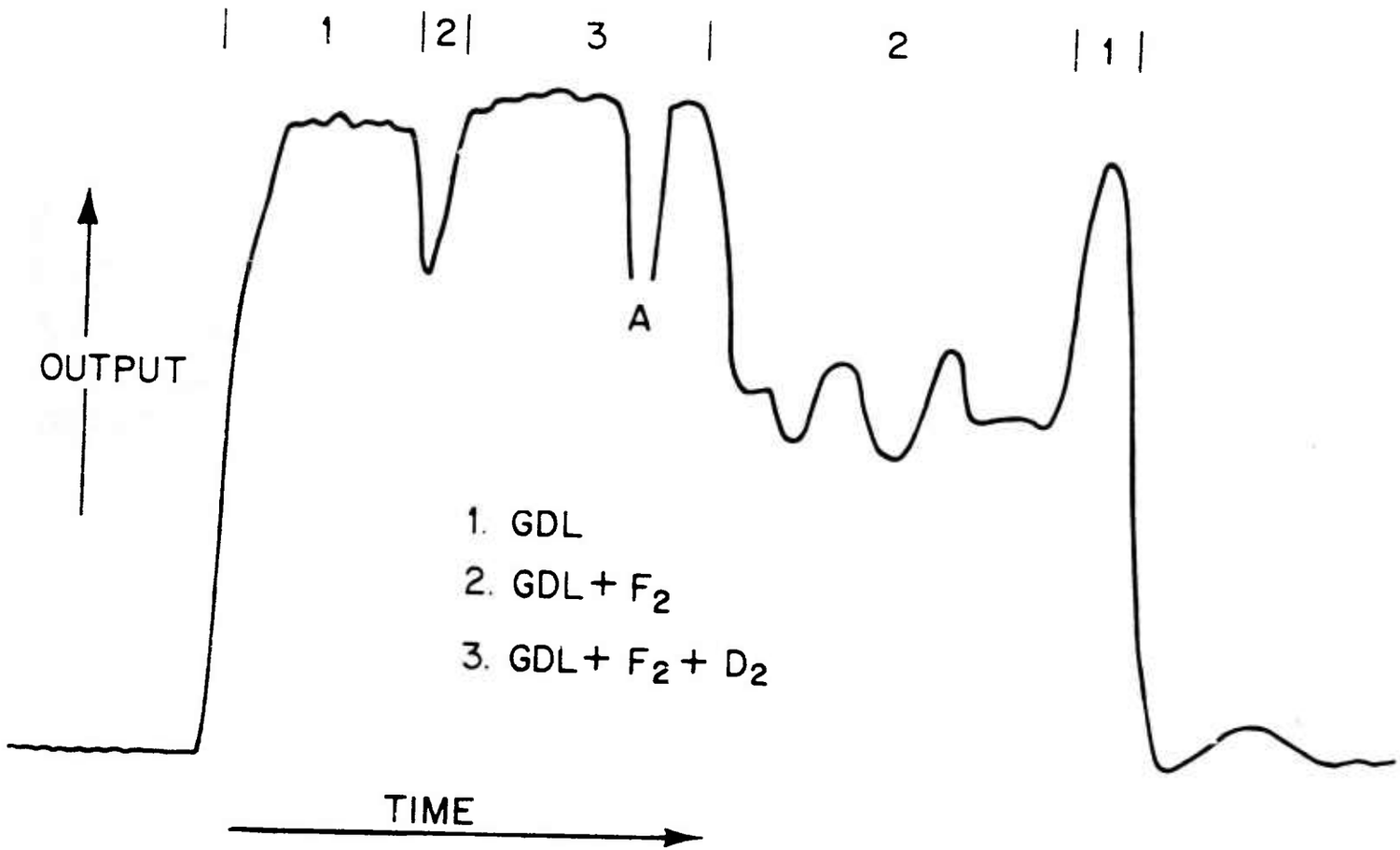

Fig. 3 — Chemical pumping of CO_2 gasdynamic laser

2. CARBON MONOXIDE ENERGY TRANSFER STUDIES

Measurements of energy transfer rates in CO are continuing using the previously reported vibrational fluorescence method. This technique employs a frequency-doubled CO_2 laser to pump ground state CO molecules to the CO(v=1) level. Previous studies stressed energy transfer rates relevant to CO lasers. It is also possible through rapid vibration to vibration energy transfer from CO to additive molecules to measure quenching rates for the additive species as well. This has been recently accomplished for CO-CO_2 and CO-N_2O mixtures over the temperature range 150-400^{o}K. Here, the emphasis was placed on measuring energy transfer rates out of the upper laser levels for CO_2 and N_2O which, until this study, were not available below room temperature. Cryogenic storage of laser gases and initiation of lasing at low temperatures is a desirable feature for those systems where rapid temperature rise deleteriously affects laser output power.

The upper laser level in CO_2 and N_2O is excited via the following near resonant V → V processes:

$$CO(v=1) + CO_2 \rightleftarrows CO + CO_2(001) + \Delta E = -206\ cm^{-1} \qquad (1)$$

$$CO(v=1) + N_2O \rightleftarrows CO + N_2O(001) + \Delta E = -81\ cm^{-1} \qquad (2)$$

An additional V → V transfer process in $CO-CO_2$ mixtures may also be occurring:

$$CO(v=1) + CO_2 \rightarrow CO + CO_2(11^10) + \Delta E = -67\ cm^{-1} \quad . \qquad (3)$$

The latter reaction is not reversible due to the rapid relaxation of $CO_2(11^10)$ in collisions with ground state CO_2 molecules. Rate constants for intermolecular V → V transfer from CO to CO_2 and N_2O are reported in Tables I and II respectively.

Vibrational quenching of $CO_2(001)$ in collisions with CO and CO_2 from 158 - 406°K are reported in Table I. Table II summarizes collisional deactivation rates of $N_2O(001)$ with N_2O, CO, and Ar in the range 144 - 405°K. The temperature dependence of the intramolecular deactivation of $N_2O(001)$ is shown in Figure 1. The N_2O self-relaxation rate exhibits a minimum near 250°K with a sharp increase in rate at lower temperatures.

The present measurements will be shortly extended to the $CO-CS_2$ system. It is quite possible that this system could produce an efficient $CO^{\dagger}-CS_2$ vibrational transfer laser and research to produce such a laser is already underway. Initial temperature studies for the rate measurements will cover the range 250 - 600°K.

During this contract period final reports have been submitted on CO room temperature energy transfer measurements[1] and CO-H_2, CO-N_2 temperature dependent studies from 100 - 650°K.[2] (See Appendix A on p. 130.)

REFERENCES

1. J.K. Hancock, D.F. Starr, and W.H. Green, "Measurement of the Rate of Excitation and Deactivation of OCS(001), N_2O(001), CS_2(001) and C_2N_2(00100) using Laser Excited CO as a Pumping Source", J. Chem. Phys., Oct. 1974.

2. D.F. Starr, J.K. Hancock and W.H. Green, "Vibrational Deactivation of Carbon Monoxide by Hydrogen and Nitrogen from 100 - 650°", J. Chem. Phys. (submitted for publication).

TABLE I

ENERGY TRANSFER RESULTS IN CO-CO_2 MIXTURES

PROCESS	TEMPERATURE	RATE (SEC^{-1} $TORR^{-1}$)
$CO^+ + CO_2 \rightarrow CO + CO_2^+$	406	3.2×10^3
	353	2.7×10^3
	301	2.5×10^3
	248	1.7×10^3
	196	1.4×10^3
	158	1.1×10^3
$CO_2(001) + CO \rightarrow CO_2 + CO$	406	290
	453	260
	301	260
	248	290
	196	420
	158	700
$CO_2(001) + CO_2 \rightarrow 2\ CO_2$	406	440
	353	370
	301	330
	248	350
	196	400
	158	420

TABLE II

$N_2O(00^0_1)$ VIBRATIONAL ENERGY TRANSFER RESULTS

RATE PROCESS	TEMPERATURE	RATE CONSTANT $k(sec^{-1}torr^{-1})$	DEACTIVATION[b] PROBABILITY	COLLISION CROSS SECTION $\sigma(Å^2)$
$N_2O(001) + CO(v=0) \rightleftarrows$	144	3.44(5)[a]	2.67(-2)	1.24
$N_2(000) + CO(v=1)$	196	2.79(5)	2.52(-2)	1.17
	247	2.50(5)	2.54(-2)	1.18
	300	2.25(5)	2.52(-2)	1.17
	353	2.08(5)	2.52(-2)	1.17
	405	1.93(5)	2.51(-2)	1.17
$N_2O(001) + N_2O \rightleftarrows$	144	1.53(3)	1.25(-4)	6.25(-3)
$N_2O(mno) + N_2O$	196	7.56(2)	7.18(-5)	3.60(-3)
	247	6.52(2)	6.95(-5)	3.49(-3)
	300	7.14(2)	8.39(-5)	4.21(-3)
	353	9.18(2)	1.17(-4)	5.87(-3)
	405	1.23(3)	1.68(-4)	8.43(-3)
$N_2O(001) + CO \rightleftarrows$	144	3.80(2)	2.95(-5)	1.37(-3)
$N_2O(mno) + CO$	196	3.74(2)	3.39(-5)	1.58(-3)
	247	4.22(2)	4.28(-5)	1.99(-3)
	300	5.37(2)	6.01(-5)	2.79(-3)
	353	7.35(2)	8.92(-5)	4.15(-3)
	405	9.90(2)	1.29(-4)	5.98(-3)
$N_2O(001 + Ar \rightleftarrows$	144	2.78(1)	2.58(-6)	1.11(-4)
$N_2O(mno) + Ar$	196	3.68(1)	3.99(-6)	1.71(-4)
	247	5.03(1)	6.12(-6)	2.63(-4)
	300	7.31(1)	9.80(-6)	4.21(-4)
	353	1.01(2)	1.47(-5)	6.31(-4)
	405	1.42(2)	2.21(-5)	9.50(-4)

(a) $3.44(5) = 3.44 \times 10^5$

(b) Deactivation probabilities were calculated using $P_{10} = (2.31 \times 10^{-8})\ KT^{\frac{1}{2}}\ \mu^{\frac{1}{2}}/d_{AB}^2$ where K is the rate constant in $sec^{-1}\ torr^{-1}$, μ is the reduced mass (AMU units) and $d_{AB} = \frac{1}{2}(d_A + d_B)$ is collision diameter in Angstroms (d = 3.7 CO, 4.0 N_2O, and 3.4 Ar).

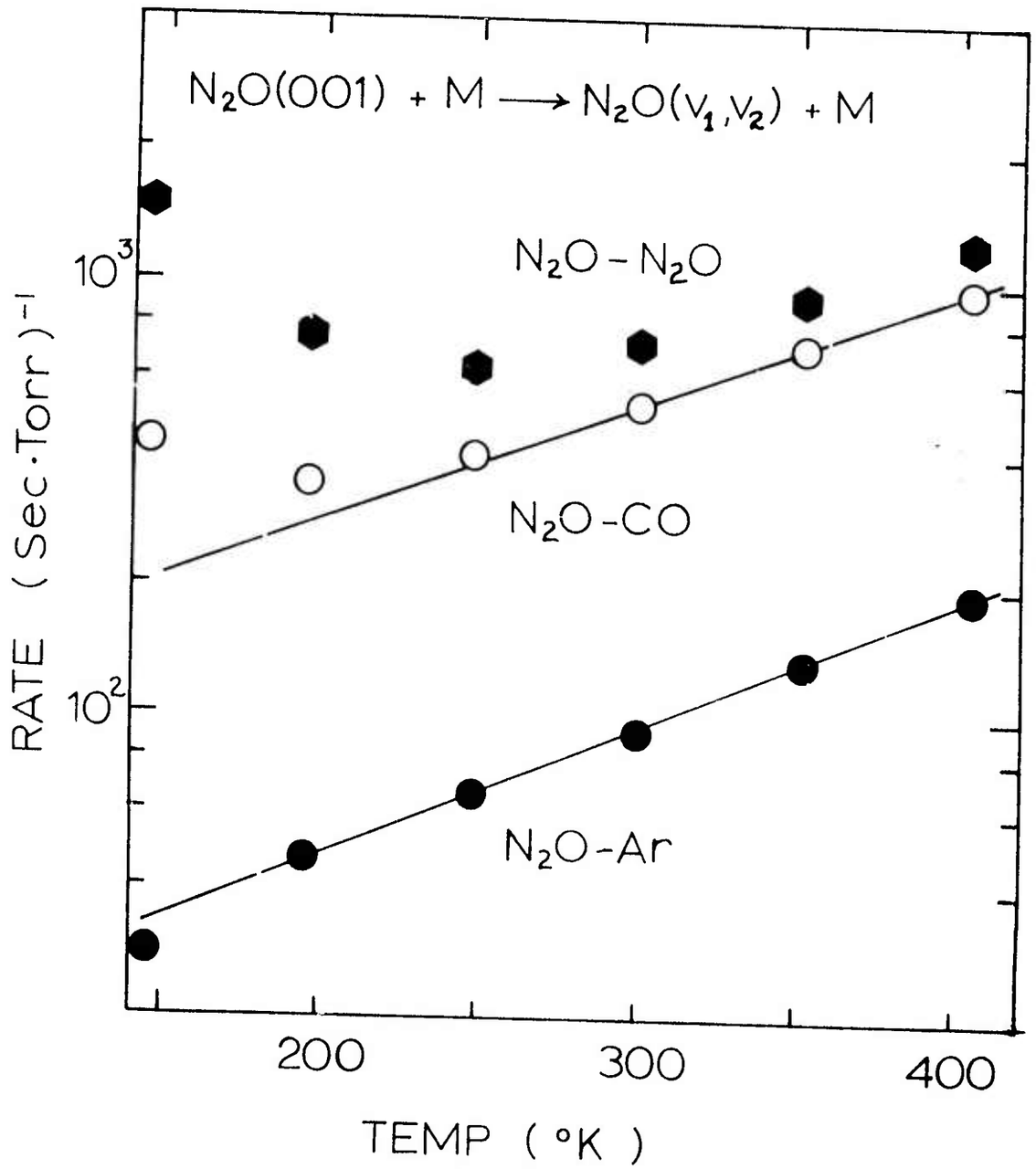
N2O(001) + M ⟶ N2O(V1,V2) + M
N2O - N2O
N2O - CO
N2O - Ar
RATE (Sec·Torr)-1
10^3
10^2
200
300
400
TEMP (°K)

Figure 1

ELECTRICAL INFRARED LASERS

1. SHORT PULSE CO_2 MOLECULAR LASER

In the present reporting period the work being carried out under this section of the ARPA/NRL high energy laser program has been completed. In the previous reporting period (1 July - 31 December 1973) the high power, nanosecond pulse CO_2 laser had been assembled and was operating at an output pulse energy $\sim$ 50 J.[1] Our work in the period 1 January - 31 June 1974 has been concerned with improving the system reliability and upgrading its performance to what we consider close to its maximum operating level. A new, higher power mode-locked oscillator has been installed and by using a large aperture, low absorption, CdTe Pockels cell in the pulse switchout system, a single pulse energy output of 12 mJ has been achieved. A fourth 3 x 3 x 50 cm amplifier has been added to the chain to increase the single pulse energy into the Lumonics amplifier. The pulsed power supplies which drive the 3 x 3 x 50 cm amplifiers have been reworked to improve their reliability and triggering jitter. We have also increased the operating pressure of the Maxwell e-beam amplifier to 1810 torr thereby increasing the energy storage of this device.

In addition we have developed a compact, high pressure (15 atm) electron-beam-controlled CO_2 laser and have succeeded

in mode-locking this laser by using p-type germanium as a saturable absorber. The mode-locked pulsewidths from this device are expected to be < 100 psec and should be suitable for amplification in a high pressure amplifier chain.

High Power Oscillator Design

For our previous work the single nanosecond pulse energy available from the helical pin mode-locked laser oscillator was limited to $\lesssim$ 3 mJ. In an effort to increase this energy, the pin laser was replaced with a 2 x 2 x 100 cm gain tube of a design similar to the first amplifier of the chain (solid electrode Lamberton-Pearson design). This oscillator has been operated using a laser gas mixture of 7½:½:2 ($He:N_2:CO_2$) and an energy loading $\sim$ 100 J/ℓ. The laser discharge is driven by a single capacitor (0.1 μF) operating at a voltage of 28 kV yielding an $E/N \approx 5.7 \times 10^{-16}$ V cm^2 in the gas.

The laser was mode-locked using the germanium acousto-optic modulator described in a previous report.[1] However the high gain of this laser necessitated use of a higher RF drive power to the modulator to obtain stable mode-locking. The energy in the mode-locked pulse train was typically 100 mJ in a clean TEM_{oo} mode in a beam diameter $\sim$ 3 mm. This was obtained using a laser cavity consisting of a 60% reflectivity output coupler and a 4 m radius 100% reflectivity

mirror separated by $\sim$ 350 cm. The 100 mJ pulse train energy is greater than the < 70 mJ as previously obtained in the pulse train from the helical pin laser. In addition the energy output from the solid electrode laser occurs in a small number of high intensity mode-locked pulses whereas the helical laser emitted a long, low intensity pulse train. The peak pulse energy from the present system is about a factor of four higher than previously achieved. Laser emission occurred only on the P(20) line of the $00^{0}1$ - $10^{0}0$ band of CO_2. While use of a single line oscillator does reduce the energy extracted from some of the amplifiers, it will be seen that high energy extraction efficiency is still obtained with the e-beam amplifier. This is achieved due to the high input energy density of the pulse at this amplifier and due to the fast rotational relaxation time obtained by operating the e-beam at high pressure.

As before, single pulse selection is carried out using a switch-out system consisting of a Pockels cell placed between crossed, stacked germanium plate polarizers. The switch-out system has been improved by replacing the GaAs Pockels cell crystal with a larger one made of CdTe. The physical and electro-optical properties of CdTe and GaAs are compared in Table 1. The small optical absorption and large electro-optic coefficient of CdTe make it superior

to GaAs for electro-optic modulator applications. For the present application the switch-out system should have a high extinction ratio (ER). The extinction ratio is defined by:

$$ER = \frac{T_p}{T_c} \qquad (1)$$

where T_p is the transmission of the polarizer-Pockels cell-analyzer arrangement when the polarizer and analyzer are parallel and T_c is the transmission when they are crossed. The extinction ratio of the system has been measured using the setup shown in Fig. 1. A stable cw CO_2 laser beam is directed through the switchout system onto a sensitive Ge:Cu detector. The cw laser is chopped and the signal from the detector is monitored using a lock-in amplifier. This permits direct measurement of the weak leakage signal obtained when the polarizer and analyzer are crossed. Saturation of the Ge:Cu detector must be avoided when measuring the large signal transmitted when the polarizer and analyzer are parallel. Saturation effects are eliminated by using calibrated attenuators to measure this signal thus keeping the light level within the linear range of the detector.

The polarizer and analyzer used each consist of four, 3" diameter germanium plates. The plates are held at the Brewster angle giving a clear aperture, through the setup, of 3/4". Using this arrangement the extinction ratio of the

polarizer and analyzer alone has been measured as $\sim 2 \times 10^4$. This is considerably less than the theoretical maximum value of 1.7×10^5. Light scatter inside the stacks is not considered a problem due to the large stack aperture (0.75") achieved by using 3" diameter germanium plates held at Brewsters angle. However, since the faces of the plates are parallel, multiple internal reflections could cause the observed reduction of ER. This problem could be resolved by wedging the plate surfaces at a small angle ($\sim$ 13 min). When the CdTe Pockels cell is placed in the system ER drops to $\sim 8 \times 10^3$ for a 3 mm probe beam diameter. This is caused by the residual birefringence in the CdTe crystal.

The Pockels cell was designed in a manner similar to that previously described for our GaAs cell. Figure 2(a) shows the details of the system. The crystal dimensions are 10 x 10 x 40 mm, which were chosen to minimize diffraction effects, to provide a convenient operating voltage, and to permit good electrical matching of the Pockels cell to the 30 ohm cable used in the system. The electrical matching characteristics of the system were checked using a time domain reflectometer and the TDR trace is shown in Fig. 2(b). The electrical reflections from the Pockels cell is $\sim$6%.

The mode-locked laser and pulse selection system were operated in the setup shown in Fig. 3. A beam-splitter directs ∿ 10% of the laser output to fire the laser triggered spark gap thus applying a short (∿13 nsec) high voltage (11.7 kV) pulse to the Pockels cell. Synchronization of the voltage pulse with the arrival of a mode-locked laser pulse at the Pockels cell is achieved by adjustment of the length of cable connecting the laser triggered sparkgap to the Pockels cell. After passing through the Pockels cell the high voltage pulse is propagated down a length of 30 ohm coaxial cable and terminated in a matched 30 ohm resistive load. The triggering jitter of the system was ∿ 1 ns and the pulse selection procedure is shown in Figure 4. Complete switching of the main pulse in the mode-locked train is achieved giving a selected pulse of energy ∿ 12 mJ. This pulse is then directed down the amplifier chain for amplification to a high energy level.

Preamplifiers

In our previous work this section of the chain consisted of one 2 x 2 x 100 cm amplifier followed by three (3 x 3 x 50 cm) devices. With this setup the energy available at the input of the Lumonics was ∿ 1.5 J. The beam diameter after the beam expander is ∿ 8.1 cm giving an input energy density to the Lumonics ∿ 30 mJ/cm^2 which is much lower than the

saturation energy of atmospheric pressure CO_2 amplifiers ($\sim$ 130 mJ/cm^2). Thus the pulse energy at this point in the chain can be increased with advantage. We have therefore added a fourth 3 x 3 x 50 cm amplifier to this part of the chain. Coupled with the improved oscillator pulse energy available, this has increased the single pulse energy into the Lumonics to $\sim$ 3 - 4 J ($\sim$60 - 80 mJ/cm^2).

The driving circuits of these five amplifiers have been rebuilt to provide better operating reliability at the high voltages used. In addition the amplifiers are now triggered using a high voltage pulse generator having five independent output channels resulting in a firing jitter, for each unit, of < 50 nsec. This is necessary due to the short time ($\sim$400 nsec) during which the gain of these amplifiers is near maximum.

Large Aperture Amplifiers

Most of the energy stored in the amplifier chain is in the two Lumonics amplifiers and the Maxwell electron-beam-controlled device. As a means of increasing the overall operating level of the system it would seem to be most profitable to concentrate on upgrading the performance of this section of the laser chain. Since the Lumonics amplifiers are operating at their maximum level, we have investigated the possibility of increasing the energy stored in the Maxwell amplifier.

The stored energy (E_{ST}) in a CO_2 amplifier is given by:

$$E_{ST} = cp\alpha \quad J/\ell \qquad (2)$$

where p is the operating pressure in torr, α is the small signal gain and c is a constant which is dependent on various properties of the laser gas and the gain measurement wavelength. The derivation of this equation is given in a later section of this report. Thus an increase in E_{ST} can be achieved by increasing either the operating pressure or the gain of the device. In practice, self-oscillation problems limit the maximum value of α that can be used (in the present system $\alpha_{MAX} = 0.05\ cm^{-1}$). Thus the pressure should be increased to maximize E_{ST}. We have previously operated the e-beam amplifier at a pressure of 1550 torr and we have since investigated its gain performance at pressures up to 2050 torr.

In the present system an upper limit on the operating pressure is set by the maximum voltage that can be applied to the sustainer capacitor bank. As the gas pressure is increased the sustainer voltage should also be increased to optimize the electron energy distribution in the discharge for maximum pumping of the upper laser levels of CO_2 and the strongly coupled levels of N_2. For the 3:¼:1 ($He:N_2:CO_2$) gas

mixture normally used in this amplifier the optimum coupling to the $00^0 1$ level of CO_2 and the vibrational levels of N_2 is obtained[2] for E/N $\approx 1.5 \times 10^{-16}$ V cm^2. The sustainer bank has a maximum charging voltage of 75 kV thus optimum E/P can be reached for a maximum pressure of 1500-torr (amplifier electrode separation = 10 cm). For higher pressures of course the pumping process will be less efficient. This was obvious as an increase in the input energy density/atm. required to achieve a given gain, as the gas pressure was increased.

Based on the gain results an operating pressure of 1810 torr was chosen as optimum for the system. This gives a large $p\alpha$ product for a gas energy loading which is not excessive. This operating pressure could be increased by fitting the amplifier with a higher voltage sustainer bank.

Pulse Amplification

The complete laser system was assembled as shown in Figure 5. Saturable absorber cells 1 and 2 are included to prevent amplification of leakage and self-oscillation in the amplifier chain, respectively. The construction of these cells and their important dimensions are shown in Figure 6. Cell 1 was filled with an SF_6/He mixture to a total pressure of 760 torr. The SF_6:He mixture ratio used was typically 1:6. Cell 2 was typically filled with pure

SF_6 to a pressure of 15 torr.

The output pulse at the end of the amplifier chain was monitored using the setup shown in Figure 7. A sodium chloride beam-splitter splits off 8% of the beam for energy monitoring using a Gen-Tec calorimeter (sensitive area 23 cm^2). A further sodium chloride beam splitter directed part of the laser pulse onto an Oriel photon drag detector for temporal measurements using a Tektronix 7904 oscilloscope. The oscilloscope was placed in a screened room to isolate it from electro-magnetic noise generated by the electron gun. Figure 8 shows oscilloscope records of the output pulse. The lower trace, which is on a long time scale demonstrates the absence of large leakage pulses around the main pulse. In this case the measured energy was ~70 J. Energy measurements taken without activating the Pockels cell show a leakage energy < 4 J. The pulse energy obtained at various stages in the amplifier is shown in Figure 5.

Some indication of the spatial energy profile and coherence properties of the laser pulse have been obtained by replacing the energy monitoring calorimeter with a suitable beam stop to obtain laser burn patterns. Unexposed, developed Polaroid film was used as a simple means of obtaining the above patterns. A typical burn pattern is shown in Figure 9. In the above setup the sodium chloride beam splitter acts as a shear plate interferometer. Each

face of the plate reflects 4% of the incident pulse energy. The wavefronts from each surface have a lateral shear with respect to each other due to the thickness of the plate and the angle of incidence ($\sim 20^{o}$). The wavefronts also are inclined at an angle to each other due to the plate wedge ($\sim 3'$) and are time delayed by 2nd cos ϕ/c where n is the refractive index of sodium chloride, c the velocity of light, d the plate thickness ($\sim$ 3 cm) and ϕ is the internal angle of incidence on the plate.

The first thing that can be deduced from the burn pattern concerns the temporal coherence of the laser pulse. Since the burn pattern is formed by two superimposed inclined and delayed beams the fact that high contrast interference fringes are formed shows that the coherence time of the pulse is at least 2nd cos ϕ/c which in this case is $\sim$250 psec. The relative straightness of the fringes indicates that the spatial coherence of the beam is good. A large variation of phase across the beam would cause curvature of the fringes. The pattern in Figure 9 indicates a wavefront distortion of $\lesssim \lambda$ across the beam. Finally the variation of burn intensity along one fringe gives an indication of the beam intensity variation. In the present case some spatial intensity modulation is evident on the pulse.

These results are interesting in view of the fact that little effort was made to avoid interaction of the beam with diffracting apertures as it propagated down

the amplifier chain. The only criterion used was that the beam diameter at any part of the chain should be less than the amplifier aperture at that point. This did produce diffraction effects which were evident in the preamplifier stages. No window damage problems occurred due to this beam non-uniformity. However these non-uniformities would disappear due to diffraction as the pulse propagates towards an experimental area. It would thus seem that large CO_2 amplifier chains can be built with minimum attention being paid to "aperturing problems". An estimation of the beam divergence of the laser is obtained from consideration of the beam expansion from the input to the Lumonics amplifiers to the point where the burn patterns were taken. The beam expands from 8.1 cm diameter to 8.7 cm diameter over a distance $\approx$ 500 cm giving a full angle divergence of $\leq$1 mR.

Finally we should consider the output energy obtained from the laser system. The laser pulse sweeps a volume $\sim 5\ell$ in the Lumonics amplifiers and $\sim 6\ell$ in the Maxwell e-beam amplifier. We wish to compare the energy available from each amplifier with the actual energy extracted by the laser pulse. The small signal gain (α), and rotational population inversion (δ) on the one line of a CO_2 laser are related by:

$$\alpha = \sigma \delta \qquad (3)$$

where σ is the stimulated emission cross-section. For a 3:4:1($He:N_2:CO_2$) laser gas mix (which is approximately the mixture used in both amplifiers) the stimulated emission cross-section on the P(20) line of the 10 μm band of CO_2 is given by:[3]

$$\sigma\left[P(20)\right] = 1.5 \times 10^{-18} \left\{\frac{760}{p}\right\} cm^2 \qquad (4)$$

where p is gas pressure in torr. Thus the rotational inversion on the P(20) transition is given by

$$\delta\left[P(20)\right] = \frac{\alpha\left[P(20)\right]}{1.5 \times 10^{-18}\left\{\frac{760}{p}\right\}} . \qquad (5)$$

The rotational inversion (δ), and the $00^0 1 - 10^0 0$ vibrational inversion (Δ) are related by:

$$\delta(J) = f(J)\ \Delta \qquad (6)$$

where f(J) is the fraction of molecules in the Jth rotational level. Assuming these levels are in thermal equilibrium the fraction f(J) is given by:

$$f(J) = g_J \exp\left\{\frac{-\varepsilon(J)}{kT}\right\}\left[\sum_J g_J \exp\left\{\frac{-\varepsilon(J)}{kT}\right\}\right]^{-1} \qquad (7)$$

where $g_J = (2J + 1)$ is the statistical weight and $\varepsilon(J)$ is the energy of the Jth rotational level, and k is the Boltzmann constant. Thus assuming a gas temperature of $300^{\circ}K$ we obtain:

$$f(19) \approx 0.068 \quad . \qquad (8)$$

We can therefore relate gain measurements on the P(20) transition of the $00^{\circ}1 - 10^{\circ}0$ band to the vibrational inversion on this band by:

$$\Delta(00^{\circ}1\text{-}10^{\circ}0) = \frac{\alpha[P(20)]}{f(19) \times 1.5 \times 10^{-18}\left\{\frac{760}{P}\right\}} \qquad (9)$$

$$\therefore \Delta = 1.29 \times 10^{16}\ p\ \alpha \quad . \qquad (10)$$

The $00^{\circ}1\text{-}10^{\circ}0$ vibrational stored energy in one liter of gas is given by:

$$E_{ST} = 10^3\ \Delta\ \frac{hc}{\lambda} \quad J/\ell \qquad (11)$$

which for the 10 μm CO_2 wavelength gives:

$$E_{ST} \approx 1.875 \times 10^{-17} \Lambda \quad J/\ell \quad . \qquad (12)$$

Combining equations (10) and (12) we obtain:

$$E_{ST} = 0.24\ p\ \alpha \quad J/\ell \quad . \qquad (13)$$

For nanosecond pulse amplification the lower laser level does not have time to empty during the pulse passage thus the maximum energy available (E_{AV}) for nanosecond pulse amplification in a CO_2 amplifier is:

$$E_{AV} = E_{ST}/2 \qquad (14)$$

$$\therefore E_{AV} \approx 0.12\ p\ \alpha \quad J/\ell \quad . \qquad (15)$$

The small signal gain in the Lumonics amplifiers is $\sim 0.038\ cm^{-1}$ and in the Maxwell e-beam amplifier is $\sim 0.05\ cm^{-1}$. Thus the maximum energy available in these amplifiers is 17.3 J in the Lumonics and 65.2 J in the Maxwell amplifier. From Fig. 5 it is seen that the energy extracted from the Lumonics amplifiers is $\sim$13.5J and from the Maxwell amplifier is $\sim$ 55 J. These numbers are consistent with the energy available from the amplifiers. A high percentage of available vibrational inversion is removed from the Maxwell

device due to the large input pulse energy density and fast rotational relaxation time (because of the high pressure), which overcome the problem of single line oscillation of the driving oscillator.

Conclusion

We have successfully demonstrated the operation of a 70 J, nanosecond pulse, CO_2 laser system. The present amplifier chain seems to be a good combination of uv preionized and electron-beam-controlled amplifiers. The less expensive uv preionized amplifiers have been used for pulse pre-amplification whereas the main energy amplification in the chain is supplied by the more sophisticated electron-beam-controlled amplifier. The reliability and reproducibility of the various components in the system (amplifiers, trigger generators, oscillator, switching system, etc.) have been developed to the point where the system is suitable for long term operation for laser-matter interaction studies.

Certain aspects of the system could however benefit from further investigation. For critical experiments the output beam intensity profile should be improved. Further work on the properties of the saturable absorbers is required to obtain the best compromise between effective amplifier isolation and minimum attenuation of the propagating laser pulse. In addition an experimental program should be under-

taken to clarify the dynamics of short pulse amplification in CO_2 amplifiers and for comparisons with existing theory[4] which describes the process. Finally, for laser-target interaction studies, the development of convenient and effective optical isolators are required to prevent possible damage problems due to laser light reflected from the target.

High Pressure CO_2 Laser Development

For some experiments on the interaction of high energy CO_2 laser pulses with matter, it would be desirable to use high energy picosecond laser pulses. An atmospheric pressure CO_2 laser operating on a single rotational line is limited, by bandwidth considerations, to giving output pulses $\gtrsim$ 250 psec. In practice the output pulses are typically $\sim$ 1 nsec. However at very high pressure ($\sim$ 10 - 15 atm) pressure broadening causes spectral overlap of neighboring CO_2 rotational lines. For this type of CO_2 laser the available bandwidth for mode-locking is greatly increased. As an example, if locking could be achieved over ten rotational lines, the available bandwidth would be $\Delta\nu \sim 400$ GHz which, using $\Delta\nu \cdot \Delta t \sim 1$, could give a mode-locked pulsewidth $\Delta t \sim$ 2.5 psec. Thus a mode locked multi-atmosphere CO_2 laser should be a good method of producing picosecond pulses at 10.6 μm.

We have developed a mode locked high pressure electron-beam controlled CO_2 laser. For these experiments the large

area Maxwell e-beam machine was used to investigate the operation of a small high pressure CO_2 laser. The Maxwell machine is well suited to this type of experiment due to its high output current (> 1 A/cm^2) and variable voltage and pulse length. A small high pressure chamber was attached to the front of the Maxwell machine (Fig. 10) and we have investigated the operation of the laser at a pressure of 15 atm. The potential performance of any laser can be predicted from small signal gain measurements on the active medium. Thus in our first experiments we investigated the dependence of the laser gain on the laser gas mixture. The gain measurement setup is shown in Figure 11. The Maxwell electron gun was operated at a pulse length of 0.5 μsec and the sustainer voltage was set at 52 kV giving an E/N $\simeq$ 1.3 x 10^{-16} V cm^2. The laser discharge volume was (1 x 1.1 x 20) cm^3. The laser current, and therefore the energy deposition in the gas, could be varied by changing the electron beam current.

Gain measurements have been taken, using a cw CO_2 probe laser, for gas mixtures ranging from 70% He; 30% CO_2 to 70% He; 5% CO_2; 25% N_2. We have also taken gain measurements for various wavelengths on the CO_2 9 and 10 μm bands. Figure 12 shows the important results of these measurements. Highest gain was measured in mixtures containing a small amount of N_2 and the best mixture tested was 70% He; 25% CO_2;

5% N_2. In addition highest gain was measured on the 10 μm R-branch of CO_2. A maximum gain of 5.2%/cm was measured for this mixture. This was achieved at an energy input to the gas of 115 J/ℓ.atm and using an electron gun current ∿ 1.5 A/cm^2. Thus, provided large electron gun currents are available, the high pressure laser operates with best efficiency using high concentrations of CO_2.

However in some setups there might be an upper limit on the electron-gun current available in which case the laser gas mixture should be chosen to maximize the discharge current, and therefore the energy deposited in the gas. This is necessary since the gain increases rapidly with energy input for all gas mixtures. Figure 13 shows a set of results obtained for the discharge current versus percentage CO_2 in the laser mix for a fixed electron-gun current and a constant sustainer voltage. It can be seen that the laser current is much higher for the 5% CO_2 mixture than for the 30% CO_2 mixture. The energy input to the gas would also be correspondingly higher. Thus for an electron-beam current limited system, highest gain operation (but not necessarily highest efficiency) is achieved by using high N_2 concentration mixtures. The lower measured current for the high concentration CO_2 mixtures is caused by a reduction of the electron number density in the discharge due to the large attachment rate coefficient of CO_2. A laser

energy output $\sim$ 1.2 J has been obtained from this device for a laser efficiency $\sim$ 2.5%. The maximum output from the laser is limited by damage to the cell windows. By using apertures in the laser cavity TEM_{00} mode operation was easily achieved.

The high pressure laser has been mode-locked using the configuration shown in Figure 14. For these experiments the laser was operated at 12 atm using a 70% He; 15% CO_2; 15% N_2 gas mixture. Passive mode locking is obtained using p-type germanium as a saturable absorber. The important characteristics of this material are shown in Table 2. The very short lifetime of the absorbing transition is an important requirement for obtaining picosecond pulses from the laser.

The output from the mode-locked laser was monitored using a photon-drag detector and a Tektronix 7904 oscilloscope. By operating the laser close to oscillation threshold it was possible to obtain clean output trains of mode locked pulses. A typical pulse train is shown in Figure 14. The temporal width of individual pulses could not be resolved with the above detection system but it is expected that the pulsewidths are < 100 psec. These short laser pulses could be amplified in a high pressure amplifier chain to provide multi-joule picosecond CO_2 pulses for target interaction studies for comparison with similar experiments being performed with Nd^{3+}:glass lasers.

REFERENCES

1. ARPA-NRL Laser Program, Semiannual Technical Report, 1 July 1973 - 31 December 1973.
2. O.P. Judd, J. Appl. Phys. 45 (1974) 4572.
3. E.E. Stark, Jr., W.H. Reichelt, G.T. Schappert, and T.F. Stratton, Appl. Phys. Lett. 23 (1973) 322.
4. G.T. Schappert, Appl. Phys. Lett. 23 (1973) 319.

TABLE 1

	GaAs	CdTe
Refractive Index (n_o)	3.3	2.6
Symmetry Group	$\bar{4}3$ m	$\bar{4}3$ m
Electro-optic Coefficient (r_{41} m/V)	1.6×10^{-12}	6.8×10^{-12}
Bulk Absorptivity (cm^{-1} @ 10.6 μm)	.02	.002
Resistivity (Ohm-cm)	4×10^{8}	2×10^{8}
Breakdown Field (V/cm d.c.)	4×10^{3}	2.1×10^{3}
Dielectric Constant ($\varepsilon_{d.c.}$)	12.5	11
Transmission (μ)	1-18	1-30

TABLE 2

p-TYPE GERMANIUM

Absorption Cross-Section (σ)	=	6×10^{-16} cm^2
Carrier Mobility	=	1800 cm^2/V sec.
Carrier Lifetime	=	3 - 4 psec
Doping Concentration	$\approx$	$1 - 2 \times 10^{15}/cm^3$
Saturation Intensity	=	11 Megawatts/cm^2

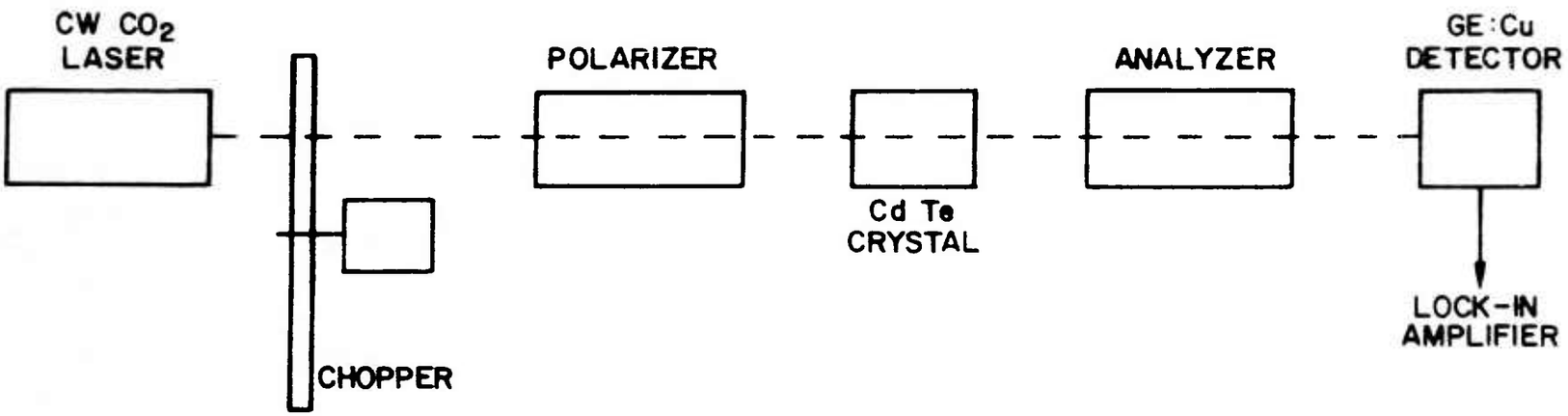

Fig. 1 — Experimental arrangement used for extinction ratio measurements

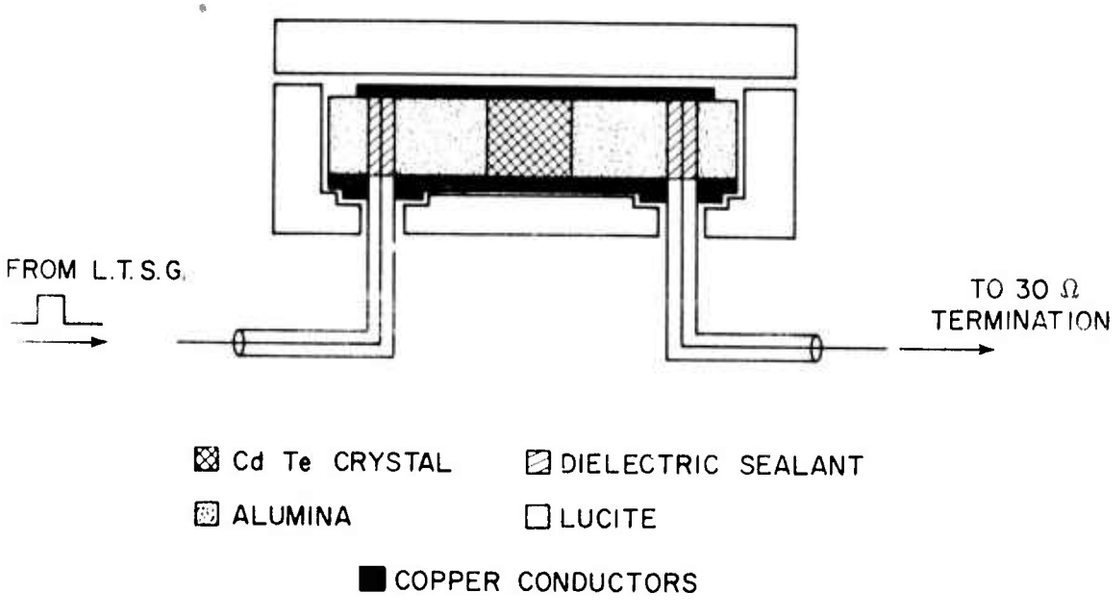

(a)

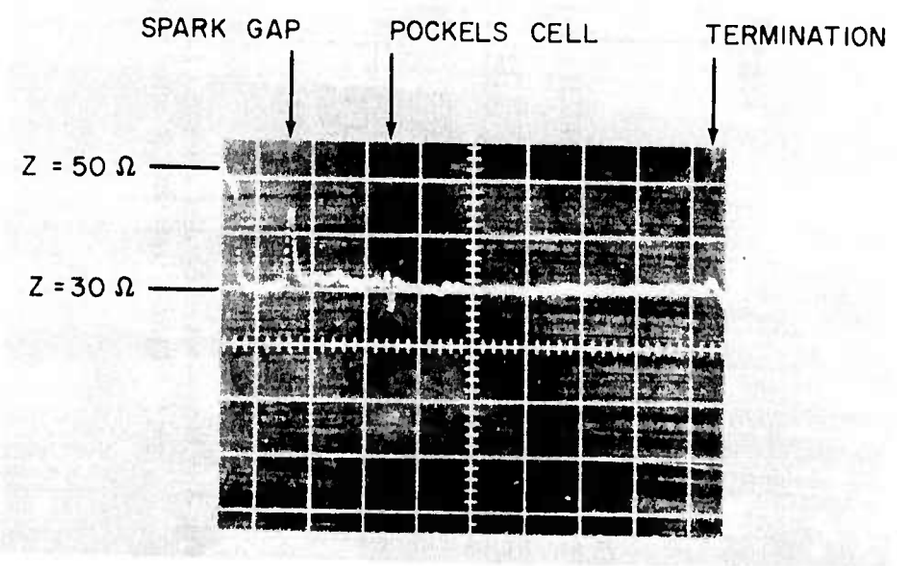

(b)

Fig. 2 — (a) Constructional details of the CdTe Pockels cell, and (b) TDR trace of the complete Pockels cell switching system. Time scale: 10 nsec/div.

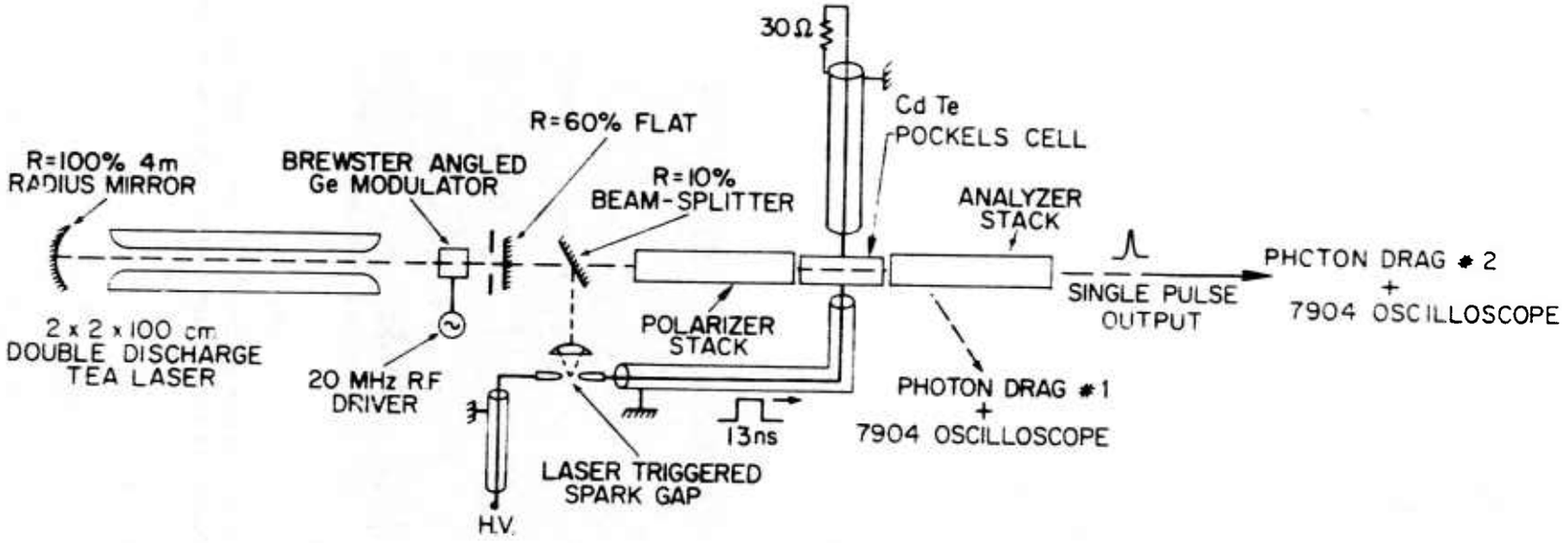

Fig. 3 — Mode-locked oscillator setup. Detectors no. 1 and 2 monitor the rejected pulse train and selected single pulse respectively

(a)

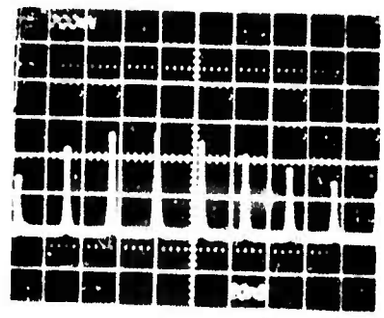

(b)

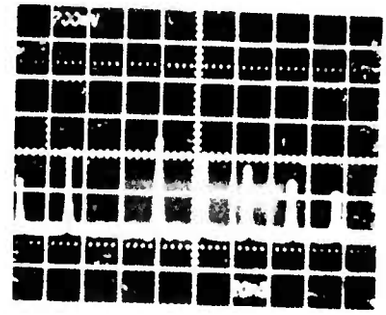

Fig. 4 — Oscillator operation as monitored by: (a) and (b) detector no. 1; (c) and (d) detector no. 2;
Trace details:
(a) Spark-gap blocked. 200 mV/div; 20 nsec/div
(b) Spark-gap blocked. 200 mV/div; 20 nsec/div
(c) Single selected pulse. 500 mV/div; 1 nsec/div
(d) Single pulse contrast. 20 mV/div; 10 nsec/div

(c)

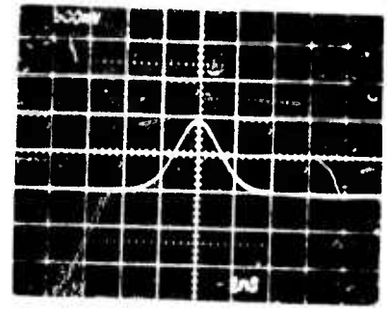

(d)

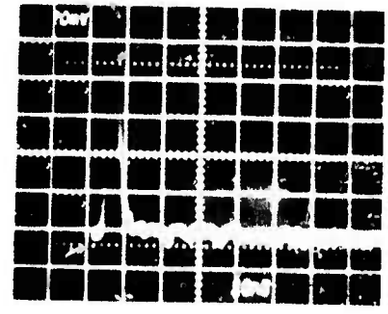

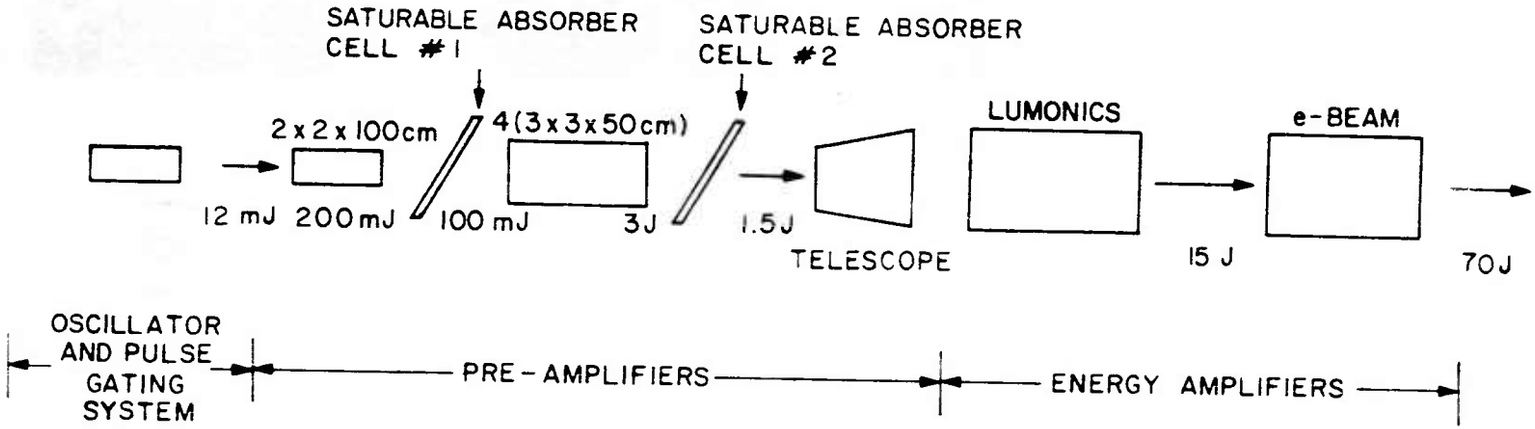

Fig. 5 — High power laser setup

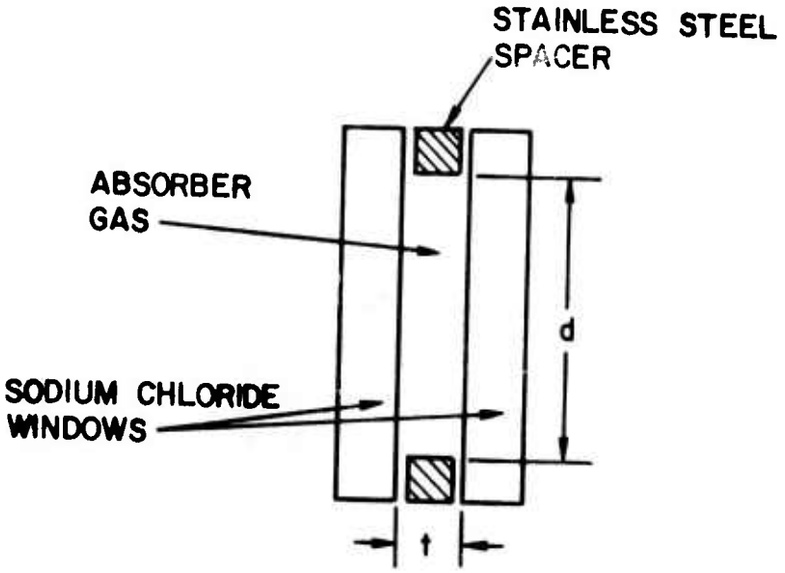

CELL 1 d = 40mm; t = 1mm
CELL 2 d = 60mm; t = 8mm

Fig. 6 — Details of absorber cells

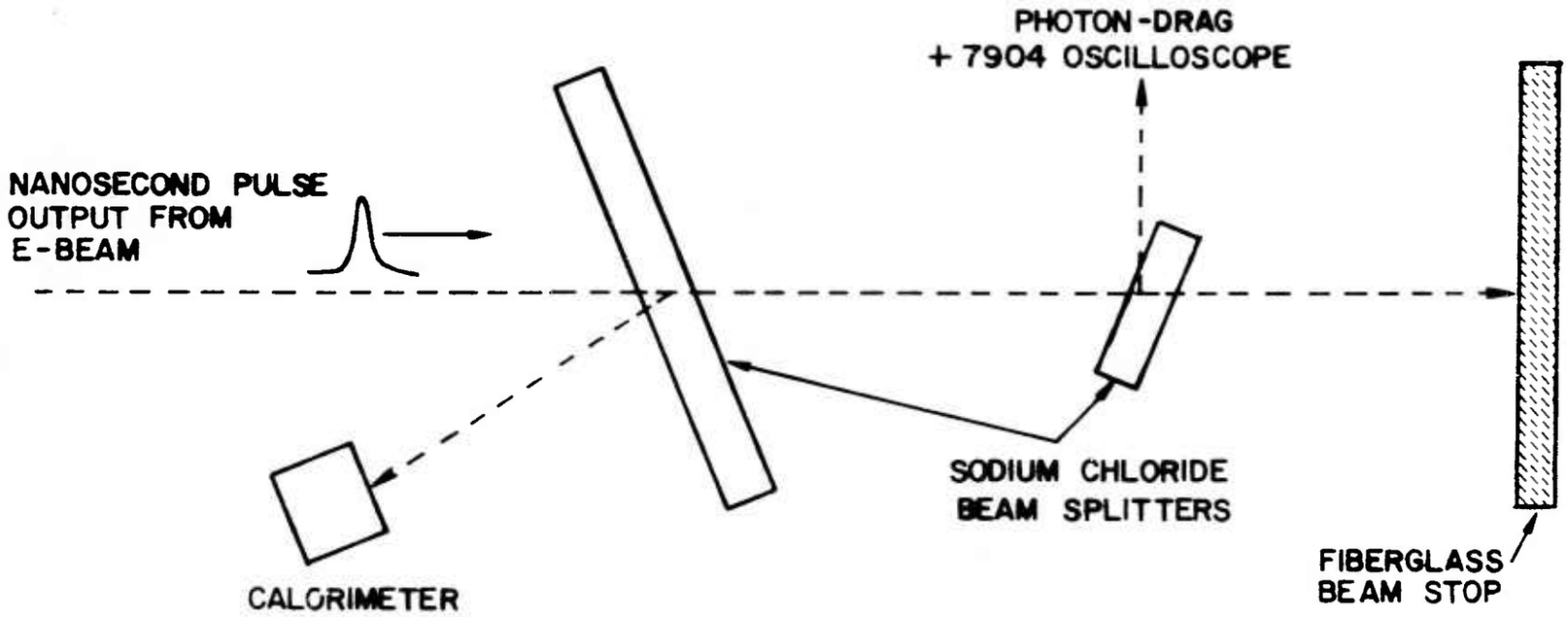

Fig. 7 — Output pulse monitoring setup

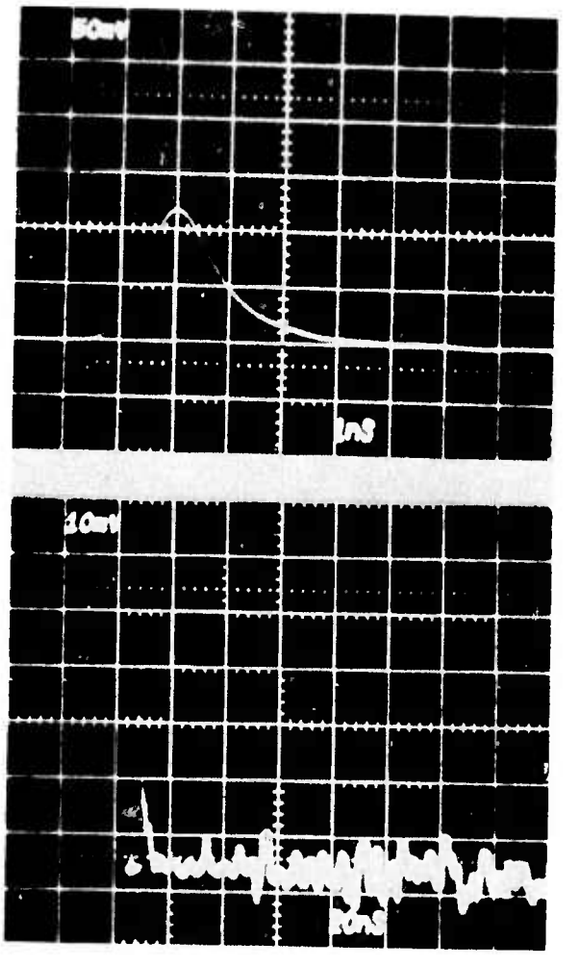

Fig. 8 — Output pulse from laser system. Upper: Pulse shape on 1 nsec/div. Lower: Output on 20 nsec/div and a more sensitive voltage scale.

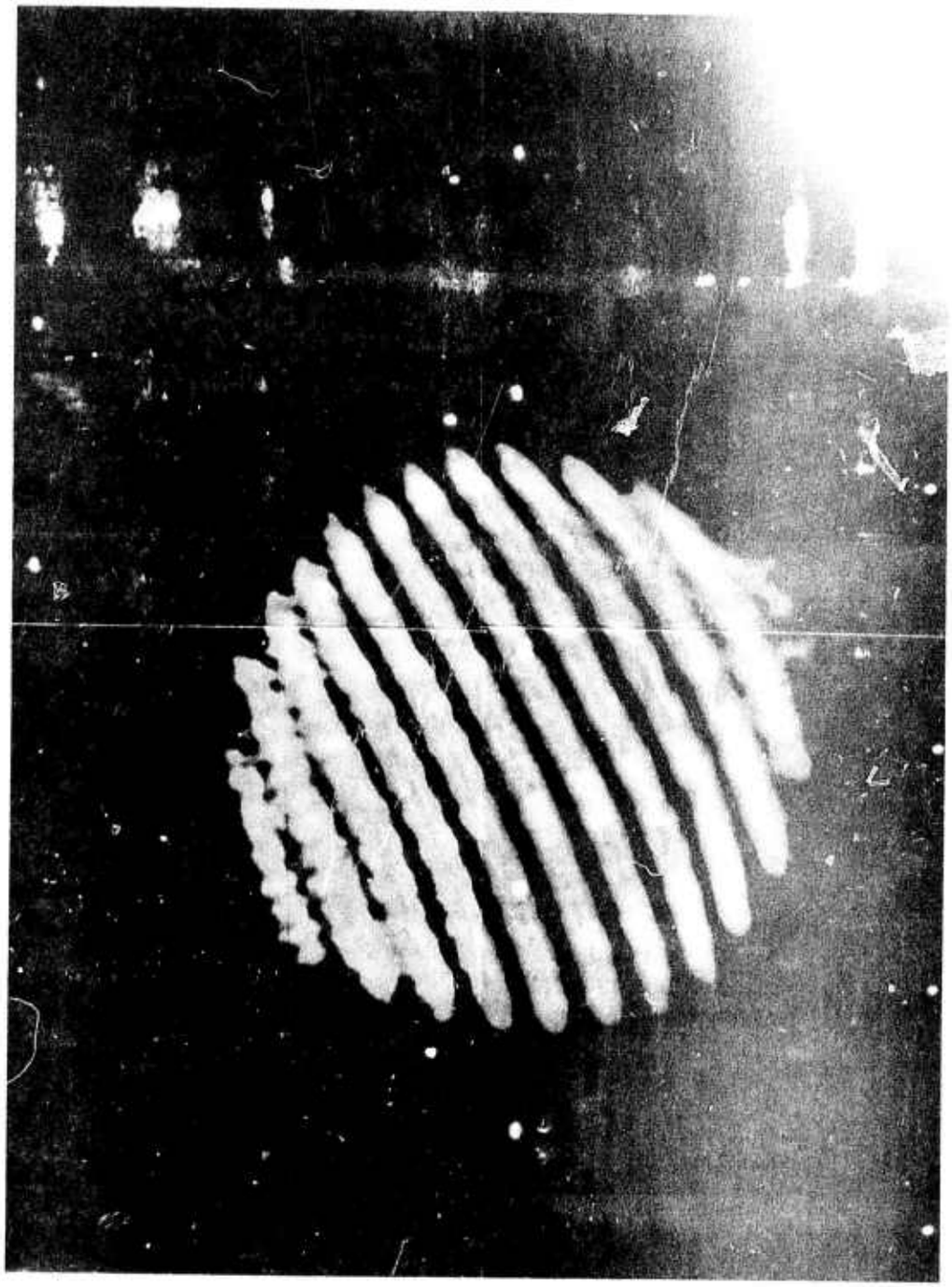

Fig. 9 — Output pulse burn pattern. Beam diameter is 8.7 cm.

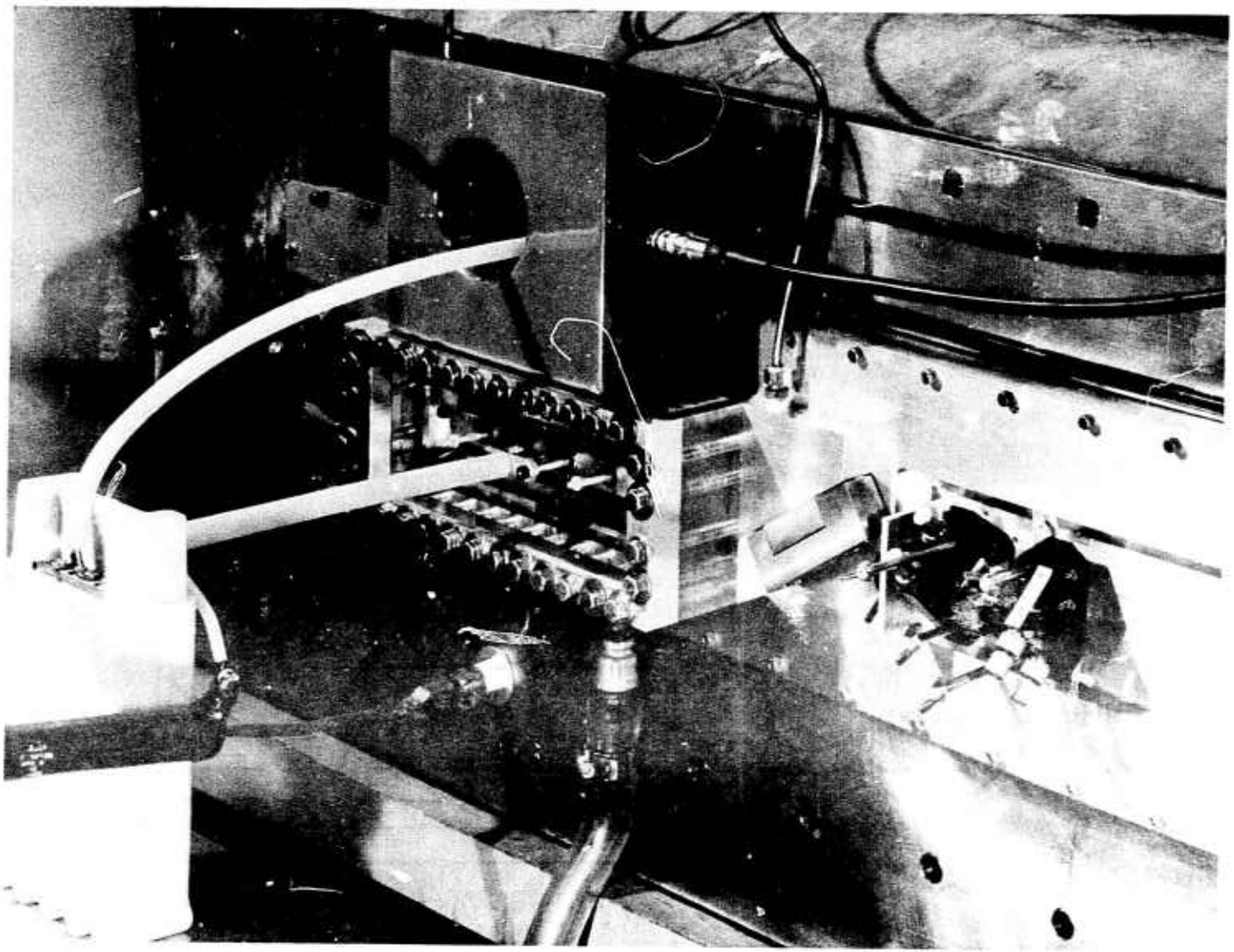

Fig. 10 — 15 atm. CO_2 laser chamber attached to Maxwell e-beam macl.ine

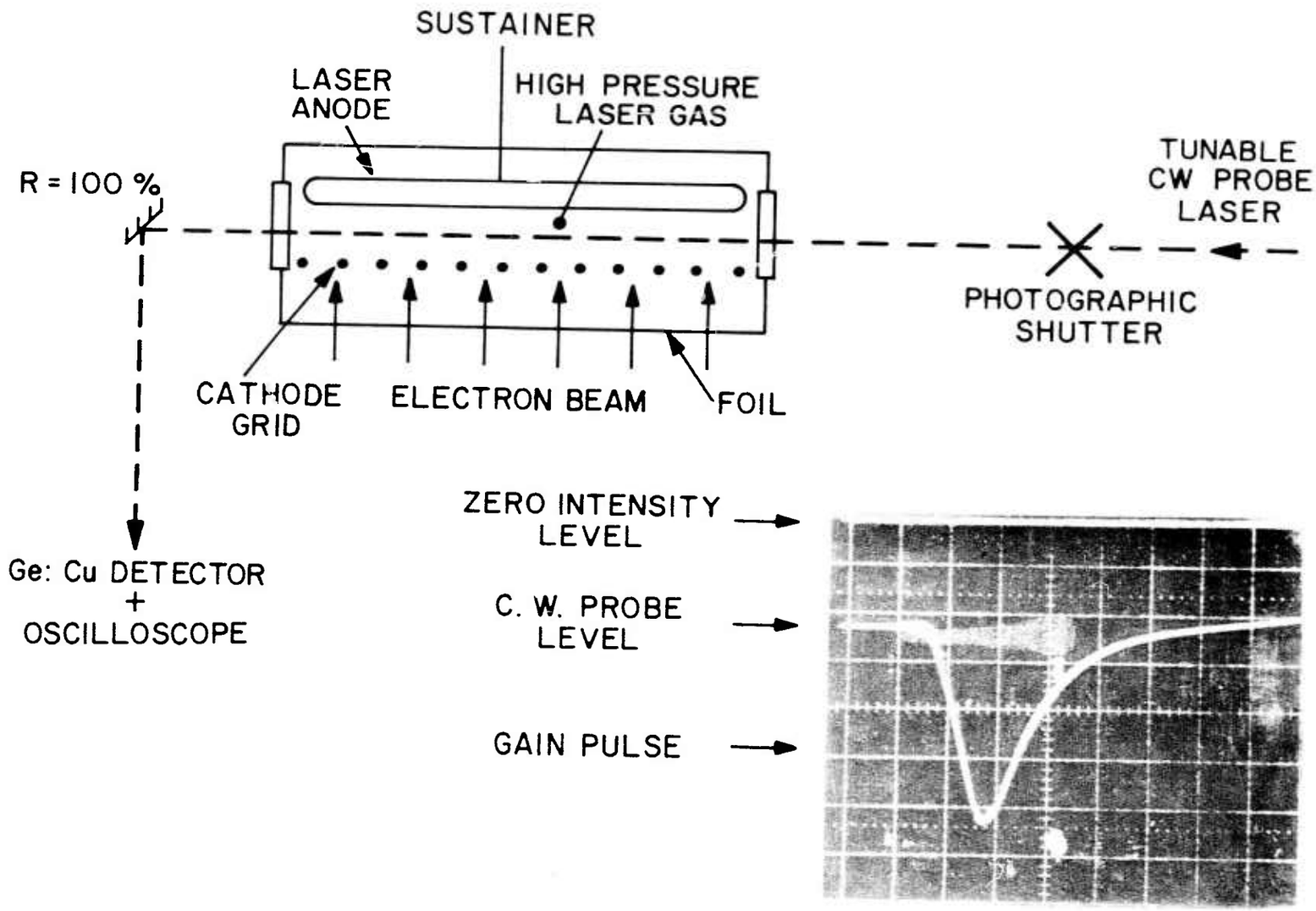

Fig. 11 — High pressure laser gain measurement setup. Inset: a typical gain result.

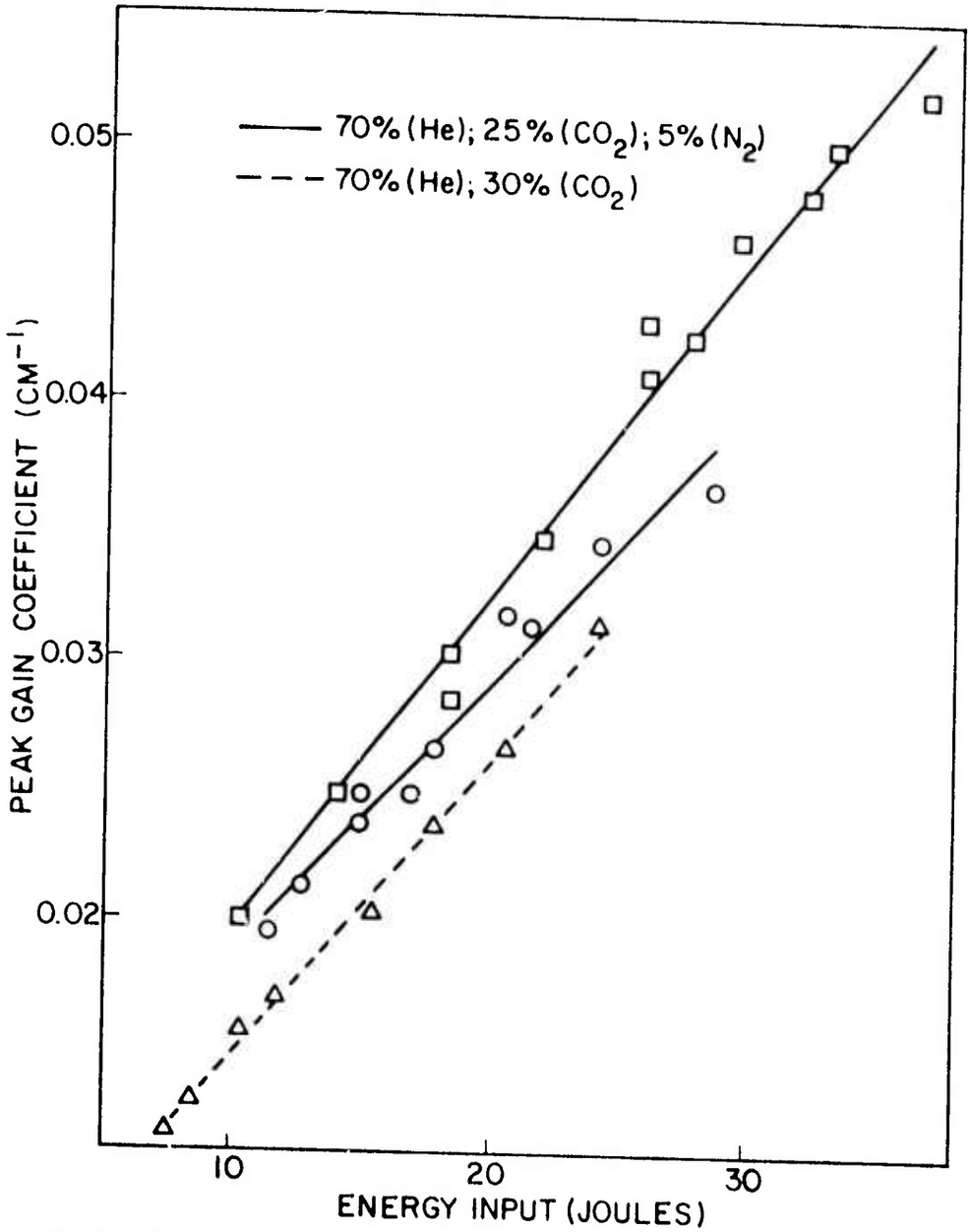

Fig. 12 — Gain characteristics of high pressure CO_2 laser for results taken on (0, Δ) the R(20) line of the 00°1-02°0 transition and on (□) the R(16) line of the 00°1-10°0 transition

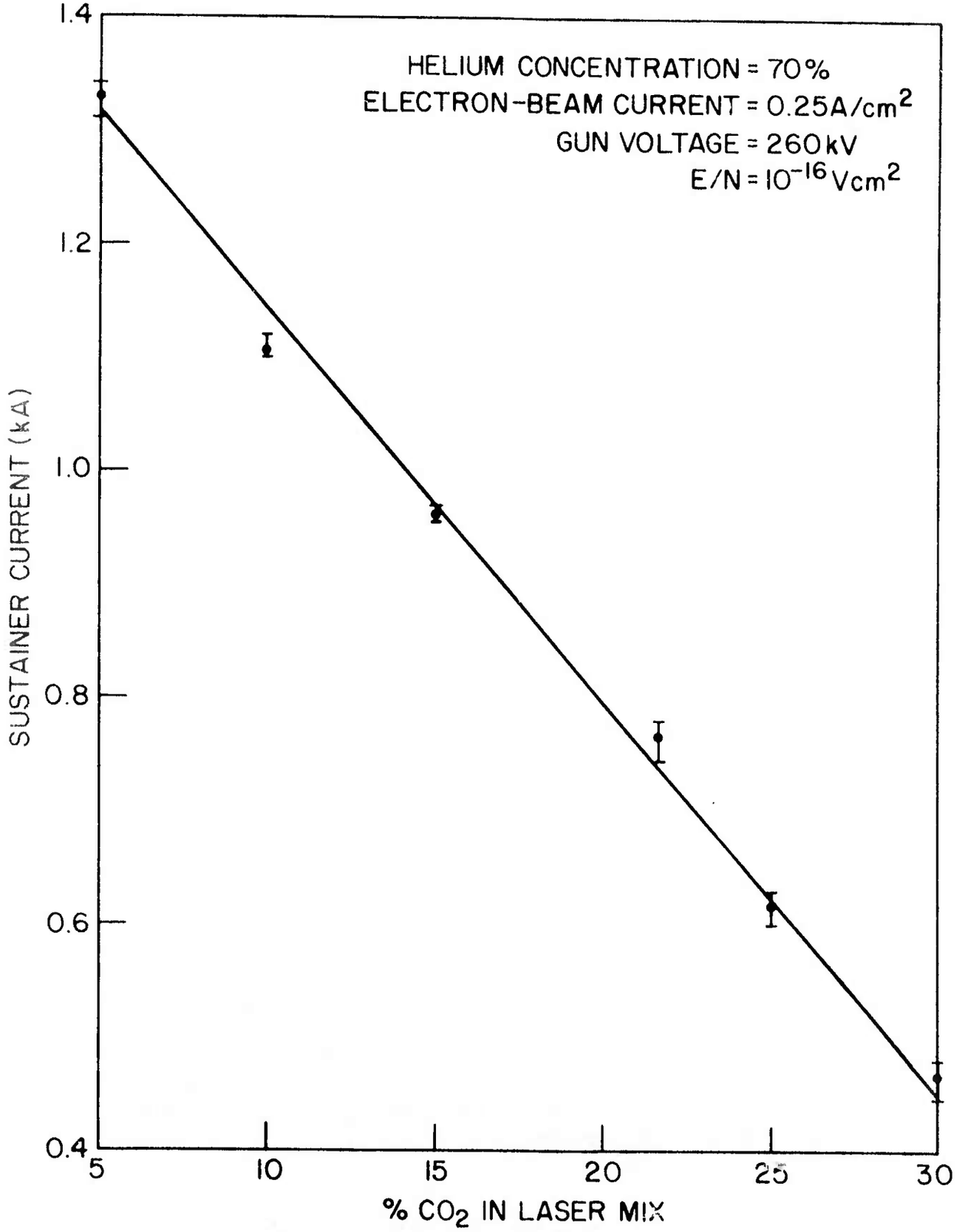

Fig. 13 — Sustainer current variation in high pressure CO_2 laser

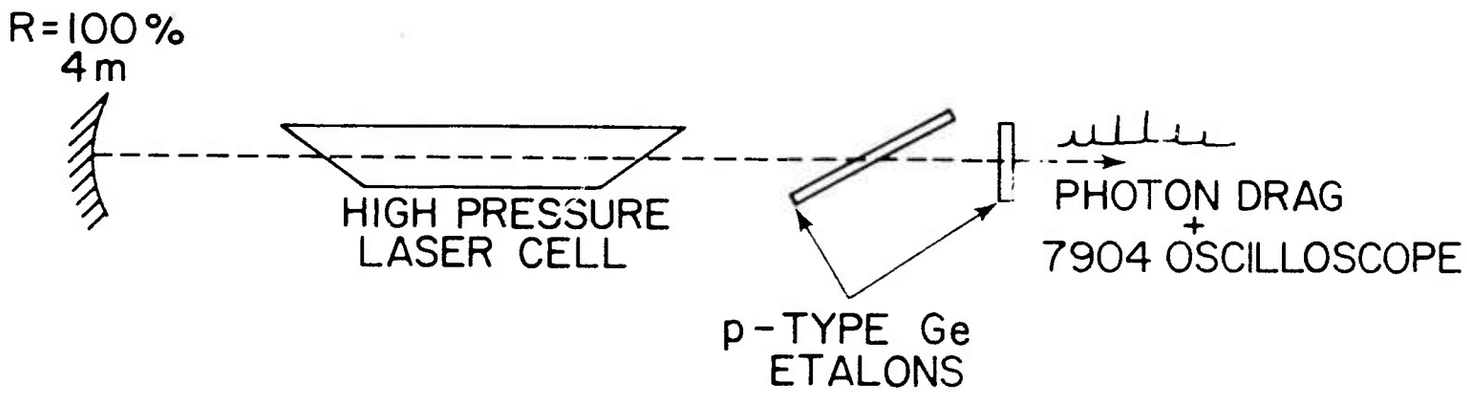

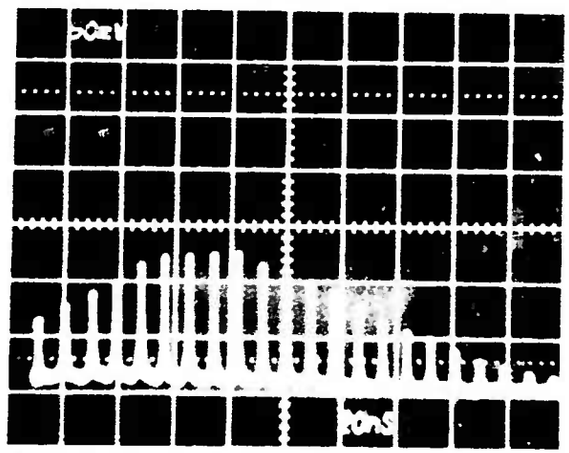

Fig. 14 — Cavity arrangement for mode-locking of high pressure CO_2 laser and typical mode-locked pulse train

2. ELECTRIC DISCHARGE GASDYNAMIC LASER (EDGDL)

A subatmospheric plenum EDGDL has been fabricated in order to study the D_2-HCl transfer laser system. A description of the apparatus is presented in reference 1. A picture of the assembled apparatus is shown in Figure 1 and a schematic is shown in Figure 2. The D_2 (diluted in either Ar or He) is vibrationally excited by an electric discharge in the subsonic plenum prior to undergoing supersonic expansion. HCl is injected part way through the nozzles with mixing and vibrational energy transfer continuing into the cavity region.

During this reporting period preliminary HCl fluorescence studies have been performed. Figure 3 is a trace of the total HCl fluorescence as monitored with a Ge:Au detector, as a function of position along the flow. The fluorescence can be seen to increase as the optics translate away from the exit plane of the nozzles. The fluorescence then levels off before decreasing near the end of the available window. To date the signals have been too weak to resolve the HCl spectra, however, filters have been used to identify the signal as 3.5 → 4.0 μ HCl fluorescence. HCl fluorescence has also been observed when the D_2 has been replaced by H_2. Attempts at producing a laser were unsuccessful.

Ref. 1. ARPA-NRL Laser Program Semiannual Technical Report 1 July 1973 - 21 December 1973, NRL Memorandum Report No. 2846.

Further studies to characterize the mixing, D_2 vibrational excitation in the discharge, and transfer to HCl will continue in order to optimize the HCl excitation. These experiments will be followed by the construction of a high Q cavity to investigate the lasing potential of this system.

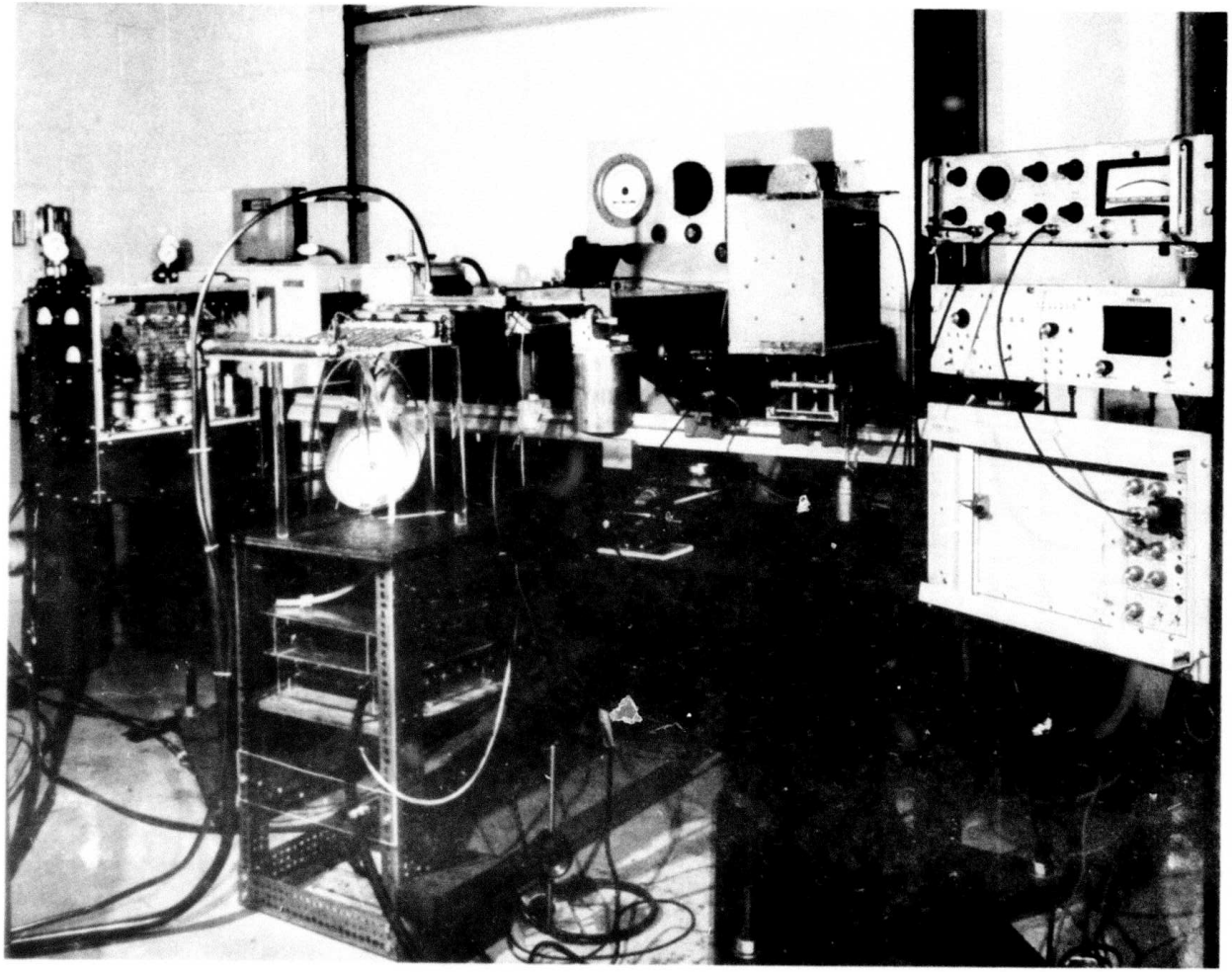

Fig. 1 — Assembled D_2-HCl transfer laser

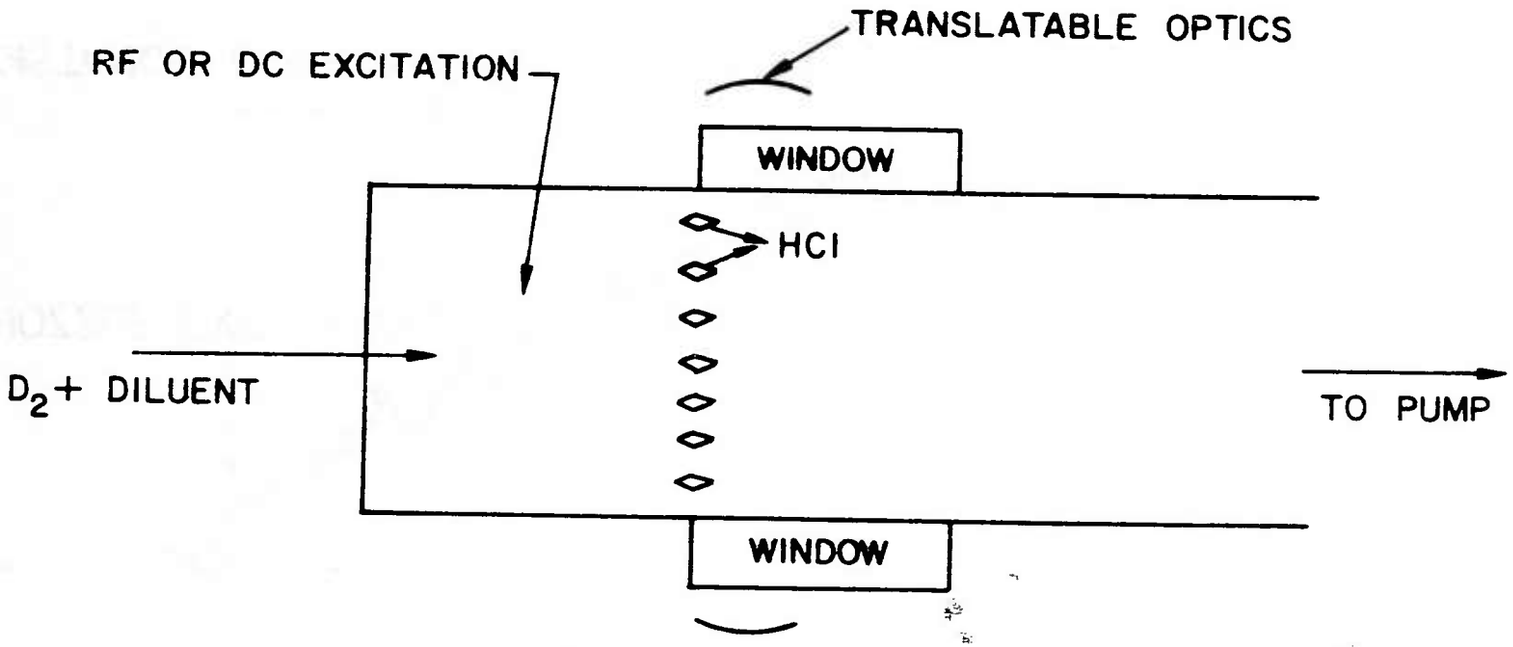

Fig. 2 — Schematic of EDGDL

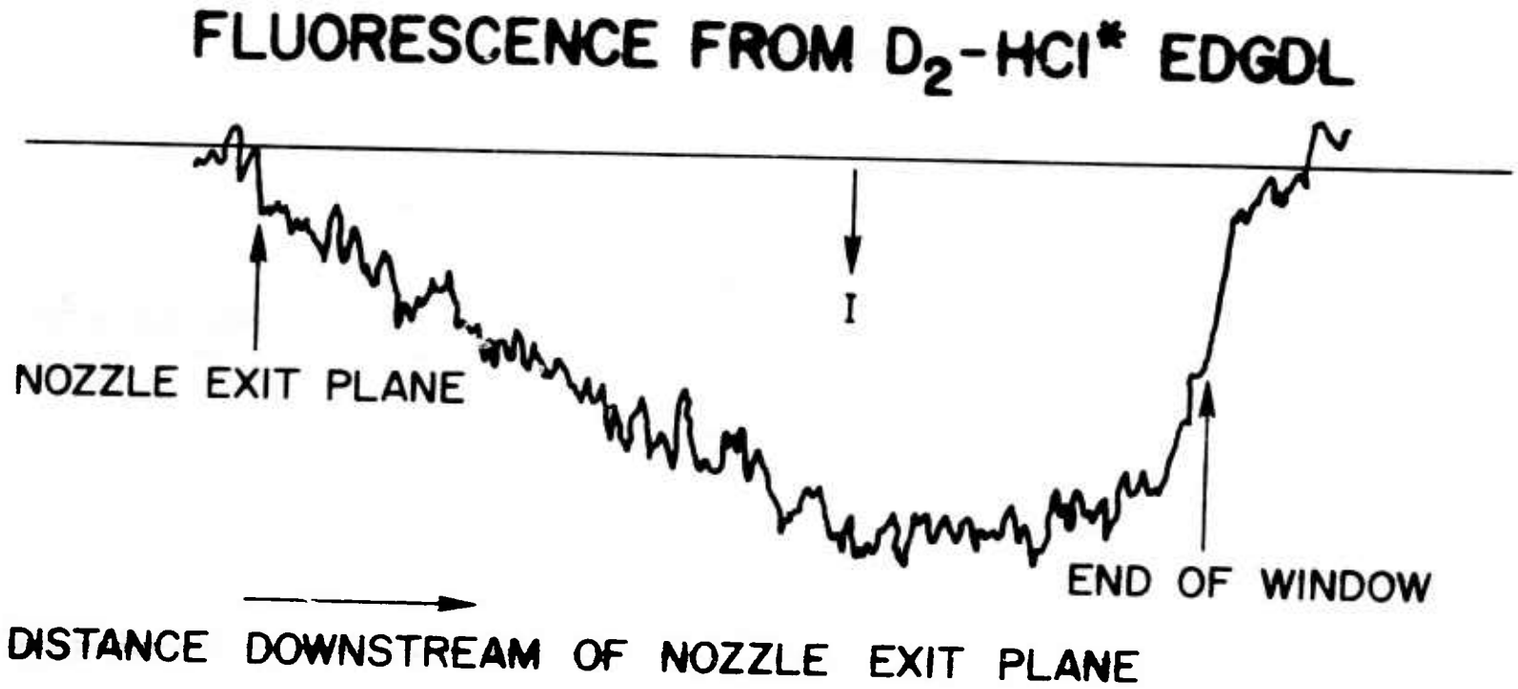

Fig. 3 — Trace of total HCl fluorescence as monitored with a Ge:Au detector

APPENDIX 1

Volume 11, number 1 OPTICS COMMUNICATIONS May 1974

RELIABLE HALF WAVE OPERATION OF A GaAs POCKELS CELL *

L.F. CHAMPAGNE, F. O'NEILL and W.T. WHITNEY
Naval Research Laboratory, Washington, D.C. 20375, USA

Received 15 February 1974

The design and operation of a GaAs Pockels cell suitable for reliable selection of a single nanosecond pulse from the output of a mode-locked atmospheric pressure CO_2 laser is described. Careful construction of the Pockels cell and use of a short (~ 13 nsec) high-voltage switching pulse permits reliable operation of the crystal at its half wave voltage (~ 15 kV).

GaAs Pockels cells have presiously been used in double pass [1] and transmission [2,3] arrangements to select single nanosecond pulses from the mode-locked pulse trains produced by high pressure CO_2 lasers. While the double pass configuration can in theory give high switching efficiency at a low operating voltage, it is not the optimum arrangement to use in practice because light can leak back into the laser resonator making it difficult to obtain reliable mode-locking. In addition the system is highly lossy due to absorption and diffraction after a double pass in the small aperture crystal. Previous work [2] with a single pass transmission arrangement has been restricted to a low operating voltage on the GaAs (1.2 kV/mm) with the result that the switching efficiency was low. This constraint was imposed to stay below the dc breakdown voltage of the crystal. It is expected however that the breakdown strength of the GaAs will be higher for short pulses because resistive heating of the crystal is reduced. Thus thermally induced runaway can be avoided. Hill et al. [4] have recently reported pulsing a GaAs Pockels cell to its half wave voltage but no details of the long-term operation of the device were given. In this paper we describe the design and operation of a GaAs Pockels cell which can be pulsed to its half wave voltage. The system has also been designed to minimize reflection of the voltage pulse applied to the Pockels cell, since the reflected pulse can return at a later time and produce secondary switching [5]. This can be a serious problem when the Pockels cell is used for selection of a single mode-locked pulse for amplification in a high-gain amplifier chain [5,6].

In the GaAs crystal used for the present experiments the electric field is applied perpendicular to a (110) plane with the laser beam propagating normal to a (110) plane. For this configuration the half wave retardation voltage is given by [7]

$$V_{\frac{1}{2}} = \frac{\lambda_0 d}{2n_0^3 r_{41} l},$$

where λ_0 is the vacuum wavelength of the laser, n_0 is the refractive index at the laser wavelength, r_{41} is the electrooptic coefficient, d is the thickness and l is the length of the crystal. The crystal dimensions are $8.6 \times 8.6 \times 50$ mm and using $\lambda_0 = 10.59\ \mu$m, $n_0 = 3.34$ [9] and $r_{41} = 1.6 \times 10^{-12}$ m/V [9] gives $V_{\frac{1}{2}} = 15.3$ kV. The crystal has a resistivity $\sim 2 \times 10^8\ \Omega$cm and was anti-reflection coated on both ends. The optical loss of the crystal (reflection and absorption losses) was measured to be ~ 13% using a cw CO_2 laser. Using this laser the extinction ratio of the crystal when placed between crossed polarizers was measured to be ~ 1300 : 1 indicating the GaAs was of good quality with low residual birefringence. The extinction ratio of the crossed polarizers alone was ~ 3500 : 1.

The pulse selection system consists of a pulse forming cable, a laser triggered spark gap (LTSG) and the GaAs Pockels cell. The LTSG and Pockels cell have been constructed to match the 30 Ω impedance of the high voltage co-axial cable used to connect them. The

* This work was supported by the Defense Advanced Research Projects Agency under RPA Order 2062.

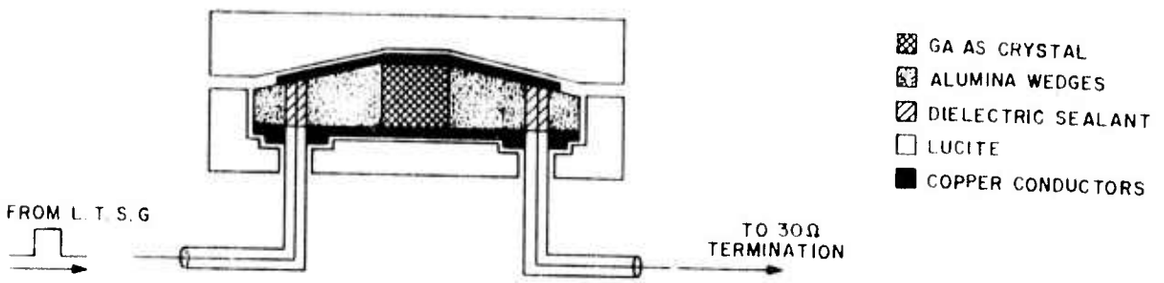

Fig. 1. Schematic showing constructional details of the GaAs Pockels cell.

LTSG is similar in construction to that described by Milam et al. [10]. The Pockels cell was constructed by placing the GaAs between two alumina wedges and the whole assembly (fig. 1) was held in a Lucite box taking care to avoid stressing the crystal. Stripline connections were made to the top and bottom of the crystal and the strips were tailored to achieve a smooth electrical transition through the Pockels cell. The output cable from the Pockels cell is terminated in a 30 Ω resistive load. The electrical characteristics of the complete system were observed using time domain reflectometry and in the final arrangement voltage reflections at the various components were ~ 10%. A calibrated voltage monitor was connected across the Pockels cell to facilitate synchronization of the applied high voltage pulse with an individual mode-locked laser pulse.

The switching system was tested using the arrangement shown in fig. 2. The output of an acousto-optically mode-locked [11], helical-pin, atmospheric-pressure CO_2 laser [12] was directly through the GaAs Pockels cell which was positioned between crossed, stacked germanium plate, Brewster angled polarizers. The output of the laser was a train of 1.2 nsec pulses with a total pulse train energy of 70 80 mJ and a peak pulse energy ~ 5 mJ. The laser operated in a clean TEM_{00} mode. A small portion (~ 15%) of the beam is used to trigger the LTSG by focusing it in the gas ~ 0.2 mm from the cathode of the device using a 25 mm focal length anti-reflection coated germanium lens. The LTSG and pulse forming cable were charged to 31 kV with the gap filled with nitrogen at a pressure of 140 psig. The electrode spacing was 0.75 mm. The beam intensity was carefully adjusted to trigger the LTSG at the peak of the laser pulse train and the triggering jitter was < 2 nsec. The length of the pulse forming cable was adjusted to give a 13 nsec high voltage pulse from the spark gap. The length of the cable connecting the LTSG and the Pockels cell was adjusted to synchronize the high voltage switching pulse with

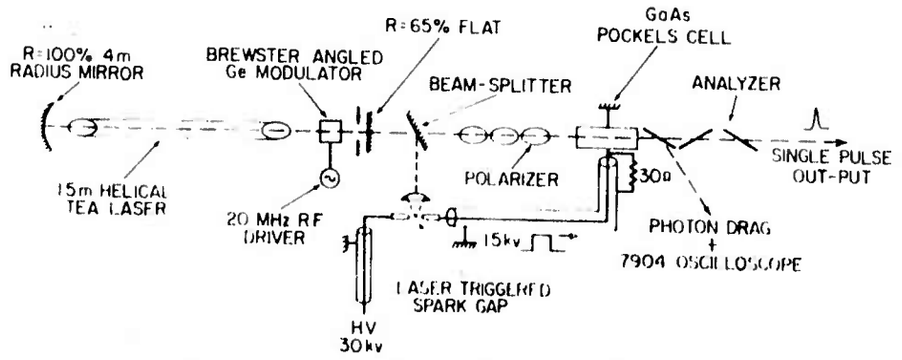

Fig. 2. Experimental arrangement used for testing the Pockels cell system.

12

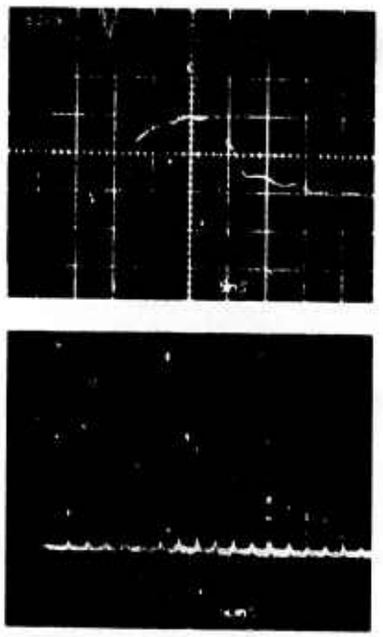

Fig. 3. Operation of Pockels cell. Upper trace: high-voltage switching pulse. Lower trace: mode-locked pulse train showing 100% switching of a single mode-locked pulse.

the arrival of a mode-locked laser pulse.

A typical voltage pulse as applied to the Pockels cell is shown in fig. 3 (upper). The switching efficiency of the system is observed by monitoring the laser beam rejected from the first plate of the analyzer stack (see fig. 2), using a fast risetime photon drag detector and a Tektronix 7904 oscilloscope. A typical recording using this system is shown in fig. 3 (lower). The missing pulse has had its plane of polarization rotated by 90° by the Pockels cell and has been transmitted by the analyzer stack. It can be seen that complete switching of the single mode-locked pulse has been achieved. The Pockels cell has been operated at its half-wave voltage for more than 10,000 shots without degradation.

In conclusion we have shown that GaAs Pockels cells can be used for reliable and efficient extraction of single pulses from the mode-locked pulse trains produced by high pressure CO_2 lasers. The system described in this paper routinely delivers pulses, with energy $\gtrsim 3$mJ, for driving a high gain CO_2 amplifier chain [6]. Due to the large aperture components used in the present set up the pulse spatial intensity profile is smooth and spherically symmetric. This is an important advantage of the present arrangement over those employing reflection analyzers [1,4]. With these systems the beam will contain interference fringes due to reflections at the parallel surfaces of the germanium plates.

The authors wish to thank Mr. Neville Harris for his many helpful suggestions. The technical work of Mr. J. Peele who designed and constructed the equipment is also acknowledged. We wish to thank Mr. D Shores for his assistance in some of the experiments.

References

[1] D.T. Davis, D.L. Smith and J.S. Koval, IEEE J. Quant. Electron. QE-8 (1972) 846.
[2] J.F. Figueira, W.H. Reichelt and S. Singer, Rev. Sci. Instrum. 44 (1973) 1481.
[3] F. Rheault, J.L. LaChambre, J. Gilbert, R. Fortin and M. Blanchard, Opt. Commun. 8 (1973) 132.
[4] G.A. Hill, D.J. James and S.A. Ramsden, Opt. Commun. 9 (1973) 237.
[5] E.E. Stark, Jr., W.H. Reichelt, G.F. Schappert and T.F. Stratton, Appl. Phys. Lett. 23 (1973) 322.
[6] L.F. Champagne, N.W. Harris, F. O'Neill and W.T. Whitney, Paper 22.2, Technical Digest, Internat. Electron Devices Meeting, Wash., D.C., Dec. 1973 and to be published.
[7] A. Yariv, Quantum Electronics (Wiley, New York, 1967), p. 313.
[8] A. Yariv, C.A. Mead and J.V. Parker, IEEE J. Quant. Electron. QE-2 (1966) 243.
[9] I.P. Kaminow, IEEE J. Quant. Electron. QE-4 (1968) 23.
[10] D. Milam, C.C. Gallagher, R.A. Bradbury and E.S. Bliss, Rev. Sci. Instrum. 43 (1972) 1482.
[11] O.R. Wood, R.L. Abrams and T.J. Bridges, Appl. Phys. Lett. 17 (1970) 376.
[12] R. Fortin, M. Gravel and R. Tremblay, Can. J. Phys. 49 (1971) 1783.

APPENDIX 2

Operation of a 15-atm electron-beam-controlled CO_2 laser

N. W. Harris, F. O'Neill, and W. T. Whitney

Laser Physics Branch, Optical Sciences Division, Naval Research Laboratory, Washington, D.C. 20375

(Received 2 May 1974)

We describe the operation of a 15-atm electron-beam-controlled CO_2 laser. Stable glow discharges have been sustained in the high-pressure $He:CO_2:N_2$ mixtures for 0.5 μsec using an electron-beam current of $\lesssim 1.5$ A/cm^2. A small-signal gain ~ 0.052 cm^{-1} has been measured in a 70:25(He):5(CO_2):5(N_2) mixture for an energy input to the gas ~ 115 J/l atm. We have obtained a laser output energy of 1.2 J from a volume of 22 cm^3 for an overall efficiency of 2.5%.

At present there is much interest in the operation of high-pressure molecular gas lasers because the broad bandwidth provided by the mutual overlapping of pressure-broadened rotational lines will permit continuous frequency tuning and picosecond pulse generation using infrared-emitting gases. The continuous tunability of these lasers is particularly attractive for infrared spectroscopy and for selective vibrational-rotational excitation of molecules as a first step in isotope separation experiments[1] or for studies on laser-induced chemical reactions.[2] By using various gases (e.g., HF, CO, CO_2, N_2O) it should be possible to obtain high-power tunable coherent radiation in the spectral range 2–17 μm. Many vibrational energy levels of molecules lie in this region. In addition, these molecular gas lasers potentially offer higher power levels than presently available from tunable infrared sources, viz., diode lasers, spin-flip Raman lasers, and frequency-mixing devices.

High-pressure CO_2 lasers have previously been operated using optical pumping[3] and by electron-beam[4,5] or uv[6] preionization of gas discharges. More recently Blanchard *et al.*[7] have reported the operation of a 6-atm double-discharge CO_2 laser. In addition high-pressure operation of a HF chemical laser[8] and an optically pumped N_2O laser[9] has recently been demonstrated. Highest gain has been achieved with atmospheric-pressure CO_2 lasers using electron-beam-controlled discharges.[10,11] In this paper we report on the extension of this technique to pressures ~ 15 atm. The present system differs considerably from the laser described in Ref. 5 where a short (~ 10 nsec) high-current (~ 20 A/cm^2) electron-beam pulse was used to preionize the laser gas. The main discharge energy was then supplied by a low-inductance high-voltage capacitor connected across the laser electrodes. In the present system the laser discharge is sustained in the $He:CO_2:N_2$ mixtures using a low-current ($\lesssim 1.5$ A/cm^2) long-pulse (~ 0.5 μsec) electron beam. The electron number density produced in the gas by the electron beam determines the laser discharge current supplied by a high-voltage sus-

Applied Physics Letters, Vol. 25, No. 3, 1 August 1974

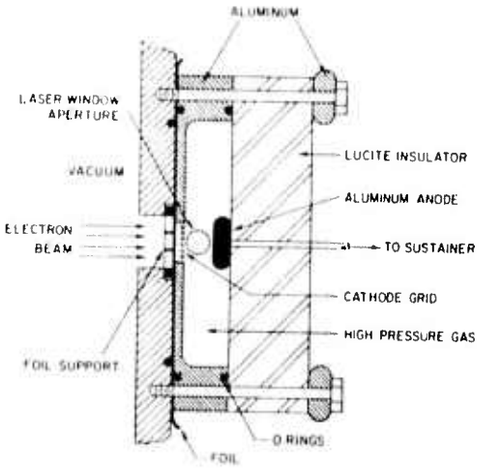

FIG. 1. Cross-sectional view of the high-pressure laser chamber.

tainer capacitor. The laser is characterized by simplicity of operation and high optical gain. Extremely reliable arc-free operation is obtained for pressures up to 15 atm. Higher-pressure performance has not been investigated since almost complete rotational line overlap is achieved for pressures ≥ 10 atm.[3,5,6]

A cross-sectional view of the laser chamber is shown in Fig. 1. The high-voltage electron beam generated by a variable-voltage variable-pulse-length cold-cathode gun enters the laser chamber through a 0.001-in.-thick titanium foil. The beam current, and therefore the laser discharge current, could be varied by changing either the gun's operating voltage or its internal cathode-anode separation. For the present experiments, the pulse length was fixed at 0.5 μsec. The titanium foil is supported by a perforated $\frac{1}{4}$-in.-thick stainless steel structure. The ionization produced by the electron beam controls a discharge between a smooth aluminum anode and a fine copper grid cathode placed 2 mm from the foil. The purpose of the grid is to protect the foil from possible arcs in the laser chamber.

The aluminum anode, which is connected to a 0.22-μF low-inductance sustainer capacitor, is supported by a 2-in.-thick Lucite insulator. The laser discharge volume is $1 \times 1.1 \times 20$ cm^3 and the ends of the laser chamber are sealed by 2-cm-thick Brewster-angled polycrystalline NaCl windows (clear aperture 1 cm) held in steel supports. The chamber withstood pressures up to 35 atm and no optical distortion was evident at the working pressure of 15 atm. The laser gas flowed through the chamber at a rate sufficient to renew the gas between shots. Electrical probes were used to monitor the sustainer voltage and current, to allow calculation of energy deposition in the laser gas.

Optimization of the laser was carried out by taking gain measurements using a low-power cw CO_2 laser. The gain signals were observed using a sensitive Ge:Cu detector system, with a measured rise time of 35 nsec and an exponential fall time of 170 nsec. A typical laser current pulse and corresponding gain recording are shown in Figs. 2(a) and 2(b). Measurements were taken at a pressure of 200 psig and an $E/N \sim 1.32 \times 10^{-16}$ V cm^2. This value of E/N is close to that required for optimum pumping of the 00°1 level of CO_2 and the strongly coupled levels of N_2.[12,13] Various gas mixtures were investigated ranging from 70% (He) 30% (CO_2) to 70% (He) 10% (CO_2): 20% (N_2). Arcing did not occur in any of these mixtures. The highest gain was measured for small added amounts of N_2 and the best mixture tested was 70% (He): 25% (CO_2): 5% (N_2) which is close to the optimum mixture for atmospheric-pressure electron-beam-controlled devices.[14] These comparison measurements were taken with the cw probe laser tuned to line center of the $R(20)$ line of the 00°1–02°0 CO_2 transition. The gain-versus-energy input results for the best mix are shown in Fig. 3 and, for comparison, results for 70% (He) 30% (CO_2) are also given. With all gas mixtures the gain increased linearly with time and peaked at the end of the current pulse. As expected the gain pulse decay time increased with N_2 concentration due to the energy transfer from the N_2 vibrational levels to the 00°1 level of CO_2.

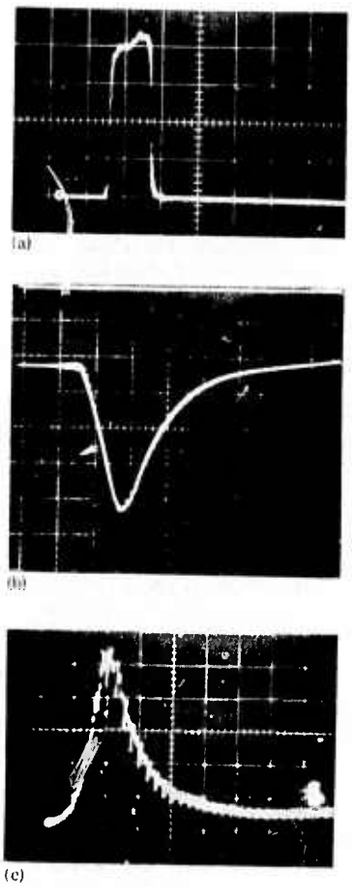

FIG. 2. Typical oscilloscope traces showing the operation of the laser system. (a) Laser current pulse; vertical: 330 A/div; horizontal: 0.5 μsec/div. (b) Gain pulse; 0.5 μsec/div. (c) Laser pulse; 20 nsec/div.

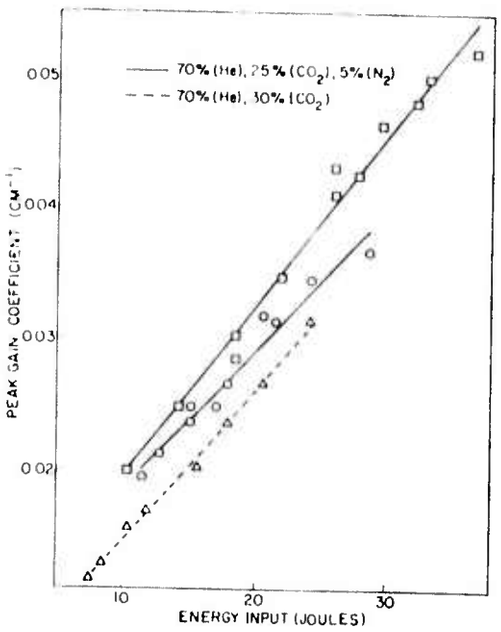

FIG. 3. Gain characteristics of CO_2 laser for results taken on (□, △) the $R(20)$ line of the 00°1-02°0 transition and on (○) the $R(16)$ line of the 00°1-10°0 transition.

Gain measurements have also been taken on various rotational lines of the 00°1-10°0 and 00°1-02°0 laser bands to determine the wavelength of maximum gain. Results were taken for the $R(20)$ and $P(20)$ lines of both bands and for the $R(16)$ line of the 00°1-10°0 band. Maximum gain was measured on the $R(16)$ line of the 00°1-10°0 transition and results for this line are shown in Fig. 3. This agrees with the results of Ref. 3 where the authors observed laser action on this line at high pressure, but differs from the observations of Ref. 6 where lasing occurred on the $R(20)$ line of the 00°1-02°0 band. The maximum gain coefficient measured was 0.052 cm^{-1} which was achieved for an energy input to the laser of 115 J/l atm and a gun current ~ 1.5 A/cm^2. The gain was still increasing linearly with energy at the highest input energy used. From Fig. 3 it is seen that a gain of 0.05 cm^{-1} is obtained for an energy input ~ 100 J/l atm. This is a significantly lower energy density than is required to obtain similar gain in atmospheric-pressure devices, the corresponding energy being ~ 150 – 200 J/l atm.[13,15,16] This lower energy requirement could be caused by gain enhancement due to rotational line overlap at high pressure.

The system was operated as a laser using a cavity consisting of a 100% reflectivity 4-m-radius mirror and a 50% reflectivity flat, both dielectric coated. A typical laser pulse, as detected using a photon drag detector and a Tektronix 7904 oscilloscope, is shown in Fig. 2(c). The laser emission occurred close to the peak of the gain pulse. Using the highest-gain mix and maximum available gun current, a multimode laser output of 0.875 J was obtained for an energy input of 35 J giving a laser efficiency of 2.5%. Using the same gun current, a larger sustainer current was obtained for a 70% (He):15% (CO_2):15% (N_2) mix, and an energy output of 1.2 J was obtained at an energy input of 47 J. The smaller sustainer current in the high-percentage CO_2 mixture is caused by the reduced electron number density due to the large attachment rate coefficient of CO_2.[17]

The laser oscillation wavelength was checked using an Optical Engineering spectrum analyzer. The fluorescent screen normally used for detection purposes in the instrument was replaced by a strip of developed unexposed Polaroid film. Burn marks on the film indicated the laser output wavelength. For these measurements, the dielectric-coated laser mirrors were replaced by a 7% gold mirror and an uncoated 3-mm-thick germanium etalon. Under these conditions the laser oscillated strongly in the vicinity of the $R(14)$, $R(16)$, and $R(18)$ lines of the 00°1-10°0 CO_2 transition, with strongest emission in the region of the $R(16)$ line. The laser oscillated at seven separate wavelengths corresponding to the resonances of the etalon output mirror, including a wavelength midway between the $R(16)$ and $R(18)$ rotational lines. This demonstrates the possibility of using narrow-gap Fabry-Perot interferometers, rather than diffraction gratings,[6] to obtain frequency tuning of the high-pressure laser.

In conclusion, we have demonstrated the operation of a high-gain high-efficiency electron-beam-controlled 15-atm CO_2 laser, and we have presented preliminary results on the effect of gas mix and energy input variation on the performance of the laser. A more complete investigation is at present being carried out and will be reported elsewhere. In addition we have clearly demonstrated the possibility of using Fabry-Perot interferometers as tuning elements in this type of laser.

The authors wish to thank L. F. Champagne for many helpful suggestions. They also acknowledge the technical assistance of J. Peele and D. Shores.

[1]R. V. Ambartsumyan, V. S. Letokhov, G. N. Makarov, and A. A. Puretskii, JETP Lett. 17, 63 (1973).
[2]N. V. Karlov, Appl. Opt. 13, 301 (1974).
[3]T. Y. Chang and O. R. Wood, Appl. Phys. Lett. 23, 370 (1973).
[4]N. G. Basov, V. A. Danilychev, O. M. Kerimov, and A. S. Podsosonnyi, JETP Lett. 17, 102 (1973).
[5]N. G. Basov, E. M. Belenov, V. V. Danilychev, O. M. Kerimov, I. B. Kovsh, A. S. Podsosonnyi, and V. F. Suchkov, Sov. Phys. JETP 37, 58 (1973).
[6]A. J. Alcock, K. Leopold, and M. C. Richardson, Appl. Phys. Lett. 23, 562 (1973).
[7]M. Blanchard, J. Gilbert, F. Rheault, J. L. Lachambre, B. Fortin, and R. Tremblay, J. Appl. Phys. 45, 1311 (1974).
[8]V. N. Bogratashvili, I. N. Knyazev, Uy. A. Kudev (olsev and V. S. Letokhov, JETP Lett. 18, 62 (1973).
[9]T. Y. Chang and O. R. Wood, Appl. Phys. Lett. 24, 182 (1974).
[10]C. A. Fenstermacher, M. J. Nutter, J. P. Rink, and K. Boyer, Bull. Am. Phys. Soc. 16, 49 (1971).
[11]J. D. Daugherty, E. R. Pugh, and D. J. Douglas-Hamilton, Paper T1, 24th Annual Gaseous Electronics Conference, Gainsville, Florida, 1971 (unpublished).
[12]J. J. Lowke, A. V. Phelps, and B. W. Irwin, J. Appl. Phys. 44, 4664 (1973).

[13]H. G. Ahlstrom, A. L. Pindroh, J. Holzrichter, T. Kan, G. Inglesakis, A. C. Kolb, and H. J. Jansen, IEEE J. Quantum Electron. QE-10, 26 (1974).
[14]C. A. Fenstermacher, M. J. Nuller, W. T. Leland, and K. Boyer, Appl. Phys. Lett. 20, 56 (1972).
[15]L. F. Champagne, N. W. Harris, F. O'Neill, and W. T. Whitney, Paper 22.2, Technical Digest, IEEE International Electron Devices Meeting, Washington, D. C., 1973 (unpublished).
[16]J. P. Rink, In Ref. 15, Paper 22.3.
[17]W. L. Nighan and W. J. Wiegand, Phys. Rev. (to be published).

ELECTRONIC STATE LASERS

1. ELECTRON BEAM INITIATED VISIBLE TRANSITION LASERS

ABSTRACT

The Ar-N_2 laser, which was discovered during the previous reporting period, has been more fully investigated. Laser peak powers of nearly 200 kW have been obtained on the N_2(C-B) transition at 357.7 nm. A computer code has been used to quantitatively predict the concentrations of the upper and lower laser levels. Comparison between the N_2(C-B) fluorescence measurements and the computer predictions show excellent agreement.

The inorganic halide new laser project has also received attention. A number of experimental difficulties arose and are discussed in the experimental section.

INTRODUCTION

Laser emission depends on the excitation of atoms or molecules to a specific energy level. In the present project, a powerful relativistic electron beam (e-beam) was used to excite rare gas-additive mixtures. The high velocity electrons, 86% of the speed of light, primarily cause ionization of the gaseous species. The challenge is to use the rare gas ions and the following rare gas collision processes for laser pumping. By

1. $\vec{e} + R \rightarrow R^+ + \vec{e} + e$

2. $R^+ + 2R \rightarrow R_2^+ + R$

3. $R_2^+ + e \rightarrow R^* + R$

4. $R^* + 2R \rightarrow R_2^* + R$

5. $R_2^* \rightarrow 2R + h\nu$

controlling the partial pressures of R and A (additive) separately, one can choose the species which will interact with the A and thereby effect an inversion in the electronic levels of A. As indicated in steps 1 - 5, R^+, R_2^+, R^*, R_2^* or $h\nu$ can be used to transfer energy to A.

Let us consider three examples. Collins et al[1] have studied the resonant charge transfer step (6).

6. $He_2^+ + N_2 \rightarrow N_2^+(B) + 2He.$

Resonant charge transfer theory predicts the selective excitation of N_2 to the $N_2^+(B)$ state. To achieve significant optical gain via step (6), one must adjust the concentrations of He and N_2 such that rate (2) > rate (7) and rate (6) < rate (3) where R represents He and A represents N_2.

7. $He^+ + N_2 \rightarrow$ products.

Experimentally optical gain was measured by Collins to be

0.05 cm^{-1} on the (0,1) vibrational component of the $B\ ^2\Sigma_u^+ \rightarrow X\ ^2\Sigma_g^+$ transition at 427.8 nm. The partial pressures of He and N_2 were 2280 and 0.8 torr respectively.

A second example of specific excitation involves the photolysis of N_2O by the radiation emitted by Ar_2^*. The absorption step is indicated in step (8).

$$8. \quad h\nu + N_2O \rightarrow O(^1S) + N_2 \quad .$$

The quadrupole transition given by step (9)

$$9. \quad O(^1S) \rightarrow O(^1D) + h\nu = 557.7 \text{ nm}$$

is expected to show significant optical gain. In this scheme it is important that rates (2) - (5) be faster than any competing process with N_2O. In this example R represents Ar and A represents N_2O. This implies very high pressures of Ar and relatively low pressures of N_2O. Murray et al[2] have observed a high level of $O(^1S)$ emission from e-beam excited mixtures containing Ar at 23 ktorr - 68 ktorr and N_2O at 0.1 - 10 torr.

We have seen examples of energy transfer to an additive by charge transfer and by photolysis. In the present work argon metastable species were used to transfer their energy to N_2 as shown in step (10).

10. $Ar^* + N_2 \rightarrow N_2(C) + Ar$

11. $N_2(C) \rightarrow N_2(B) + h\nu = 357.7$ nm.

Laser emission was detected on the second positive transition, step (11). The relevant energy levels of both N_2 and Ar are shown in Figure 1. Both the Ar-N_2 laser and a theoretical model were developed during the current reporting period. A published paper on this subject is included in the appendix.

EXPERIMENTAL

A. Optics

Figure 2 illustrates the optics, laser cell, and e-beam device. Initial experiments were performed with a low loss optical cavity consisting of a > 99.7% reflectance dielectric mirror and a partially transmitting dielectric mirror. The transmission of the latter was 10% at 357.7 nm and 36% at 380.5 nm. Quartz Brewster angle windows attached to holders with a 0.67 cm diameter bore were used. Further work was carried out with normal incidence windows spaced 31.9 cm apart. The windows had a useful diameter of 1.27 cm. In most of the shots with the normal incidence windows, a single > 99.7% R mirror was used.

B. Laser Cell

The stainless steel laser cell had an internal dimension of 1.27 cm along the direction of the e-beam. The e-beam

entered the cell through a 25 μ thick titanium foil supported by a 0.67 cm thick steel plate with fourteen 0.95 cm diameter holes in a linear array over 15.4 cm. The maximum beam width as defined by the 0.95 cm diameter holes compares to the internal cell width of 1.27 cm.

C. Calorimetry

The e-beam energy delivered to the laser cell and deposited in the gaseous mixtures is an important parameter. This parameter determines the efficiency of an e-beam pumped laser. It can also be used, in conjunction with absolute fluorescence measurements, to obtain an estimate of a specific reaction rate constant such as the one for step (10). Consequently, the energy deposition problem was examined closely. Two different approaches were taken. In the first, a calorimeter was used to measure the e-beam energy at the titanium foil entrance window of the laser cell. The deposited energy can be calculated from the known stopping powers of the gases[3] and the depth of the cell, 1.27 cm. This technique should be valid for the thin gas targets where e-beam scattering by the gas does not increase the high energy electron path length nor decrease the high energy electron velocity sufficiently to increase the stopping power.

Previously the e-beam energy was determined to be 36 ± 6 J. This measurement was made with a carbon block

calorimeter 1 x 1 x 15.4 cm^3. The measurement was repeated with an aluminum calorimeter 1 x .079 x 15.4 cm^3. Great care was taken to insure that the iron-constantan thermocouple was in good contact with the calorimeter; that a low inductance return path existed; and that the calorimeter was sufficiently adiabatic. The sensitivity of the calorimeter was 62 J per mV. By coincidence the new measurements exactly reproduced the old measurements, 36 $\pm$ 6 J.

D. Scattering

After this verification, the electron beam scattering was investigated. One atmosphere of lab air was the scattering medium. The electron beam spatial distribution was observed by photographic detection of the induced fluorescence. The laser cell was replaced by a folded piece of stainless steel sheet metal whose back wall was 1.90 cm from the e-beam entrance window. An open end and a wide top slot allowed the e-beam induced fluorescence to be photographed. A Graphex camera with Polaroid type 57 film or Royal X Pan film was used to record the fluorescence at f16-f32. A Joyce, Loebl and Co. microdensitometer MK-IIIC was employed to generate the traces shown in Figure 3. Two things are apparent from these traces. One is that the beam is quite uniform across the 14 - 0.95 cm diameter holes in the foil support plate. The other is that the beam

divergence due to scattering or other phenomena is not a serious problem at one atmosphere. The conclusion is that the method of calculating the e-beam energy deposition with the assumption of no scattering is quite acceptable.

E. Chemical Dosimetry

Although the technique described above was found to be satisfactory, it was decided to verify it by chemical dosimetry. In chemical dosimetry, the stable and product yield from the e-beam excitation of a gas is measured. The most common dosimeter utilizes N_2O as the target gas. After the e-beam excitation of the N_2O gas, the N_2O is condensed out at liquid nitrogen temperature. The remaining gas is mostly N_2. From a knowledge of the pressure and the volume, one can readily calculate the N_2 yield. This yield is related to the deposited e-beam energy in tables compiled by NBS[4]. The yield is expressed in g-units or the number of product molecules formed per 100 eV absorbed. The g value for N_2 from N_2O is 12.4 at high dose rates and N_2O pressures from about 400 - 2000 torr.

After purification, N_2O samples were irradiated over a wide pressure range. g-values were calculated from the measured N_2 yield and the absorbed energy determined from the calorimetric method. These results are presented in Figure 4. There is a discrepancy of approximately a factor

of five between the present results and the 12.4 g-value. This suggests that the calorimetric technique underestimated the absorbed e-beam energy by a factor of five.

Such a large factor could be caused by energy deposition from low energy electrons backscattered from the laser cell walls. Since this effect depends on the atomic number of the wall material[5], an aluminum liner (Z=13) and a lead liner (Z=82) were inserted into the cell. The chemical dosimetry measurements were repeated. However $g(N_2)$ was not affected. Thus backscattered electrons were not identified as a major problem although the number of backscattered electrons is expected to be significant[5].

It is apparent that an accurate determination of the energy deposited by an e-beam in a gas is difficult to carry out. The difficulty stems from the number of ways in which energy can be deposited in the gas. Simple absorption of the e-beam, scattering, and back-scattered electrons have been considered here. Other possibilities include the return current electrons and the energy (velocity) distribution of the e-beam.

In the original work with chemical dosimetry[6] on high dose rate devices, i.e. pulsed e-beam machines, extensive calorimetric measurements were made. Both the thickness and the position of the calorimeter were varied. The dosimetry

technique therefore should provide a better estimate of the absorbed e-beam energy.

F. Gas Handling System

An all metal bakeable gas handling system was used in the present experiments. A four inch diffusion pump allowed evacuation to 10^{-6} torr. Pressures up to 21 ktorr (400 psig) have been handled in the system. Gaseous mixtures were prepared by filling a one liter tank with the additive gas. The high pressure rare gas was suddenly admitted to the one liter tank where turbulent mixing occurred. This mixing was promoted by admitting the high pressure gas to a pipe which ran the length of the inside of the tank and which contained 30 - .079 diameter injection orifices. The mixed gas was then transferred to the laser cell from the one liter tank. Variations in the mixing time from 5 minutes to 2 days did not affect any of the results.

G. Heated Cell System

It is necessary to have a heated cell for the planned metal halide laser experiments. The vapor pressure of metal halides such as copper, mercury, and thallium become appreciable, 1 - 10 torr, only at temperatures above 700°K. The existing laser cell was designed to be compatible with that requirement. In order to test the heated cell, however, a number of changes were made. The quartz windows were replaced by sapphire windows sealed to a Kovar fitting. The fitting

was welded to a flange which was attached to the laser cell. The welding proved to be difficult. In the first attempts cracking occurred in the Kovar sleeve in the vicinity of the weld. After some experimentation with the welding configurations, the problem was solved.

Four 500 W Firerod heaters were inserted into the laser cell body. An oven was then constructed around the cell. The cell was next heated to the design temperature and allowed to cool back to room temperature. The following problem areas were noted. The windows were too cool. The attempted solution was to place a heavy copper sleeve between the cell body and the windows to improve heat conduction. Also a better oven was constructed. The oven is shown in Figure 5. A test of this arrangement indicated that it would be necessary to heat the windows directly.

These tests also showed that the e-beam cathode and prepulse hold-off plate reached excessive temperatures which caused the hold-off plate to melt. This difficulty was rectified by replacing the plexiglas plate with a Teflon plate and by redesigning the cathode and cathode holder to reduce heat conduction to the plate.

Finally a salt (metal halide) reservoir was fabricated. The reservoir has two features. Its temperature can be controlled independently. The added rare gas can be flowed directly over the surface of the salt to facilitate mixing.

With the apparatus illustrated in Figure 5, a limited number of test shots were carried out with mixtures of TlI and Ar. Emission was observed from the sought after species, the $Tl7^2S$ state, on both the 377.5 and 535.0 nm transitions. At the end of the experiment, a coating of TlI was found to cover the sapphire windows.

Overall, substantial progress has been made to build an apparatus for metal halide vapor research at temperatures above 700^oK. Heating the windows directly will allow this program to begin laser oriented experiments.

RESULTS AND DISCUSSION

A. Low Power Ar-N_2 Laser

The Ar-N_2 laser discovered during the previous reporting period was developed in the current period. Our findings were recently published[7]. A copy of the manuscript is included in the appendix. In this section the manuscript is summarized and additional comments are added to clarify certain points. Laser emission was proven to occur. Figure 6 reproduces a fluorescence spectrum and a laser spectrum. Laser performance as a function of pressure and mixture composition was described in the paper.

A theoretical kinetic model was setup to predict temporally the concentrations of the upper and lower laser levels. The model data is listed in Table 1. A sample of the computer output is presented in Figure 7. Comparison

between the model predictions and the fluorescence from the upper laser level, $N_2(C)$ is given in Figures 8 and 9. The agreement is quite good. The ramifications of the comparison have real significance. First the major laser pumping route was identified to be step A4 rather than step A9. The former was tentatively predicted from our earlier results while the latter was emphasized in the abstract of Hill et al[8] for the VIII IEEE meeting. The importance of the choice of the pumping step is that step A9 predicts a high nonlinear increase in pumping with a more intense e-beam while step A4 predicts only a linear behavior. All of this dramatically affects scaling of the laser to higher peak powers. Since both the model and the measurements were done on an absolute basis, a relative rate constant for step A4 could be obtained. The value was found to be $^{13-}_{70\%}$ of the value for step A5. This strongly disagrees with the only prior absolute measurement, 0.4%, which is cited in Table 1. According to E.C. Zipf (private communication), his value of 0.4% may have a substantial uncertainty because of the complexity of his experiment. A more detailed comparison on rate constant k A4 values are contained in Table II. The other two values in Table II are limits obtained from observations of both $N_2(C)$ and $N_2(B)$ emission. In the future we plan to monitor the $N_2(B)$ emission in order to better

understand both the laser emission and the fundamental collision processes.

B. High Power Ar-N_2 Laser

A report on the discovery of the Ar-N_2 laser at NRL prompted several groups to investigate this new laser. While the NRL work was in progress, M. Bhaumik (private communication) observed some very high power laser pulses from e-beam excited Ar-N_2 mixtures. Subsequently an anomaly in the optical cavity design was found in the present work. The anomaly was that the replacement of the Brewster angle windows by normal incidence windows substantially increased the laser output. The effect was reproducible and was not affected by rotating both Brewster angle window holders by 90^{o}. Since the effect is not expected to be a general one, its causes were not examined experimentally.

Further experiments were performed with the normal incidence windows. Two 0.67 diameter apertures placed next to the windows were removed. These apertures were essential to make a meaningful comparion between the intensity of the laser emission with the Brewster angle windows which were held by a holder with a 0.67 diameter bore opening. Removal of the stops provided windows with an effective diameter of 1.27 diameter. In general only one laser mirror was used. Superfluorescent emission occurred with or without

the single mirror. However, the highest output was observed for the single mirror cavity relative to no mirrors or to the pair of mirrors used in conjunction in the Brewster angle windows. This is shown in Fig. 10.

An overview of the experimental results is given in Fig. 11. Laser action was observed from 600 - 5000 torr in a 5% N_2-Ar mixture. Laser peak power was determined with a calibrated neutral density filter and photodiode combination. Figure 11 illustrates a typical set of traces with the scope voltage converted to absolute units. Also shown on this figure is the laser output with the single mirror blocked. Laser energy was determined from the integrated signal.

Laser emission at 600 torr commenced just before the time at which the fluorescence peaked, i.e. the maximum pumping rate. As the total pressure was increased, laser emission occurred earlier. At 5000 torr, the laser peak was reached after a delay of only 2 ns. The FWHM was 5 ns. A similar temporal behavior was noted for the low power Ar-N_2 laser.

Let us now consider the efficiency of the laser. Figure 11 shows that the highest efficiency is achieved at 1000 torr since the e-beam input rises linearly with pressure. At higher pressures, the laser energy and efficiency decrease

because the pulse width narrowed faster than the amplitude increased. The decrease in efficiency, however, would be partially offset if only the e-beam energy deposited prior to the laser termination time was used to calculate the efficiency. From the two energy deposition calculation methods, the efficiency was calculated to be in the range 0.08 - 0.4%. In any event, it is more than a factor of two higher than previously reported for an e-beam pumped N_2 laser[9]. Experiments were also carried out at 2.5% and 7.5% N_2-Ar. Laser performance indicated that 5% N_2-Ar was the best laser mixture.

Ault et al[10] have also reported laser emission from e-beam pumped Ar-N_2 mixtures. They obtained an efficiency of 0.2% from a 4760 torr Ar-400 torr N_2 mixture. Their peak power was 0.5 MW. Thus experimentally there is some agreement in the Ar-N_2 laser system.

Two additional parameters were explored with the high power Ar-N_2 laser. First the laser gain near threshold at 1500 torr was deduced from a trace of the laser emission taken at 2 ns/div with a Tektronix 7904 scope. The signal was plotted in arbitrary units on a log scale. See Figure 12. The abscissa is a distance scale derived from the speed of light, the length of the e-beam excited volume, and the mirror separation distance. The initial gain was ascertained

to be 0.22 cm^{-1}. It was felt that assignment of values for a small signal gain coefficient and saturation parameter was inappropriate since the rates are so removed from steady state equilibrium. In other words these parameters are rapidly changing functions with time.

Secondly, the high resolution laser spectrum was taken in the 5th order of a 3/4 m Jarrell-Ash spectrometer. The Ar-N_2 laser operates at pressures up to around 200 times the conventional nitrogen laser. It was of interest therefore to see if the spectra on the 357.7 nm band were similar. Figure 13 presents the spectrum of the high power Ar-N_2 laser taken with Polaroid type 57 film. The laser emission was attenuated by passing the beam through a short focal length lens and a ND2 filter. Hg lines were used in the wavelength calibration. The nearest of these lines, 253.7 nm in 7th order, is shown in Figure 13. While the spectrum does not resolve individual lines, the bandpass of the laser is $\leq$ 0.05 nm. Kaslin et al[11] ascertained that the conventional laser emits strongly from about 357.6112 - 357.6613 nm.

In summary, a theoretical model of the events in e-beam excited Ar-N_2 was completed. The Ar-N_2 laser was developed to a peak power of about 200 kW. Future work on the Ar-N_2 system centers around monitoring the lower laser level $N_2(B)$

emission. This is challenging because of its long lifetime and the poor detectivity for radiation in the 0.8 - 1.0 μ region.

The metal halide planned experiments will begin soon now that the heating problems are largely solved.

REFERENCES

1. C.B. Collins, A.J. Cunningham, S.M. Curry, B.W. Johnson and M. Stockton, Appl. Phys. Lett. 24, 477 (1974).
2. J.R. Murray, H.T. Powell and C.K. Rhodes, VIII Inter. Quant. Elec. Conf., San Francisco, June 1974, post-deadline paper.
3. M.J. Berger and S.M. Seltzer, Tables of Energy Losses and Ranges of Electrons and Positions, NASA SP 3012 (1964).
4. G.R.A. Johnson, Radiation Chemistry of Nitrous Oxide Gas, NSRDS-NBS 45 (1973).
5. R.W. Dressel, Phys. Rev. 144, 332 and 344 (1966).
6. C. Willis, O.A. Miller, A.E. Rothwell and A.W. Boyd, Adv. Chem. Ser. 81, 539 (1968) and C. Willis, A.W. Boyd, and D.A. Armstrong, Can. J. Chem. 47, 3783 (1969).
7. S.K. Searles and G.A. Hart, Appl. Phys. Lett. 25, 79 (1974).
8. R.M. Hill, D.J. Eckstrom, R.A. Gutcheck, D.L. Huestis, D.C. Lorents, D. Mukherjee and H.H. Nakano, VIII Inter. Quan. Elec. Conf., San Francisco (June 1974).

9. E.L. Patterson, J.D. Gerardo, and A. Wayne Johnson, Appl. Phys. Lett. 21, 293 (1972).

10. E.R. Ault, M.L. Bhaumik, and N.T. Olson, J. Quan. Electr. QE-10, 624 (1974).

11. V.M. Kaslin and G.G. Petrash, JETP Lett. 3, 55 (1966).

TABLE I. KINETIC DATA FOR THE Ar N_2 COMPUTER CODE

A. STEPS FOR $N_2(C)$ PRODUCTION AND LOSS

STEP		k^a	REFERENCE
1.	$Ar^+ + 2\,Ar \rightarrow Ar_2^+ + Ar$	2.5×10^{-31}	b
2.	$Ar_2^+ + e \rightarrow Ar^* + Ar$	7×10^{-7}	c
3.	$Ar^* + 2Ar \rightarrow Ar_2^* + Ar$	6×10^{-33}	d
4.	$Ar^* + N_2 \rightarrow N_2(C) + Ar$	1.2×10^{-13}	e
5.	$Ar^* + N_2 \rightarrow N_2^f + Ar$	3×10^{-11} g	d
6.	$N_2(C) + Ar \rightarrow N_2^f + Ar$	3×10^{-13}	h
7.	$N_2(C) \rightarrow N_2(B) + h\nu$	2.5×10^{7}	i
8.	$N_2(C) + N_2 \rightarrow 2N_2$	1.15×10^{-11}	j
9.	$2N_2(A) \rightarrow N_2(C) + N_2$	2.6×10^{-10}	k
10.	$2N_2(A) \rightarrow N_2(B) + N_2$	1.1×10^{-9}	k

B. ADDITIONAL STEPS FOR $N_2(B)$ PRODUCTION AND LOSS

11.	$Ar^* + N_2 \rightarrow N_2(B) + Ar$	n.d.	
12.	$Ar_2^* + N_2 \rightarrow N_2(B) + 2Ar$	1×10^{-11}	l
13.	$Ar_2^* \rightarrow 2Ar + h\nu$	1×10^{8}	m
14.	$N_2(B) + Ar \rightarrow N_2(A) + Ar$	1.6×10^{-12}	n
15.	$N_2(B) \rightarrow N_2(A) + h\nu$	1.2×10^{5}	o
16.	$N_2(B, v=1) + N_2 \rightarrow 2N_2$	2.25×10^{-12}	q

a. Radiative units, sec^{-1}; two-body units, cm^3/sec; and three-body units, cm^6/sec.
b. E.W. McDaniel, V. Cermak, A. Dalgarno, E.E. Ferguson, L. Friedman, Ion-Molecule Reactions (Wiley-Interscience, New York, 1970), p. 338.
c. J.N. Bardsley and M.A. Biondi, in Advances in Atomic and Molecular Physics (Academic, New York, 1970), Chap. 1.
d. J. LeCalvé and M. Bourène, J. Chem. Phys. 58, 1446 (1973).
e. R.A. Gutcheck and E.C. Zipf, Bull. Am. Phys. Soc. 17, 395 (1972).
f. N_2 electronic state distribution incompletely determined.
g. Total k for disappearance of Ar^*.
h. D.W. Setser, D.H. Stedman and J.A. Coxon, J. Chem. Phys. 53, 1004 (1970).
i. A.W. Johnson and R.G. Fowler, J. Chem. Phys. 53, 65 (1970).
j. P. Millet, Y. Salamero, H. Brunet, J. Galy, D. Blanc, and J.L. Teyssier, J. Chem. Phys. 58, 5539 (1973).
k. G.N. Hays and H.J. Oskam, J. Chem. Phys. 59, 1507 (1973), 59, 6088 (1973).
l. Estimate made by D.J. Eckstrom, R.A. Gutcheck, R.M. Hill, D. Huestis, and D.C. Lorents, Stanford Research Institute Technical Report MP 73-1 (1973).
m. H.A. Koehler, Lawrence Livermore Laboratory, Private Communication to D.C. Lorents, SRI.
n. R.A. Young, G. Black and T.C. Slanger, J. Chem. Phys. 50, 303 (1969)
o. B. Rosen, ed., Selected Constants Spectroscopic Data Relative to Diatomic Molecules (Pergamon Press, New York, 1970) p. 266.
q. J.W. Dreyer and D. Perner, Chem. Phys. Lett. 16, 169 (1972).

TABLE II

RATE CONSTANT FOR STEP A4 $Ar^* + N_2 \rightarrow N_2(C) + Ar$ AS A PERCENTAGE OF STEP A5 $Ar^* + N_2 \rightarrow$ ALL PRODUCTS

PERCENTAGE	RESEARCH GROUP
70%	This work using energy deposition derived from calorimetry.
13%	This work using energy deposition derived from chemical dosimetry.
0.4%	Reference e, Table I
$\leq$ 14%	Reference h, Table I
$\leq$ 40%	Reference 8

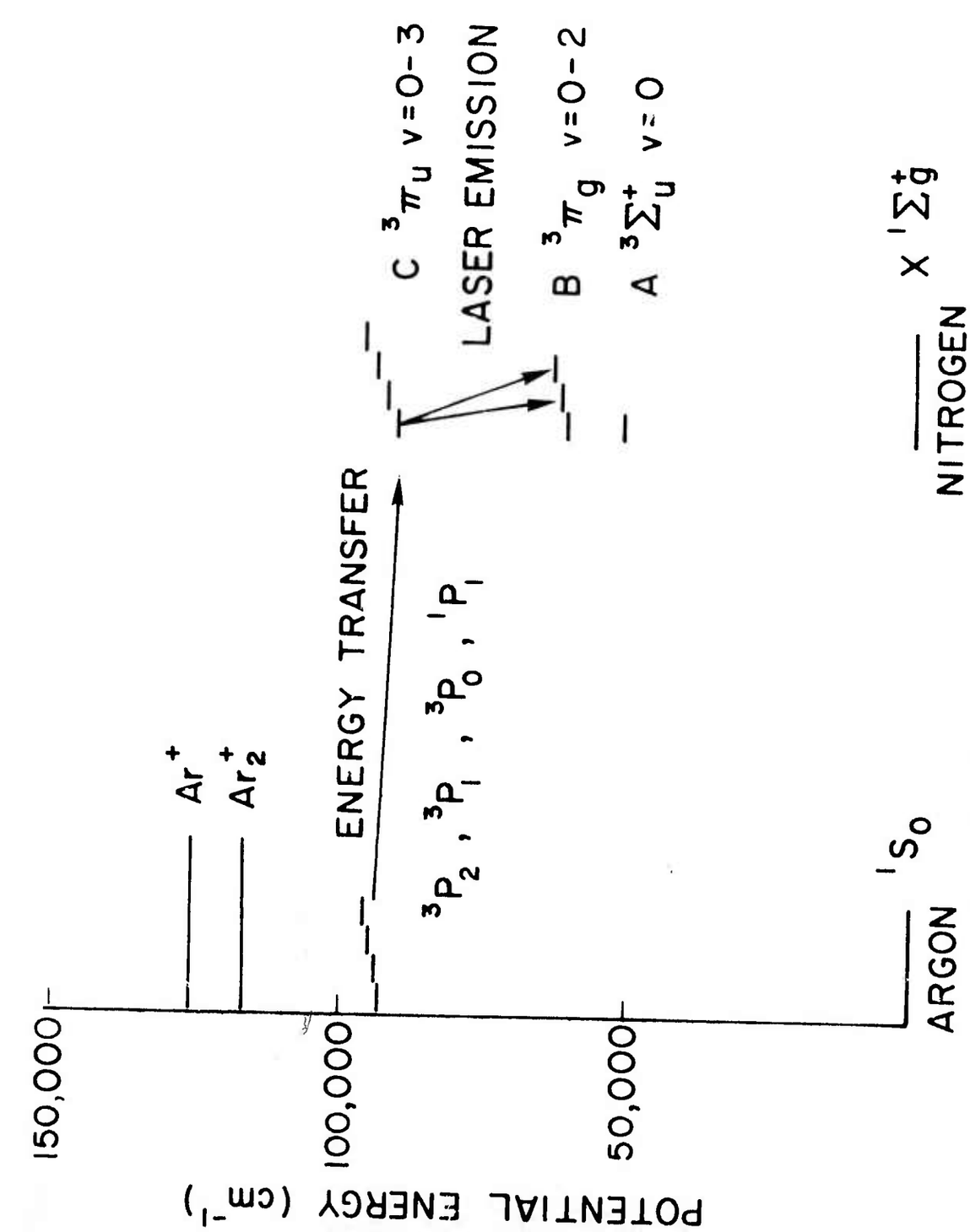

Fig. 1 — Potential energy levels of argon and nitrogen

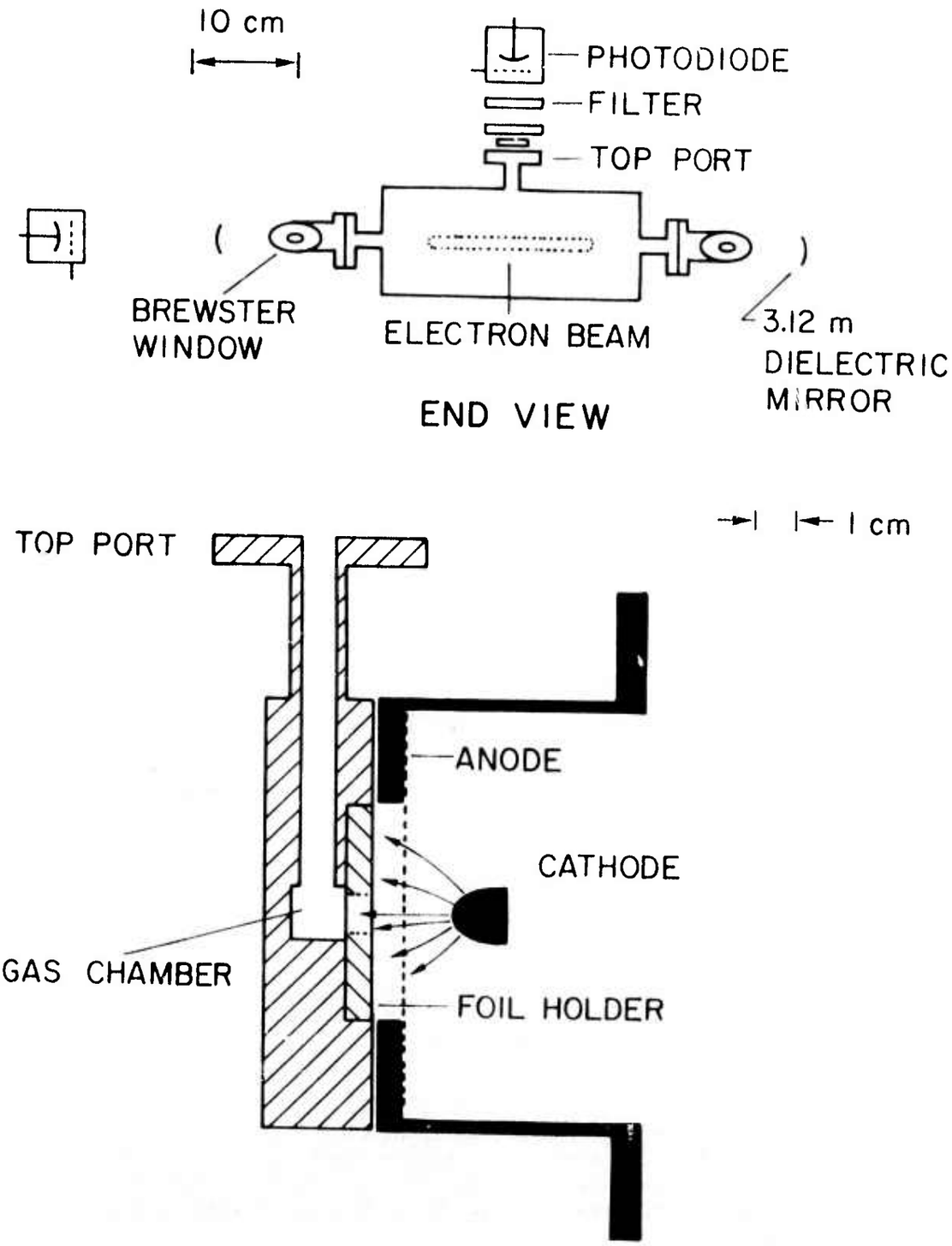

Fig. 2 — E-beam device with the laser cell and optical cavity used for the low power Ar-N_2 laser

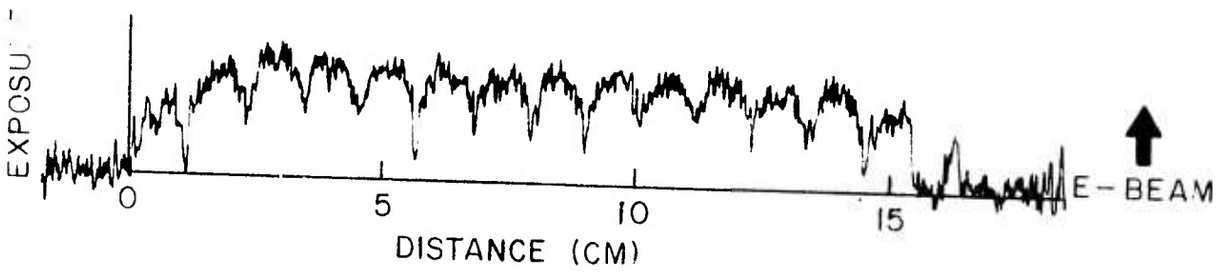

(a)

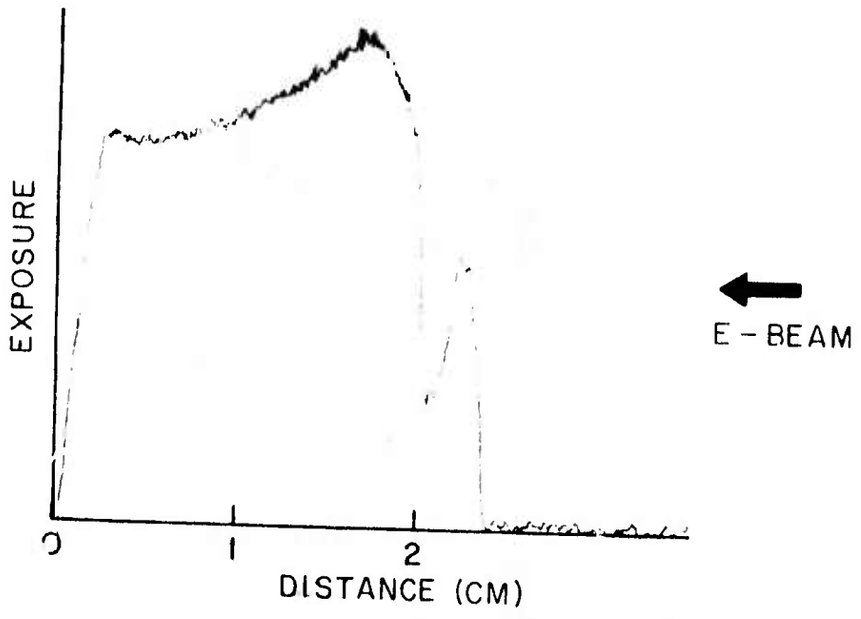

(b)

Fig. 3 — (a) Upper Trace. E-beam profile visualized by fluorescence and recorded on film. Top view, with respect to Fig. 2, microdensitometer scan taken at 6.5 mm distance from the foil. (b) Lower Trace. Side view. Scan taken along the centerline of the beam. Peak on the right is a spurious reflection.

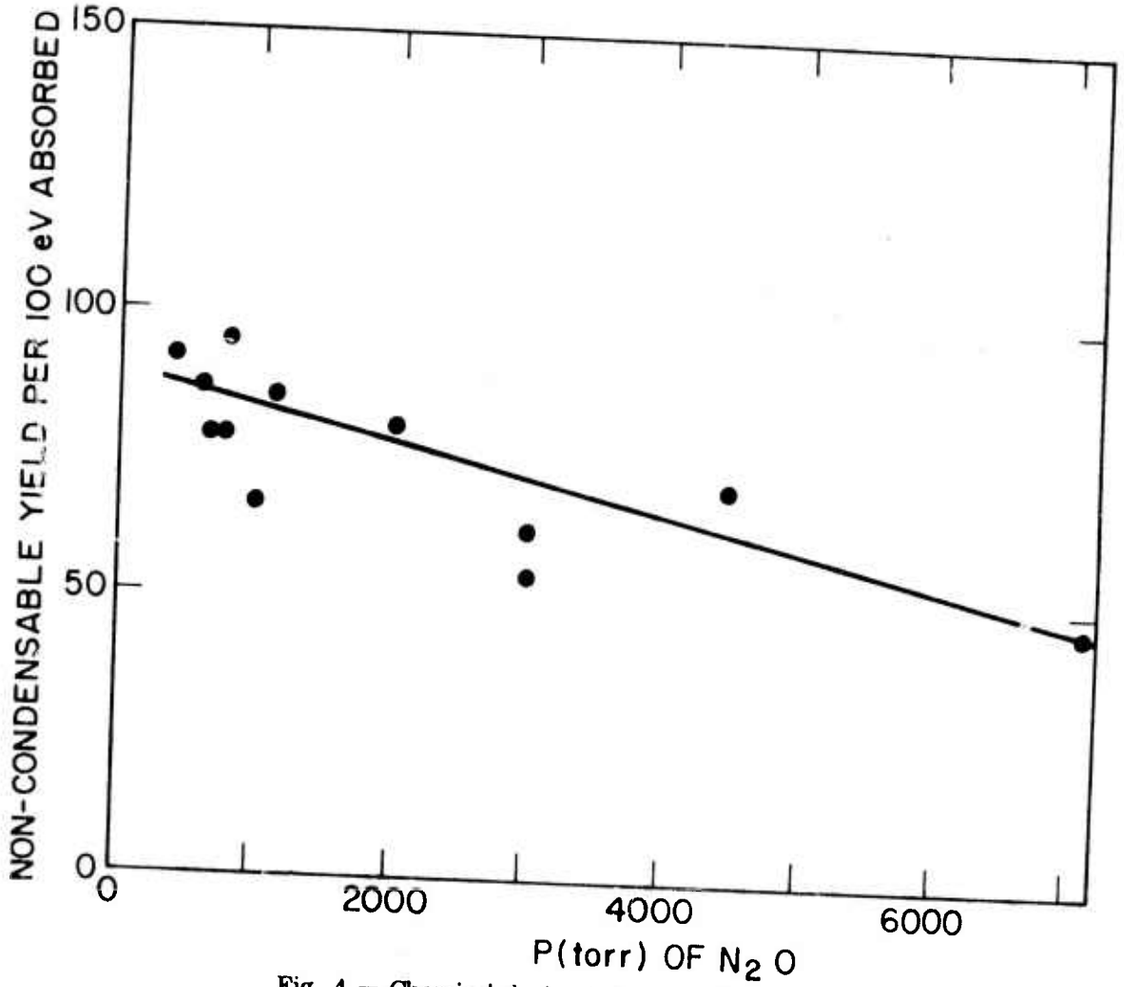

Fig. 4 — Chemical dosimetry versus pressure

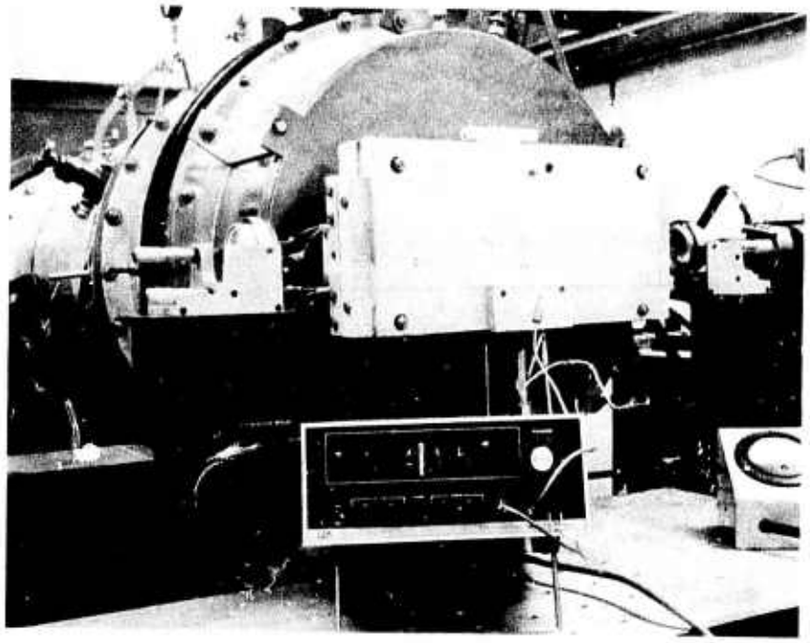

Fig. 5 — Oven and heated cell mounted on the e-beam device. Test temperature 742°K.

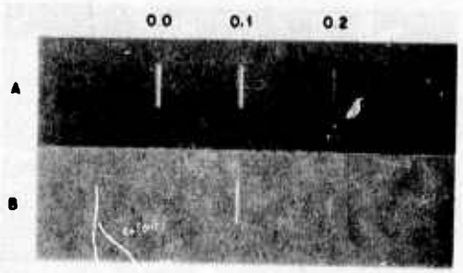

Fig. 6 — Comparison of the fluorescence spectrum (A) and the laser spectrum (B) arising from excitation of a 5% N_2-Ar mixture at a total pressure of 1500 torr. The bands all originate from v = 0 of $N_2(C)$ and terminate on v of $N_2(B)$ as indicated by the number to the right of the decimal point.

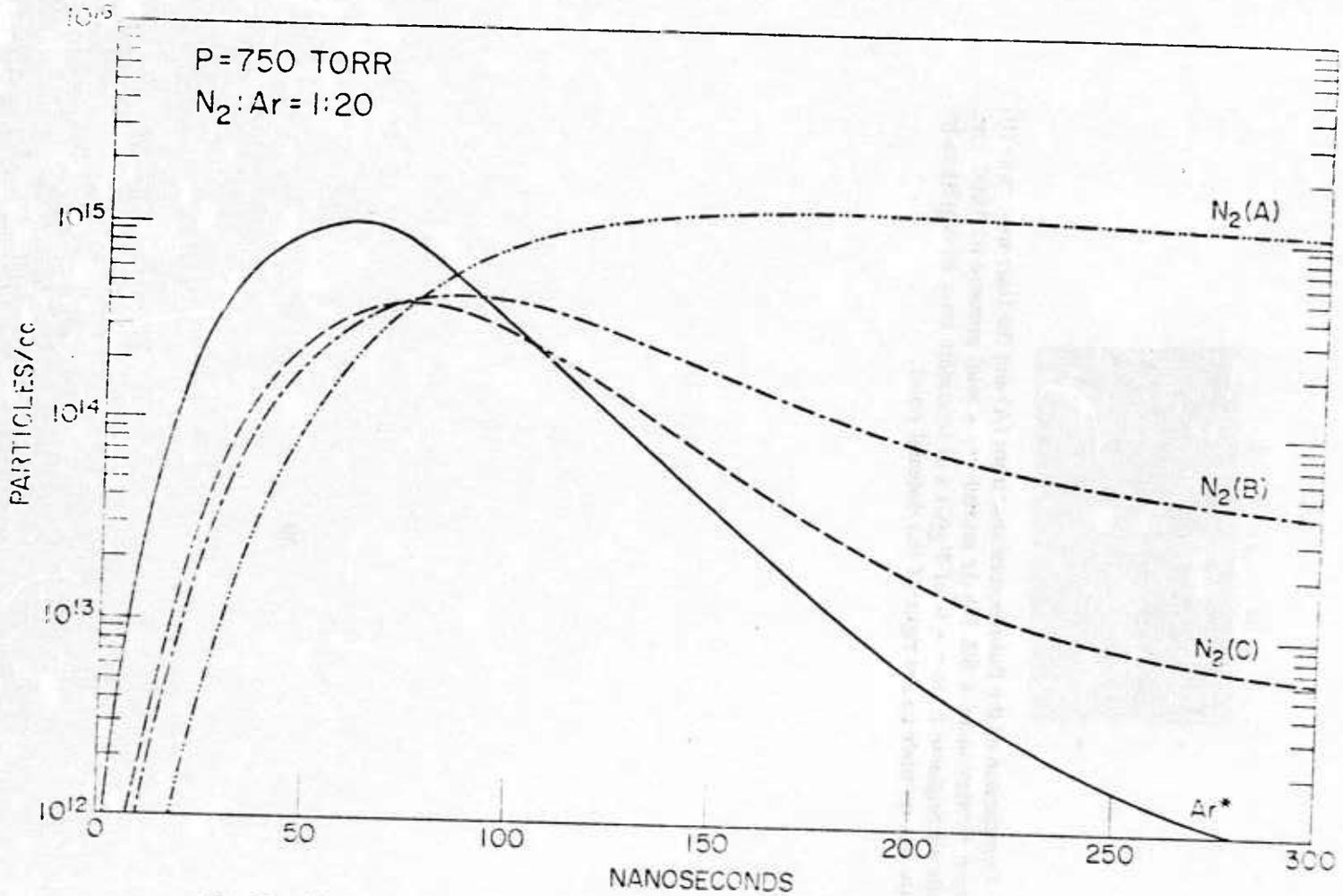

Fig. 7 — Number densities of various species in an E-beam excited N_2-Ar mixture versus time as derived from model calculation

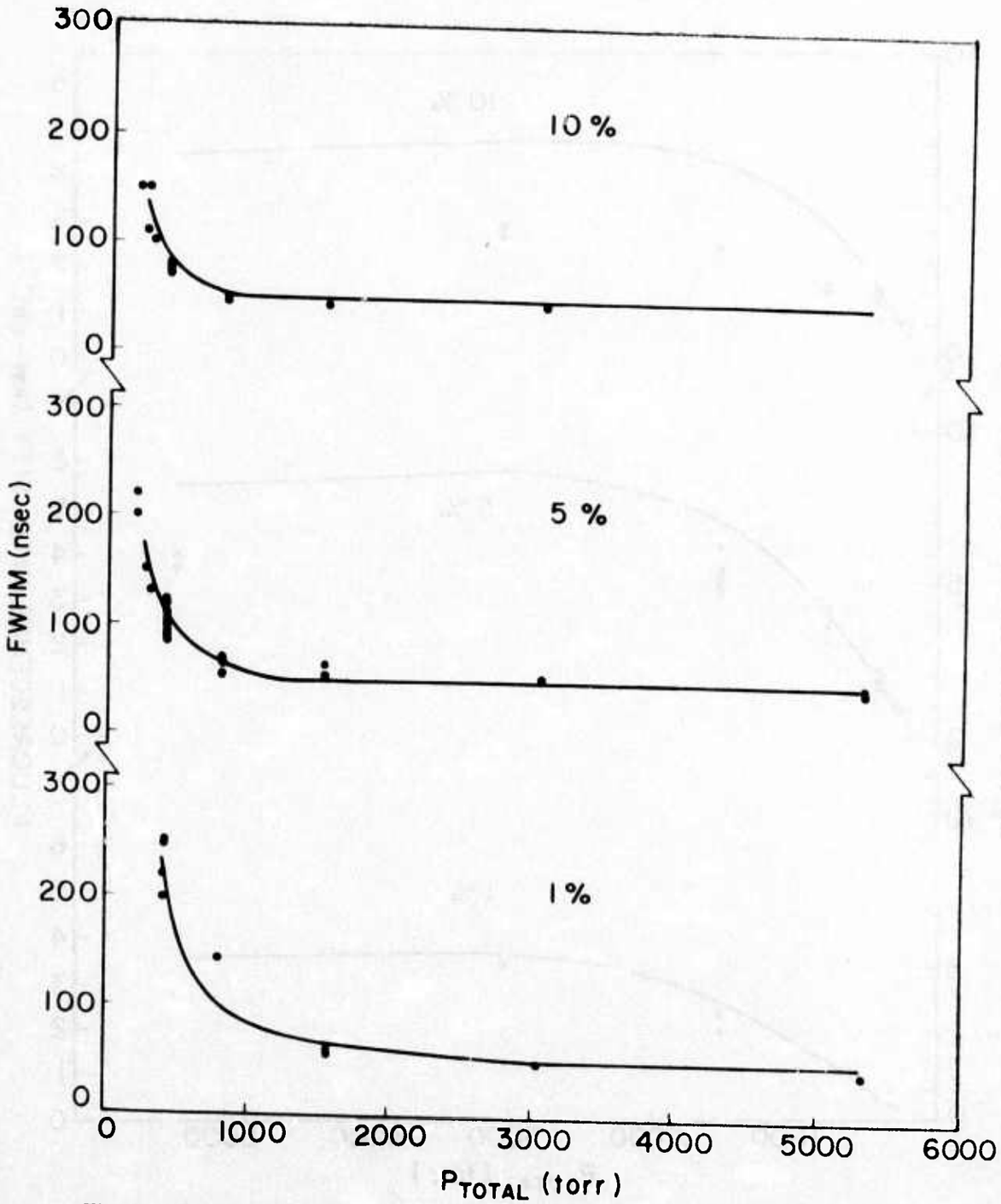

Fig. 8 — FWHM of the C-B fluorescence from 1%, 5%, and 10% N_2-Ar mixture

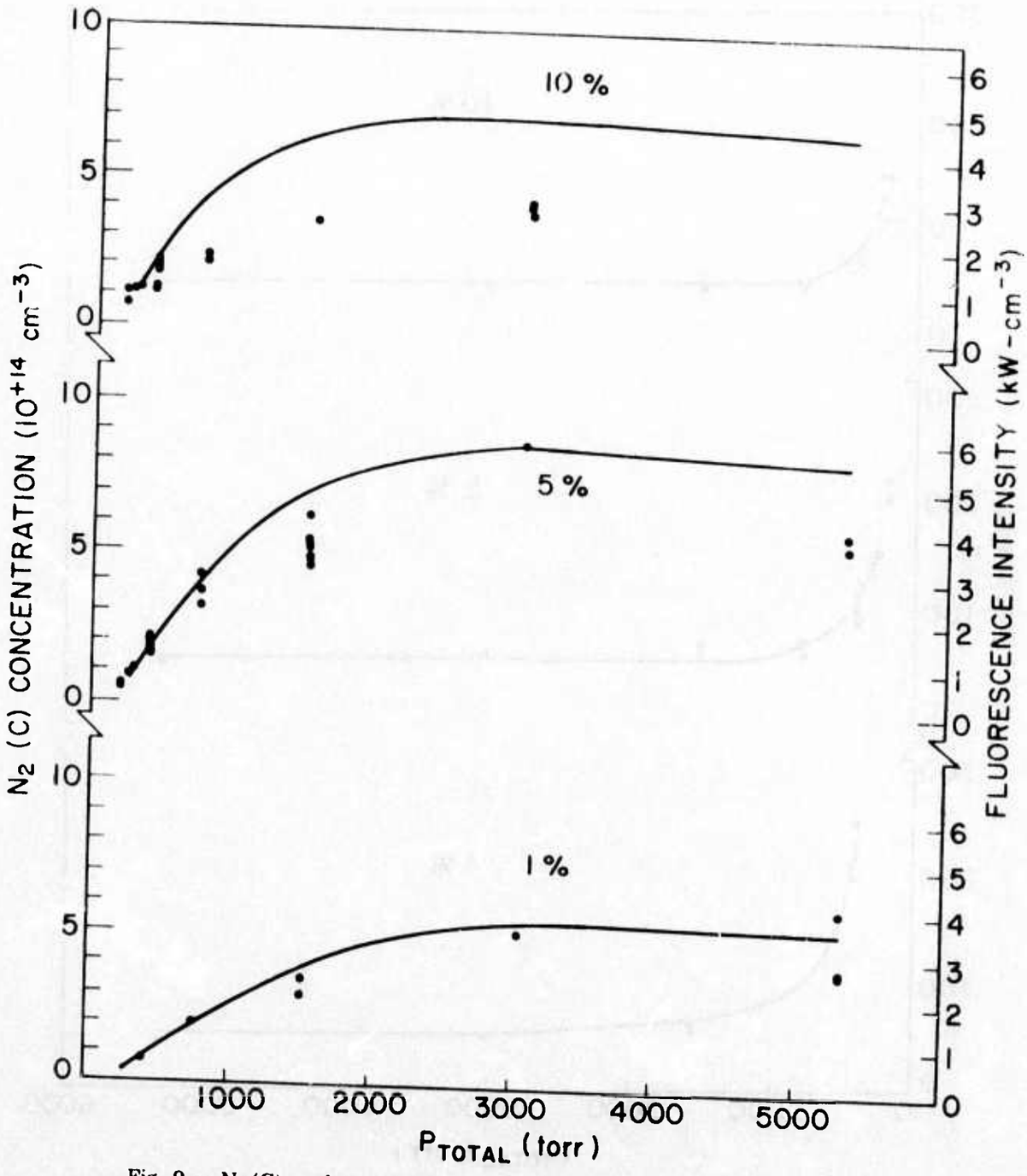

Fig. 9 — $N_2(C)$ peak concentration as a function of the total pressure

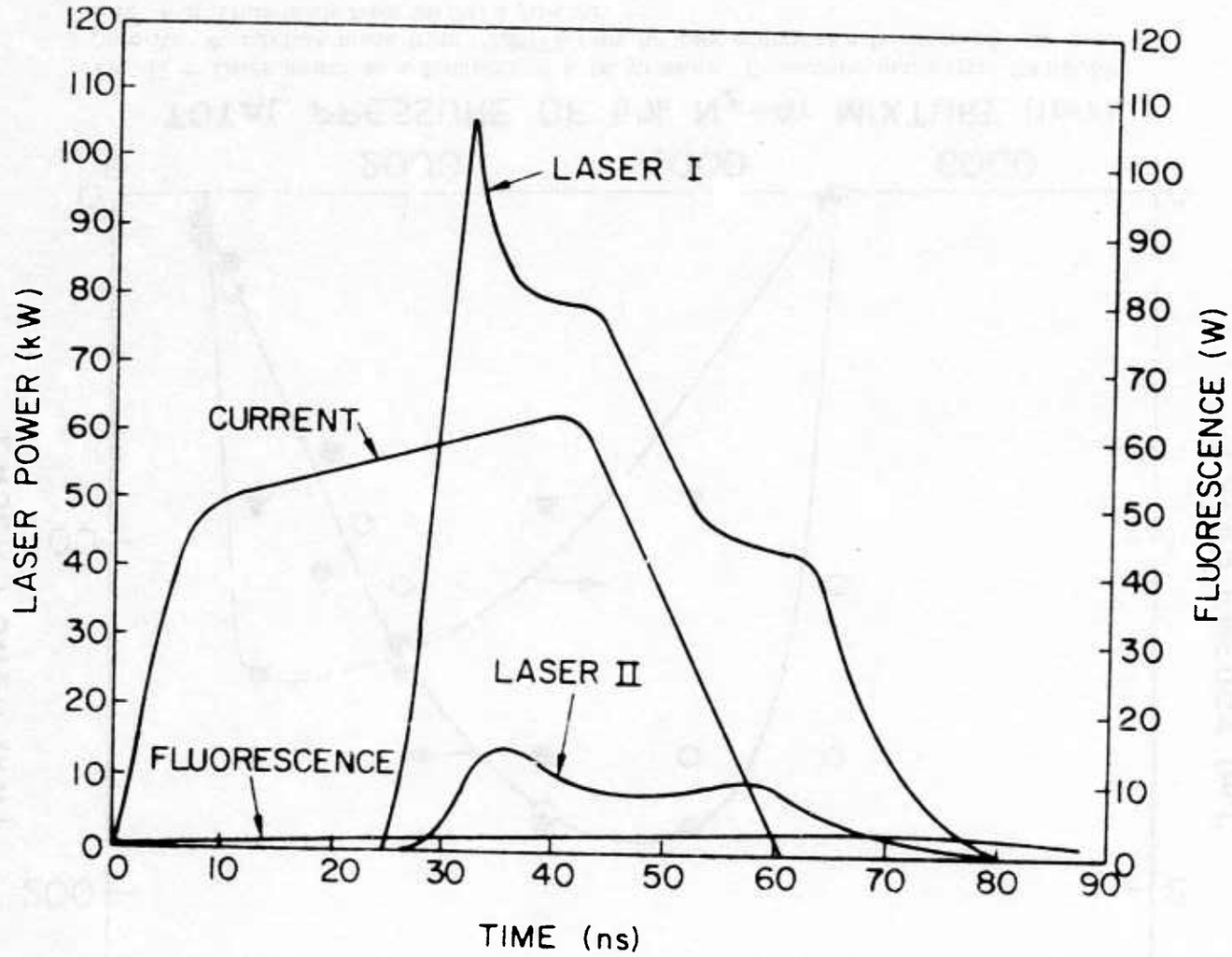

Fig. 10 — Temporal dependence of the e-beam current on an arbitrary amplitude scale, fluorescence measured at a side window. Laser I with a 99.7% R mirror and Laser II with only the quartz windows providing optical feedback to the laser cell. Total pressure 1500 torr of a 5% N_2-Ar mixture.

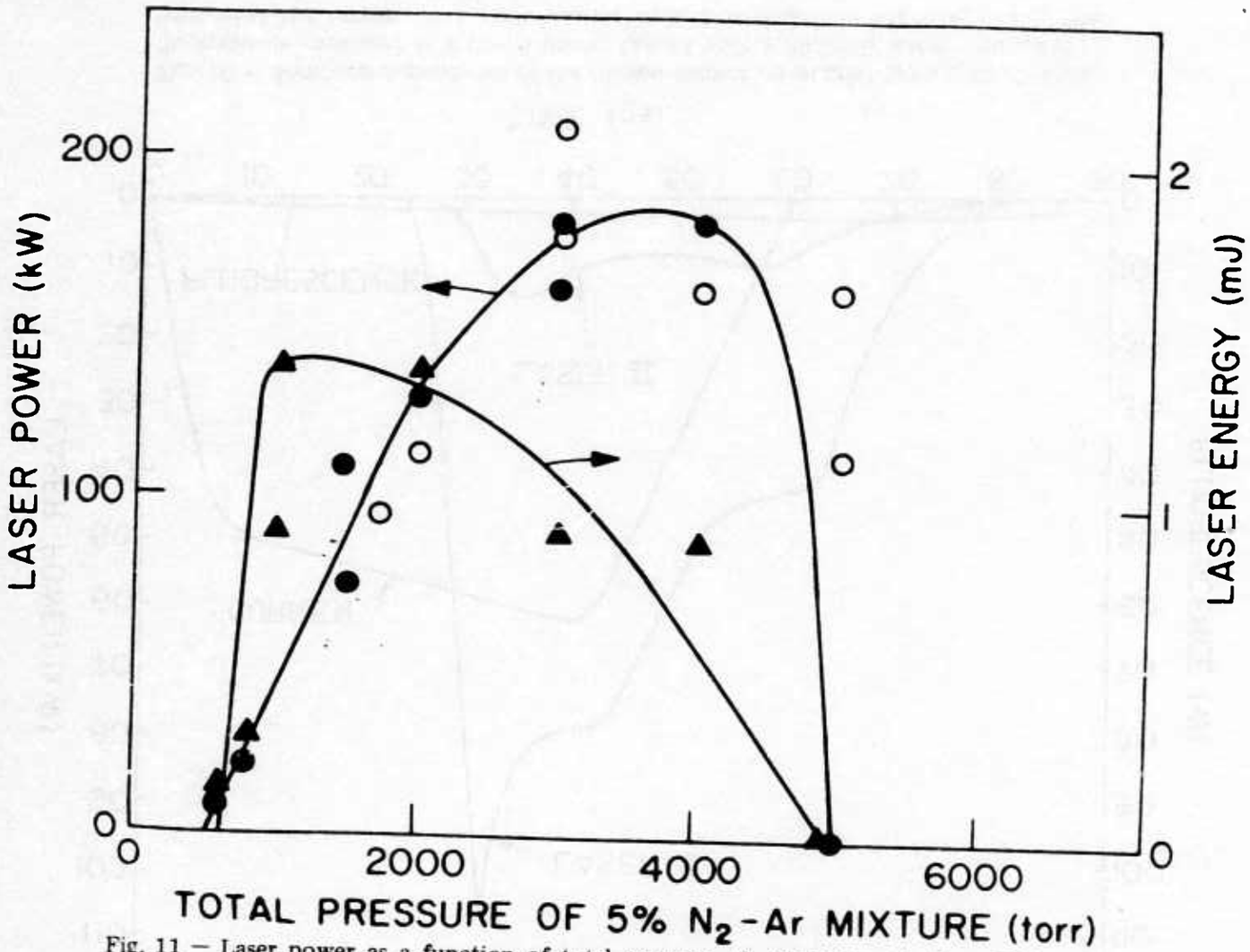

Fig. 11 — Laser power as a function of total pressure. 0 mixture made from 99.9995% pure Ar. ● mixture made from 99.997% pure Ar laser energy as a function of total pressure. ▲ mixture made from 99.997% pure Ar.

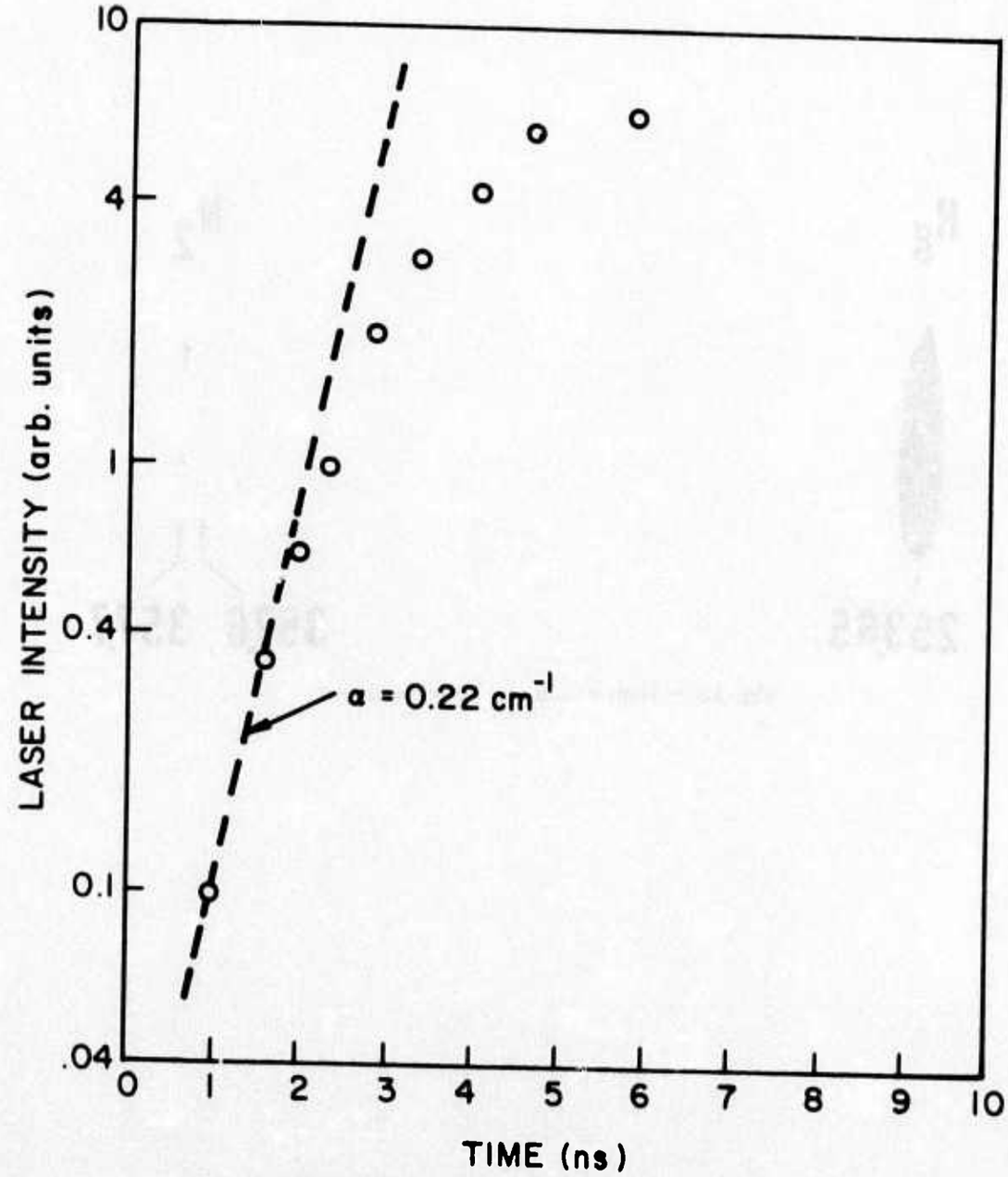

Fig. 12 — Laser gain derived from the leading portion of a laser pulse from 1500 torr 5% N_2-Ar

Fig. 13 — High resolution laser spectrum

APPENDIX 1

Laser emission at 3577 and 3805 Å in electron-beam-pumped Ar-N_2 mixtures*

S. K. Searles and G. A. Hart†

Laser Physics Branch, Optical Sciences Division, Naval Research Laboratory, Washington, D.C. 20375
(Received 11 March 1974, in final form 29 April 1974)

Experiments were performed with electron-beam-pumped Ar-N_2 mixtures. Laser emission on the second positive band transitions 3577 Å (0-1) and 3805 Å (0-2) was observed in an optical cavity fitted with Brewster angle windows. Some exc[illegible]ng preliminary experiments in which the laser windows were mounted at normal incidence were performed. These results indicated superfluorescent emission with an efficiency of 0.4%. The energy pathways in the irradiated mixtures were modeled and compared to the experimental results.

There has been a great deal of research interest in the $C\,^3\pi_u - B\,^3\pi_g$ nitrogen laser. Patterson *et al.*[1] have reported superfluorescent emission at 3371 Å arising from the electron-beam (e-beam) excitation of low-pressure nitrogen. A traveling wave tube was used by Godard[2] to obtain both high power and high efficiency. Nelson *et al.*[3] have produced exceptionally long C-B laser pulses, up to 20 μsec, from a Ar-N_2-HF mixture pumped by an e-beam sustainer system. Their observed laser transitions included 0-0, 1, 2, 3.

We report here a C-B laser operating strongly on the 0-1 (3577 Å) transition and weakly on the 0-2 (3805 Å) transition. A 50-nsec-long relativistic e-beam pulse was used to pump the gas.

The e-beam generator output was a 50-nsec-long pulse of 500-keV electrons. Figure 1 shows a typical integrated B dot signal. The pulse entered the laser cell through a 25-μ-thick Ti foil supported by a steel plate with fourteen 0.95-cm-diam holes spaced evenly over a length of 15.4 cm. The beam energy into the laser cell was determined to be 36 ± 6 J by carbon block calorimetry. The over-all beam uniformity was measured to be ±15% by thin-film dosimetry.

The laser cell was fitted with Brewster angle quartz windows in a transverse geometry to the electron beam. The optical cavity was defined by the 0.67-cm-diam holes in the Brewster window holders and a > 99.7% reflectance dielectric mirror and partially transmitting dielectric mirror. The transmission of the second mirror was 10% at 3577 Å and 36% at 3805 Å. The cavity length was 55 cm. A quartz window mounted mutually perpendicular to the optical axis and the e-beam axis allowed fluorescence measurements. Emission measurements were made with ITT F4018-S5 photodiodes. As shown in Fig. 1, the beam current, laser emission, and fluorescence were measured for each shot and synchronized with a fiducial time mark. A 1-m Jarrell-Ash spectrometer was used to identify the N_2 transitions. A 3200–3800-Å Corning band-pass filter was used to restrict the side-emission measurements to C-B fluorescence. The gases used in the experiment were 99.997% pure Ar and 99.998% pure N_2.

Emission measurements were made over the pressure range 200–5300 Torr. The partial pressure of N_2 relative to Ar was 1, 5, or 10%. Representative oscillograms are shown in Fig. 1. The following trends were observed for the three Ar-N_2 mixtures. At the lowest pressures at which laser action occurred, peak fluorescence was reached after the end of the pumping pulse and before the laser pulse. In the 5% mixture at 250 Torr the fluorescence peaked at 110 ns after the begin-

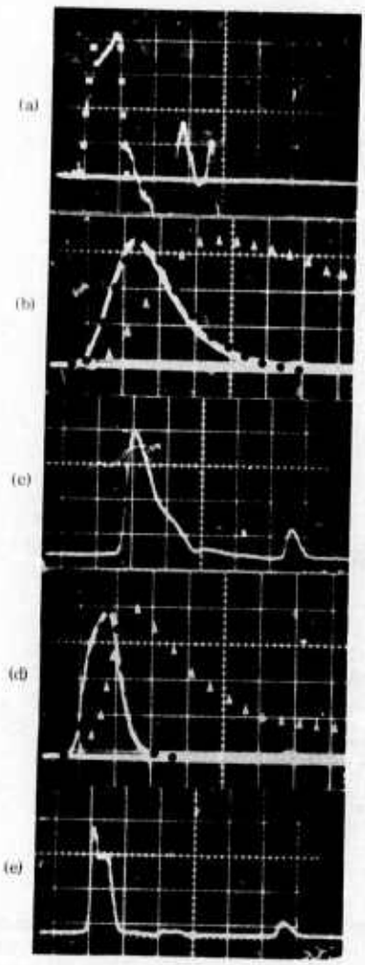

FIG. 1. (a) Typical current pulse measured at the cathode. Square points show the theoretical simulation of the pulse. A time mark appears near the end of each trace. All oscillograms originate from 5% N_2. (0.2 V/div.) (b) Fluorescence from the 0-0, 1, 2 transitions at 400 Torr. Dots, theoretical curve for steps 1–8 with $k(4)$ multiplied by 170. Triangles, theoretical curve with inclusion of steps 9 and 10. Amplitude multiplied by 50. (0.2 V/div.) (c) Laser emission at 400 Torr. (5 V/div.) (d) Fluorescence at 1500 Torr. Dots, theoretical curve for steps 1–8 with $k(4)$ multiplied by 125. Triangles, theoretical curve with inclusion of steps 9–11. Amplitude multiplied by 20. (0.5 V/div.) (e) Laser emission at 1500 Torr. (20 V/div.). Time scale for (a)–(e) 50 nsec/div.

ning of the current pulse. Laser action peaked 45 nsec later. An increase in pressure shifted the peaks toward the current pulse as shown in Fig. 1. The best laser efficiency for all three mixtures occurred at 800 Torr total pressure. Relative efficiency values were 1.1:14: 5.3 for 1, 5, and 10% mixtures, respectively. Beam output divergence was measured to be 6 mrad. The 3577-Å transition was the only laser line recorded with the exception that the 3805-Å line was weakly recorded over a narrow pressure range in the 5 and 10% mixtures.

In fluorescence the relative line intensities were in agreement with those predicted by the relative transition probabilities (A_{0-0}, 12.1; A_{0-1}, 8.6; A_{0-2}, 3.0).[4] The fluorescence signals grew linearly with pressure until about 1500 Torr and reached a maximum at about 3000 Torr.

We now consider the proof that the axial emission is due to stimulated emission. The following four factors demonstrate laser emission.

(i) Removal of the far mirror reduced the axial emission by as much as 2 orders of magnitude.

(ii) The axial pulse shape, width, and amplitude indicate laser action when comparison is made with the fluorescence signal (see Fig. 1).

(iii) The dominant line in fluorescence is absent in the laser spectrum although all lines originate from a common level.

(iv) The ratio of axial emission to side emission is a strong function of pressure and mixture composition as illustrated in Fig. 2.

A mechanism for population of the upper laser level is presented in Table I. A Runge-Kutta-Treanor computer program was used to calculate the concentration of the various species from 0 to 600 nsec. The pumping pulse had a trapezoidal shape patterned after the experimental current pulse shown in Fig. 1. The 500-

TABLE I. Mechanism for population of $N_2(C)$.

Step	k[a]	Reference
1. $Ar^* + 2Ar \rightarrow Ar_2^* + Ar$	2.5×10^{-31}	b
2. $Ar_2^* + e \rightarrow Ar^* + Ar$	7×10^{-7}	c
3. $Ar^* + 2Ar \rightarrow Ar_2^* + Ar$	6×10^{-33}	d
4. $Ar^* + N_2 \rightarrow N_2(C) + Ar$	1.2×10^{-13}	e
5. $Ar^* + N_2 \rightarrow N_2{}^f + Ar$	3×10^{-11}[g]	d
6. $N_2(C) + Ar \rightarrow N_2{}^f + Ar$	3×10^{-13}	h
7. $N_2(C) \rightarrow N_2(B) + h\nu$	2.5×10^{7}	i
8. $N_2(C) + N_2 \rightarrow 2N_2$	1.15×10^{-11}	j
9. $Ar^* + N_2 \rightarrow N_2(A) + Ar$	3×10^{-11}	
10. $2N_2(A) \rightarrow N_2(C) + N_2$	2.6×10^{-10}	k
11. $2N_2(A) \rightarrow N_2(B) + N_2$	1.1×10^{-9}	k

[a] Radiative units, sec^{-1}; two-body units, cm^3/sec; and three-body units, cm^6/sec.
[b] E. W. McDaniel, V. Cermak, A. Dalgarno, E.E. Ferguson, L. Friedman, *Ion-Molecule Reactions* (Wiley-Interscience, New York, 1970), p. 338.
[c] J. N. Bardsley and M.A. Biondi, in *Advances in Atomic and Molecular Physics* (Academic, New York, 1970), Chap. 1.
[d] J. LeCalvé and M. Bourène, J. Chem. Phys. 58, 1446 (1973).
[e] R.A. Gutcheck and E.C. Zipf, Bull. Am. Phys. Soc. 17, 395 (1972).
[f] N_2 electronic state distribution incompletely determined.
[g] Total k for disappearance of Ar^*.
[h] D.W. Setser, D.H. Stedman, and J.A. Coxon, J. Chem. Phys. 53, 1004 (1970).
[i] Reference 4.
[j] P. Millet, Y. Salamero, H. Brunet, J. Galy, D. Blanc, and J.L. Teyssier, J. Chem. Phys. 58, 5839 (1973).
[k] G.N. Hays and H.J. Oskam, J. Chem. Phys. 59, 1507 (1973); 59, 6088 (1973).

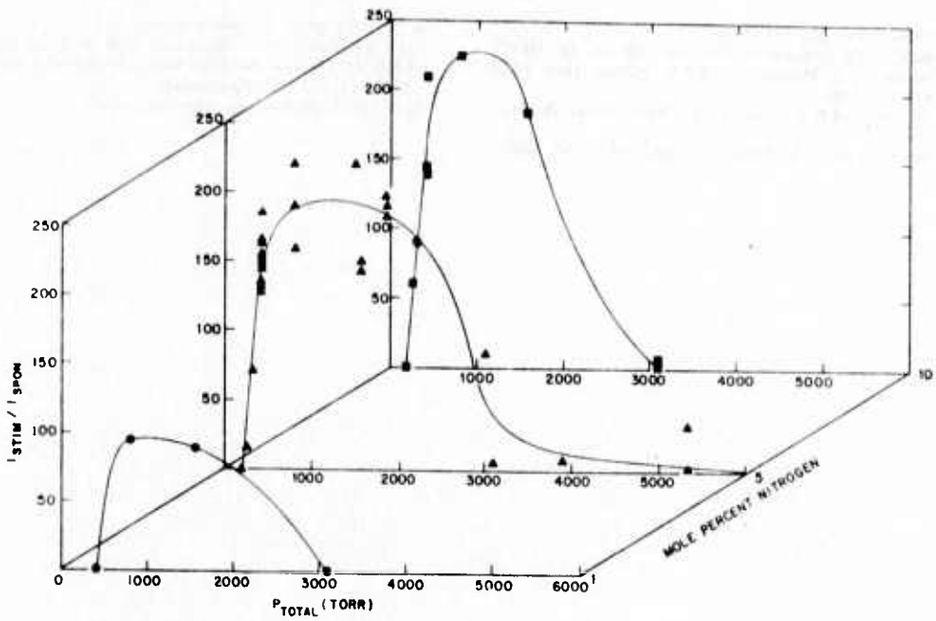

FIG. 2. Ratio of axial emission to side emission with correction for relative collection efficiencies plotted as a function of the total gas pressure and composition.

keV primary electrons gave 3.5 Ar^+ and 1.0 Ar^* per 91 eV absorbed.[5]

The secondary electrons were assumed to cool rapidly without pumping the electronic states of Ar or N_2. The return current was ignored because the inside dimensions of the cell, 1.25×1.25×15 cm long tend to favor a return path along the surface of the cell rather than through the bulk gas. Any secondary electron impact excitation of electronic states would preferentially excite Ar and not significantly affect the basic mechanism presented here. The balance of the mechanism is given by steps 1–8 in Table I. The Ar^* species was assumed to be the metastables $^3P_0$, $^3P_2$.

The computer-generated fluorescence curve was compared to the experimental curve with respect to three criteria: elapsed time to peak intensity, FWHM, and peak amplitude. Altogether 70 such comparisons can be made for experiments conducted at the three relative N_2-Ar concentrations of 1, 5, and 10% at total pressures of 250–5320 Torr taken in pressure increments of a factor of approximately 2 per step. The difference between theory and experiment for the time to reach peak fluorescence is an average of 12±6 nsec while the difference in FWHM is only 5±3 nsec. For the peak amplitude the ratio of the experimental/theoretical intensities was calculated to be 180±20 for 1%, 180±30 for 5%, and 125±15 for 10%.

The immediate conclusion from the good agreement on the elapsed time and the FWHM is that the mechanism is a reasonable one. However, the constant ratio of about 160 between experimental and theoretical intensities demonstrates that step 4 is too low by this amount. The experimental uncertainty in the $k(4)$ number cited in Table I may be considerable since it is derived from a complex plasma physics experiment in which it is quite possible that some key processes are not well understood.[6]

An alternative energy transfer mechanism given by steps 9–11 was also considered. The energy pooling step 10 has been suggested as a laser pumping process.[7] The C-B temporal emission behavior and pressure dependence predicted for this alternative model no longer displayed good agreement with experiments (see Fig. 1). Moreover the branching ratio of steps 10 and 11 makes this alternative model incapable of predicting the fluorescence observed in side emission.

The conclusion that $k(4)$ is too low is supported by some preliminary experiments in which Brewster angle windows were replaced by normal incidence windows. This change was prompted by a report that e-beam-excited Ar-N_2 mixtures gave powerful laser pulses.[8] With this window change intense superfluorescent pulses were observed in 5% Ar-N_2 mixtures over the pressure range 600–1540 Torr with a laser efficiency of 0.4%. FWHM was 40 ns and peak power was 18 kW. Further experiments are in progress.

The authors wish to thank Michael Ury for the design and construction of the pulse power generator for the electron-beam device.

*Work supported in part by DARPA.

†NRC-NRL Postdoctoral Research Associate 1973–present.

[1] E. L. Patterson, J. B. Gerardo, and A. Wayne Johnson,

Appl. Phys. Lett. **21**, 293 (1972).
[2]B. Godard, IEEE J. Quantum Electron. **QE-10**, 147 (1974).
[3]L.Y. Nelson, G.J. Mullaney, and S.R. Byron, Appl. Phys. Lett. **22**, 79 (1973).
[4]A.W. Johnson and R.G. Fowler, J. Chem. Phys. **53**, 65 (1970).
[5]L.R. Peterson and J.E. Allen, J. Chem. Phys. **56**, 6068 (1972).
[6]E.C. Zipf (private communication).
[7]D.J. Eckstrom, R.A. Gutcheck, R.M. Hill, D. Huestis, and D.C. Lorents, Stanford Research Institute Report No. SRI MP73-1, 1973 (unpublished).
[8]M.L. Bhaumik (private communication).

2. DOUBLE PULSE EXPERIMENT

For the present reporting period, the emphasis in the double pulse excitation experiments has been on the use of a fast-rising double DC pulse system for excitation of metal vapor laser systems. This appears to be a more promising area of investigation than the RF-DC system.

Using a prototype system, discharges in water vapor have been spectroscopically observed. No desired B-A state emission from the OH radical was observed over a variety of discharge conditions with various buffer gases present. Other experimentation was done with the tube operating as a N_2 laser. This mode of operation proved the fast rise-time of the excitation pulse and demonstrated the pressure range over which it could be used.

Tetraethyllead vapor, at room temperature, corresponding to a pressure of about .3 torr, was admitted to the tube. In single-pulse operation with an argon gas buffer very strong emission of the expected lines was observed. The rise time of the fluorescence at 4057 Å was about 10 ns, and it is assumed that the excitation followed the rise of the current pulse. The decay time was observed to be $\sim$ 60 ns, independent of argon pressure, much longer than the 9 ns natural lifetime. This may be due to radiation trapping or cascade from higher levels, although systematic errors cannot

cannot be ruled out at present. A heavy deposition of discharge produced Pb prevented further work with this tube to clarify this question. Observation of radiation trapping would be of use as a means of determining the metastable population density. The intensity of emission observed from single pulses in $Pb(\epsilon+)_4$ indicates that lasing may be obtained from lead compounds with this excitation scheme.

Construction of a bakeable glass discharge tube proved impractical. Hence, a stainless steel transverse discharge tube was designed and fabricated. Concurrently, a vacuum system and two thyratron-switched discharge pulse modules capable of low jitter, high repetition rate operation were constructed. The design of the stainless steel discharge tube is such as to avoid the glass and metal sealing problems which halted construction of the originally proposed tubes. The present tube has a discharge length of 20 cm and is bakeable to over 500°C. Metal vapor lamps and a boxcar integrator for time resolved studies have been procured. The discharge tube is now under test and experiments will begin shortly.

The first system to be tried is expected to be TlI. Superradiant emission at 5350 Å in a longitudinal discharge have been reported by researchers in the Soviet Union but not confirmed in this country. A large number of metal vapor compounds are candidates for investigation using the transverse discharge excitation scheme.

3. VISIBLE CHEMICAL LASER EXPERIMENTS

A series of experiments have been carried out in a newly set up discharge-flow-flash laser system involving the reactions of N atoms with a number of free radicals. The N atom, which cannot be readily generated thermally or photolytically, was produced by a 100 W microwave generator. A typical N atom concentration of $\sim 3 \times 10^{13}$ atoms/cc was obtained as determined by the NO titration method. The N atom was mixed with various radical sources, such as $CHBr_3$, CH_2Br_2, CH_2, Cl_2, $CFBr_3$ and CH_2CO, in a Suprasil flashflow tube situated in a laser cavity formed by two high-reflectivity broad-band mirrors ($\sim$ 140 nm-IR). The flash lamp has a rise time of about 5 μsec with output above 165 nm. Free radicals were produced by photodissociation reactions,[1-3] for example,

$$CXBr_3 + h\nu \rightarrow 3Br + CX(X = F,H)$$

$$CH_2CO + h\nu \rightarrow CH_2(^1A_1) + CO, \text{ etc.}$$

The radicals thus formed, then rapidly react with the N atoms present in the flow:

$$N + CH \xrightarrow{1} CN + H + 103 \text{ kcal/mole}$$

$$N + CF \xrightarrow{2} CN + F + 69 \text{ kcal/mole}$$

$$N + CH_2 \xrightarrow{3a} CN + H_2 + 106 \text{ kcal/mole}$$

$$\xrightarrow{3b} HCN + H + 122 \text{ kcal/mole.}$$

A number of experiments with varying reactant concentrations and flash energies have been performed. No stimulated emission has yet been detected. In order to test the cavity conditions and the extent of reaction occurring in the system, a small amount of H_2 ($\sim$ 0.5 torr) was added to a flow of $\sim$ 0.02 torr N atoms and $\sim$ 0.5 torr $CFBr_3$, carried by about 15 torr He. Flash photolysis of the flowing mixture produced a relatively intense HF laser pulse, probably due to the well-known $F + H_2 \rightarrow HF^{\dagger} + H$ reaction. This test clearly indicates that the system has been properly tuned, that the N + CF reaction does take place and a reasonable amount of CN has been generated chemically. Unfortunately, these reactions are new and all kinetic information including the overall reaction rates are not available in the literature. These experiments will be repeated with a 2 KW microwave generator and internal mirrors with higher reflectivities.

Many more exothermic reactions such as

$$O + C_2H \rightarrow CO + CH^*$$

$$N + C_2O \rightarrow CN^* + CO, \text{ etc.}$$

will be studied in the discharge-flow-flash system as well as the 1 μsec transverse flash unit ($\lambda \geq 105$ nm) which is now under construction. The unit will be ready for testing in early 1975. The reactions to be investigated

in the initial stage of testing include:

$$O(^1S) + CH(^2\pi) \rightarrow CO(^1\pi) + H(^2S) + 36 \text{ kcal/mole}$$

$$O(^1S) + CS(^1\pi) \rightarrow CO(^1\pi) + S(^1D) + 26 \text{ kcal/mole}$$

$$CO(^1\pi) \rightarrow CO(X^1\Sigma^+) + h\nu \ (180 \text{ nm})$$

$$O(^1S) + Xe \rightarrow XeO^{**} \rightarrow XeO^* + 558 \text{ nm}$$

where $O(^1S)$ will be produced by the photodissociation of N_2O at 120 nm,

$$COCl_2 + h\nu \rightarrow Cl_2^* + CO$$

$$Cl_2^* \rightarrow 2Cl + h\nu \ (300 - 400 \text{ nm}).$$

REFERENCES

1. M.C. Lin, Int. J. Chem. Kinet. 5, 173-176 (1973).
2. M.C. Lin, Chemiluminescence and Bioluminescence, M.J. Cormier, D.M. Hercules and J. Lee, Ed., p. 61, Plenum Press, New York (1973).
3. M.C. Lin, Int. J. Chem. Kinet. 6 1-14 (1974).

---

4. OPTICALLY PUMPED COLLISION LASERS

It has long been recognized that efficient c.w. gas lasers should utilize transitions connecting low lying energy levels. Furthermore, since the lowest lying atomic levels are as a rule either metastable or radiation trapped, it is generally understood that the lower laser level in these devices would have to be deactivated through collisions of the second kind. One immediately comes to the conclusion that direct electrical discharge excitation would not be a

suitable mode of pumping for an efficient c.w. visible laser, because the large concentration of the quenching gas required would most likely de-excite the electrons as well. However, if the laser is pumped optically, almost arbitrarily large amounts of the quenching gas would be permissible. If in addition the pumping radiation can be produced with great efficiency, there is a good chance that the resulting optically pumped collision laser would have a comparably high overall efficiency.

The basic scheme for the optically pumped collision laser is as follows:

$$(1) \qquad |0> + h\nu\ (\text{pump}) \rightarrow |1>$$

$$(2) \qquad |1> \rightarrow |2> + h\nu'\ \ (\text{laser})$$

$$(3) \qquad |2> + M \rightarrow |0> + M$$

where the three processes pertain, in order, to optical pumping of the upper laser level, stimulated emission at the laser transition, and collisional quenching of the lower laser level. A fundamental requisite for high efficiency is that $E_1 >> E_2$, with the energy of the $|0>$ state taken to be zero. The condition for gain in such a system is $g_2R_2 > g_1(A_{12} + R_{12})$, where g_i is the degeneracy of $|i>$, A_{12} and R_{12} are the radiative and collisional rates from $|1>$ to $|2>$, and R_2 is the collisional quenching rate of $|2>$.

We have demonstrated the feasibility of an optically pumped collision laser by achieving laser oscillation on the 546.1 nm transition of Hg through optically pumping a $Hg-N_2$ mixture with a low pressure Hg lamp (Appendix 1).

The relevant steps involved are the following:

(4) $Hg(6\ ^1S_o) + h\nu(253.7\ nm) \rightarrow Hg(6\ ^3P_1)$

(5) $Hg(6\ ^3P_1) + N_2 \rightarrow Hg(6\ ^3P_o) + N_2$

(6) $Hg(6\ ^3P_o) + h\nu(404.7\ nm) \rightarrow Hg(7\ ^3S_1)$

(7) $Hg(7\ ^3S_1) \rightarrow Hg(6\ ^3P_2) +$ laser (546.1 nm)

(8) $Hg(6\ ^3P_2) + N_2 \rightarrow Hg(6\ ^3P_{1,0}, 6\ ^1S_0) + N_2$.

Note that eqns. 1-3 correspond to Eqns. 6-8 in the case of the Hg laser. The $Hg(6\ ^3P_o)$ level is in effect the $|0>$ state in this modified scheme.

To assess the potential of the Hg 546.1 nm laser, we have measured R_{12} and R_2 for Hg in collisions with N_2 (Appendix 2). The results show that one should be able to convert 40% of the photons absorbed at 404.7 nm into laser output at 546.1 nm. At present, standard Hg lamps can produce 253.7 nm radiation with $\sim$ 20% efficiency at low pressure and 404.7 nm light with $\sim$ 2% at medium pressure. Thus, it is anticipated that, with the use of both types of Hg lamps, an overall efficiency close to 1% could be realized for the Hg 546.1 nm laser.

We are presently engaged in experiments to verify the high efficiency capability of the Hg laser. In addition, similar experiments are being conducted to explore the possibility of optically pumped collision lasers in other media. These include laser attempts on the 535.0 nm transition of Tℓ and a number of visible and near I.R. transitions of Na in a Hg-Na transfer system.

APPENDIX 1

Optically pumped cw Hg laser at 546.1 nm

N. Djeu

Laser Physics Branch, Optical Sciences Division, Naval Research Laboratory, Washington, D. C. 20375

R. Burnham

Science Applications, Inc., Arlington, Virginia 22209
(Received 13 May 1974)

cw laser oscillation has been achieved on the 546.1-nm line in Hg I using an optical pumping scheme. The potentials of this laser are discussed.

A cw atomic Hg laser at 546.1 nm has been realized by optically pumping a mixture of N_2 and Hg vapor. The upper and lower levels of the laser transition are the $7\,^3S_1$ and $6\,^3P_2$ terms of Hg I, respectively. Hopefully, this will become the first of a new class of atomic gas lasers which combines optical pumping by a resonance lamp with the collisional quenching of the lower laser level which is a low-lying metastable state. The physical separation of the excitation source from the laser medium allows one to use large amounts of some quenching gas to depopulate the lower laser level without interfering with the pumping process. An optically pumped collision laser could have an efficiency comparable to that for the production of the pumping line by the lamp.

The relevant energy levels and the excitation scheme employed in the N_2-Hg laser are indicated in Fig. 1. Mercury atoms in the ground $6\,^1S_0$ level absorb photons at 253.7 nm to populate the $6\,^3P_1$ level, are collisionally deactivated by N_2 to the $6\,^3P_0$ level, and accumulate there due to the latter state's long lifetime. Absorption of a second photon at 404.7 nm takes the atom from the $6\,^3P_0$ state to the upper laser level $7\,^3S_1$. After undergoing stimulated emission at 546.1 nm, the atom is quenched out of the lower laser level $6\,^3P_2$, again through collisions with N_2. Although a dashed arrow is drawn from $6\,^3P_2$ only to $6\,^3P_1$, the distribution of final states of Hg from the last process is still a matter of speculation. Also omitted in Fig. 1 is the possibility of optical pumping of the upper laser level by absorption of a 435.8-nm photon from $6\,^3P_1$. This is considered a minor process in the present device because the $6\,^3P_1$ level is expected to have a much smaller density compared to $6\,^3P_0$. Note that the N_2-Hg laser described here actually is based on an extension of the general scheme outlined in the first paragraph, but the principles are well illustrated in the present system nevertheless.

In our experiment, optical pumping of the laser medium was obtained from an electrodeless lamp coaxial with the laser tube. The lamp and the laser tube were 35 and 3 mm in diameter, respectively. An intermediate tube of 7-mm diameter was used for water cooling both the lamp and the laser medium. The apparatus was constructed with fused silica and had an active length of 30 cm. The lamp had a sidearm containing a drop of mercury (~20 mg) at room temperature and was operated at 20 MHz. The innermost tube terminated in Brewster's windows and had sidearms for varying the N_2 pressure. One of these sidearms had a U bend, in the bottom of which was placed a small drop of mercury (~20 mg), also kept at room temperature. Isotropic Hg^{200} of 89.9% purity was used in both the lamp and the laser tube.

The laser cavity was formed by two 1-m-radius-of-curvature 0.1% transmitting mirrors. The laser output power from one of the mirrors as a function of N_2 pressure is given in Fig. 2. Laser oscillation began at an N_2 pressure of 10 Torr, rose very sharply before reaching a maximum at about 25 Torr. At higher N_2 pressures the small-signal gain diminished while the saturation parameter increased, resulting in the slow fall in power output observed. Probing with a cw dye laser showed a peak gain of 3% per pass at an N_2 pressure of 25 Torr. The data in Fig. 2 were taken with 1-kW electrical input into the lamp. It was estimated that the lamp produced radiation at 253.7 and 404.7 nm with ~10% and ~0.1% efficiency, respectively. Most of the light at 253.7 nm was wasted, and approximately one-third of the light at 404.7 nm was effective in pumping the upper laser level in the present arrangement. Only a small fraction of the latter was converted to laser output, since the mirror transmission was probably an order of magnitude smaller than scattering losses in the windows and mirror coatings.

Fortunately, there exists a large body of literature dealing with the energy levels involved in the N_2-Hg laser which enables an estimate to be made of the maximum efficiency the system may ultimately attain. Assuming that output coupling constitutes the only form of cavity loss, a simple rate equation analysis shows that the power output in photons per second is given by

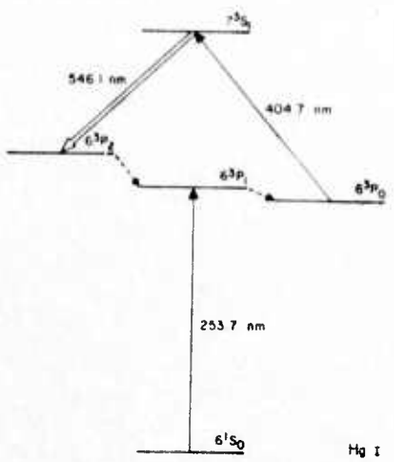

FIG. 1. Energy levels of Hg I pertinent to the N_2-Hg laser.

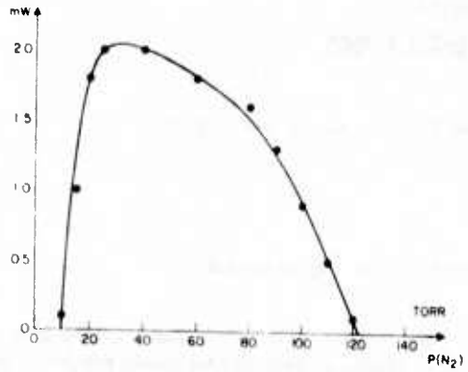

FIG. 2. cw laser output at 546.1 nm from a 0.1% transmitting mirror as a function of N_2 pressure. The laser tube had a diameter of 3 mm and an active length of 30 cm. The electrical output delivered by the power supply was 1 kW.

$$P_{\text{out}} = \frac{[R_l - (g_u/g_l)(A_{ul} + R_{ul})](t-f)}{R_l + (g_u/g_l)(A'_u + R'_u)} P_{1a},$$

where A_{ul} and R_{ul} are the radiative transition probability and collisional quenching rate by N_2 of the upper laser level into the lower laser level, A'_u and R'_u are the corresponding rates from the upper laser level to all other levels, and R_l is the total collisional quenching rate of the lower laser level by N_2.[1] The parameter f is the ratio of the laser saturated gain coefficient to the small-signal gain coefficient (assuming the transition is pressure broadened), and g_u and g_l are the degeneracies of the upper and lower laser levels. Finally, P_{1a} is the rate of pumping of the upper laser level by 404.7-nm radiation in photons per second.

For the $7\,^3S_1$ and $6\,^3P_2$ levels of Hg, $g_u = 3$, $g_l = 5$, $A_{ul} = 4.5\times10^7$ sec^{-1}, and $A'_u = 5.8\times10^7$ sec^{-1}.[2] The total quenching coefficient of $7\,^3S_1$ by N_2, $(R'_u + R_{ul})/P(N_2)$, has been measured to be 4.3×10^6 sec^{-1} Torr^{-1}.[3] Experiments recently completed by us give $R_l/P(N_2) = 2.7\times10^6$ sec^{-1} Torr^{-1} and $R_{ul}/P(N_2) < 0.5\times10^6$ sec^{-1} Torr^{-1}.[4] For a reasonable amount of output coupling, $f \ll 1$. At an N_2 pressure of 100 Torr then, one calculates $P_{\text{out}} = 0.40P_{1a}$. Thus it appears that about half the photons absorbed at 404.7 nm by the laser medium should reappear as stimulated output in a properly scaled N_2-Hg laser.

An equally important question to ask is how much light at 253.7 nm must be supplied in order to maintain a $6\,^3P_0$ density high enough to make the laser medium optically thick to 404.7 nm. With the pumping intensities at 253.7 and 404.7 nm in the present device, it appears that the major loss mechanism out of the triplet loop is the reradiation of 253.7-nm light by $6\,^3P_1$ at a rate of $\sim10^{18}$ sec^{-1} cm^{-3}. At higher 404.7-nm pump rates, a larger flux of 253.7-nm photons may be required if there is substantial quenching of the $7\,^3S_1$ or the $6\,^3P_2$ level directly to the ground $6\,^1S_0$ state by N_2. However, at present the 253.7-nm line can be produced with ~10% efficiency (in low-pressure Hg lamps such as the one we have used), whereas the 404.7-nm line with only ~1% efficiency (in higher-pressure Hg lamps). Therefore, it is felt that the over-all N_2-Hg laser efficiency probably will be determined largely by the efficiency for the production of 404.7-nm radiation and that efforts should be directed towards the enhancement of the latter.

[1] It is assumed here that the radiative decay of the lower laser level is negligible.
[2] P. Jean, M. Martin, J. P. Barrat, and J. L. Cojan, Acad. Sci. B **264**, 1791 (1967).
[3] J. P. Barrat, J. L. Cojan, and Y. Leeluse, Acad. Sci. B **262**, 609 (1966).
[4] R. Burnham and N. Djeu (unpublished).

APPENDIX 2

ABSOLUTE RATES OF COLLISIONAL DEACTIVATION Hg(6p $^3P_2$) BY NITROGEN AND CARBON MONOXIDE

R. Burnham

Science Applications, Inc.
Arlington, Virginia 22209

N. Djeu

Naval Research Laboratory
Washington, D.C. 20375

ABSTRACT

The total rates of collisional deactivation of the 6p $^3P_2$ state of mercury by nitrogen and carbon monoxide have been measured. The experimental technique involved the use of a narrow-band cw dye laser to probe the absorption at the center of the 5461 Å line of mercury in an optically pumped cell as a function of the pressure of the deactivating gases. The measured rates at 325°K were 3.0×10^6 $sec^{-1}torr^{-1}$ and 6.2×10^6 $sec^{-1}torr^{-1}$ for deactivation by N_2 and CO respectively. Also measured were the rates of collisional deactivation from the 7s $^3S_1$ level into the 6p $^3P_2$ level. These partial quenching rates were found to be less than 7×10^5 $sec^{-1}torr^{-1}$ for N_2, and equal to 4.4×10^6 $sec^{-1}torr^{-1}$ for CO.

INTRODUCTION

The collisionally induced relaxation of the component states of the 6p ^3P multiplet of mercury has been studied extensively as an example of the non-radiative transfer of energy between excited states of a particular atomic species and unexcited atomic or molecular states of another species. Recent papers have dealt with the question of the relative importance of processes which deactivate the 6p $^3P_1$ state to the 6p $^3P_0$ and 6s $^1S_0$ metastable and ground states of mercury in collisions between mercury atoms and various molecules.[1,2,3] Deactivation of the 6p $^3P_0$ state to the ground state has also been investigated.[4] However, the only studies to date dealing with the deactivation of the 6p $^3P_2$ state have been measurements of the relative rate constants for the process:

$$Hg(^3P_2) + M \rightarrow Hg(^3P_1) + M^*, \qquad (1)$$

where M represents any one of a number of the diatomic, polyatomic, and hydrocarbon molecules which were studied.[5,6]

In the present paper is described a measurement of the absolute total rate for deactivation of the 6p $^3P_2$ state of mercury in collisions with unexcited nitrogen and carbon monoxide. The investigation described in the following

sections was undertaken in conjunction with a study of the possibility of obtaining laser action on the Hg I ($7s\ ^3S_1 \rightarrow 6p\ ^3P_2$) transition at 5461 Å in an optically-pumped, collisionally-deactivated system. The realization of cw laser oscillation on the above transition[7] has pointed to an important application of the knowledge of absolute rates for collisional deactivation of excited electronic states in a new class of atomic lasers. In these devices, optical pumping of the upper level of a particular transition would be combined with collisional deactivation of the lower (possibly metastable) level of the transition in order to achieve the inversion necessary for amplification.

EXPERIMENTAL METHOD

The absolute rate of deactivation of $6p\ ^3P_2$ level of mercury was obtained through simultaneous measurements of the spontaneous emission intensity at 5461 Å and the absorption coefficient at the same wavelength in a steady-state optically-excited system. Figure 1 is an energy-level diagram of the relevant states of the mercury atom, and Figure 2 shows the apparatus used in the experiment.

The $6p\ ^3P_1$, $7s\ ^3S_1$, and higher lying levels of mercury were populated through absorption of radiation in a quartz cell containing isotopically enriched (89%) Hg^{200} at a few microns pressure together with the deactivating gas at

pressures which were varied between 1 and 100 torr. Surrounding the absorption cell was a low-pressure mercury lamp which was excited by several hundred watts of r.f. power at 20 MHz. A cooling jacket through which distilled water was circulated separated the lamp from the absorption cell. The 6p $^3P_1$ level was excited through absorption of the resonance line of mercury at 2537 Å, while the 7s $^3S_1$ level was excited through subsequent absorption at 4047 Å and 4358 Å. (The 6p $^3P_0$ level was populated through intramultiplet quenching from the 6p $^3P_1$ level.) The higher-lying 6d ^3D and 6d ^1D levels were also excited through absorption of lines in the near UV which terminate on the 6p $^3P_0$ levels and which were emitted by the lamp.

The density of atoms in the 7s $^3S_1$ level was inferred from a measurement of the absolute intensity of the line radiation at 5461 Å emitted by the column of mercury atoms in the absorption cell. Similarly, the densities of atoms in 6d ^3D and 6d ^1D levels were monitored in order to determine the contribution to the pumping rate of the 6p $^3P_2$ state from these levels. However, the cascading from these higher levels into the 6p $^3P_2$ level was found to be negligible.

For the purpose of the absorption measurement a continuously-pumped tunable dye laser was used to provide a probing beam of narrow-band radiation at 5461 Å. The

bandwidth of the radiation was limited to less than 100 MHz by a pair of quartz etalons located within the laser cavity. Tuning of the output frequency of the dye laser was facilitated through rotation of these etalons. The output of the dye laser was tuned to the center of 5461 $\mathring{A}$ transition by monitoring the absorption of the laser light passing through a small cell containing a discharge in Hg^{200}. Simultaneously, the frequency and mode structure of the beam from the laser was monitored with a scanning Fabry-Perot interferometer. It was found that with careful adjustment of the dye laser, the output frequency could be maintained within 100 MHz of the center of the 5461 $\mathring{A}$ transition.

The technique for probing the absorption coefficient of the transition at 5461 $\mathring{A}$ involved splitting the output beam from the dye laser into two beams of approximately equal intensity. One beam traversed the optically pumped absorbing region while the other served as a reference of the intensity of the output from the dye laser. The two beams impinged upon matched vacuum photodiodes, and the difference between the signals from the photodiodes was displayed on an oscilloscope. A periodic null reference was provided by a chopper which interrupted both light beams simultaneously. The ultimate detectivity of the system was limited by noise which was not cancelled in the

difference signal, however the effects of absorptions as small as 1% along the length of the cell could be readily observed. In an experimental run deactivating gas was allowed to flow over mercury contained in a sidearm at room temperature and into the absorption cell. Simultaneous measurements were made of the spontaneous emission at 5461 Å and the absorption in the cell, while the total pressure in the cell was read from a mechanical pressure gauge.

THEORETICAL CONSIDERATIONS

The absorption coefficient for radiation at the center of a doppler-broadened line may be written as:

$$\alpha(\nu_o) = k_o(N_\ell g_u - N_u g_\ell) \qquad (2)$$

where N_u and N_ℓ denote the density of atoms in the upper and lower levels of the transition and g_u and g_ℓ denote the degeneracies of the levels. The absorption cross-section at the center of the line is defined in terms of the temperature and the transition probability, $A_{u\ell}$, as:

$$k_o = \sqrt{\frac{m}{2\pi kT}} \; \frac{c^3 A_{u\ell}}{8\pi \nu_o^3 g_\ell} \; . \qquad (3)$$

The second term on the right side of Eq. 2 gives the contribution to the absorption coefficient from stimulated

emission. The magnitude of the absorption at line center by a column of gas of length L is:

$$\text{Abs} = \left[1 - \exp\left(-\int_0^L \alpha(\nu_o, x)\, dx\right)\right] \quad . \qquad (4)$$

Inversion of Eq. 4 gives the absorption coefficient in terms of the measured absorption:

$$\bar{\alpha}(\nu_o) = -\ell n(1 - \text{Abs}) \quad . \qquad (5)$$

In Eqn. 4 the integrated absorption coefficient $\bar{\alpha}(\nu_o)$, is defined as in Eqn. 2 in terms of $\bar{N}_u$ and $\bar{N}_\ell$, the densities of the excited states of mercury integrated over the length of the column of gas.

In the optically-pumped system described above, the densities of atoms in the upper and lower energy levels of the transition at 5461 $\overset{o}{A}$ may be related through the steady state solution to the rate equation for the lower ($6p\ ^3P_2$) level. This equation may be written as:

$$\frac{d\bar{N}_\ell}{dt} = 0 = \bar{N}_u \left[A_{u\ell} + k'M\right] - \bar{N}_\ell k_{21} M + \bar{N}_1 k_{12} M^* . \qquad (6)$$

The first term in Eqn. 6 includes the effects of radiative decay and possible collisionally-induced relaxation from the

upper to the lower level. In this term the rate constant for the quenching process is denoted by k', and the density in the ground state of the deactivating species is denoted by M. The transition probability for the 5461 $\mathring{A}$ transition has a measured value of $0.45 \times 10^8 sec^{-1}$.(8) The second term in Eqn. 6 gives the rate of relaxation of the lower state population, with k_{21} denoting the rate constant for collisional deactivation. The last term in Eqn. 6 allows for the effects of a back-reaction of the form,

$$Hg(^3P_{1,0}) + M^* \rightarrow Hg(^3P_2) + M \quad , \qquad (7)$$

which would tend to populate the lower level. The energy of the excited species, M*, may be in either internal motion or translation. Solving Eqn. 6 for $\bar{N}_\ell$ and inserting this quantity into the integrated form of Eqn. 2 yields:

$$\frac{\bar{\alpha}(\nu_o)}{k_o g_u} - \bar{N}_1 \frac{k_{12}}{k_{21}} \frac{M^*}{M} = \bar{N}_u \left[\frac{A_{u\ell}}{k_{21} M} + \frac{k'}{k_{21}} - \frac{g_\ell}{g_u} \right] . \qquad (8)$$

The second term on the left hand side of Eqn. 8 gives the approximately constant absorption due to population of the $6p\ ^3P_2$ level through processes of the type indicated by Eqn. 7. The magnitude of this term may be estimated from a knowledge of the temperature of the gas in the absorbing region and of the density, $\bar{N}_1$, of atoms in the $6p\ ^3P_1$ and

$^3P_0$ levels. Treatment of this quantity in the present experiment will be discussed in the following section.

In the absence of the term considered in the previous paragraph, a plot of the measured absorption coefficient, normalized to the upper state density, versus the reciprocal of the pressure of the deactivating gas should yield a straight line, the slope of which gives the rate constant for the collisional deactivation of the 6p $^3P_2$ level. Additionally, the point at which the straight line crosses the x-axis gives the ratio of the collisionally induced rates into and out of the 6p $^3P_2$ level. This ratio is of interest since if it is found to be less than g_ℓ/g_u there exists the possibility of obtaining gain on the 5461 Å transition at a finite pressure of the deactivating gas.

RESULTS AND DISCUSSION

From Eqn. 8 it is evident that in order to obtain the rate of collisional deactivation of the 6p $^3P_2$ level, the magnitudes of the quantities $\bar{\alpha}(\nu_o)$, $\bar{N}_u$, M, and k_o must be measured simultaneously. In the present experiment the value of $\bar{\alpha}(\nu_o)$ was obtained from the measured absorption; $\bar{N}_u$, the integrated density of atoms in the 7s $^3S_1$ level, was inferred from the intensity of the spontaneous emission at 5461 Å from the optically-pumped cell; the density M was obtained in terms of the pressure of the deactivating gas; and the

absorption cross-section at the center of the doppler-broadened line was determined directly from a measurement of the linewidth of the spontaneous emission at 5461 Å. The line profile was resolved with a Fabry-Perot etalon which had a free spectral range of 3 GHz and an instrumental finess of approximately 50. The measured linewidth was 500 MHz which (under the assumption that the doppler-effect was the only broadening mechanism) corresponds to a temperature of 325°K, the approximate temperature of the cooling water which circulated between the lamp and the absorption cell.

The results of the absorption measurements are presented in Fig. 3. The plotted points represent the absorption coefficient at line center normalized to the density of atoms in the 7s $^3S_1$ level at each pressure of the deact rating gas. From the slopes of the lines drawn through each set of experimental points the following values were obtained for the rates of collisional deactivation at 325°K:

$$k_{21}(N_2) = 3.0 \times 10^6 \text{ sec}^{-1} - \text{torr}^{-1}$$

$$k_{21}(CO) = 6.2 \times 10^6 \text{ sec}^{-1} - \text{torr}^{-1} \quad .$$

The cross-sections corresponding to the above rates are 6.1 $Å^2$ and 12.6 $Å^2$ for N_2 and CO respectively. Uncertainties

in the measured rates of deactivation arise principally from experimental error in the determination of the absolute intensity of the spontaneous emission at 5461 Å, which involved the calibration of the photomultiplier against a tungsten strip lamp. The overall uncertainty for the above rates is estimated to be about $\pm$ 35%.

Inspection of Fig. 3 reveals that the points at which the absorption coefficients cross the abscissa correspond to pressures of 10.5 torr and 7.5 torr for N_2 and CO respectively. Inserting these values into Eqn. 8 along with the values for the measured rates of deactivation yields the collisionally induced rates of relaxation from the $7s\ ^3S_1$ level into the $6p\ ^3P_2$ level. The resulting rates are:

$$k'(N_2) = 7 \times 10^5 \text{ sec}^{-1} \cdot \text{torr}^{-1} \pm 100\%,$$

and

$$k'(CO) = 4.4 \times 10^6 \text{ sec}^{-1} = \text{torr}^{-1} \pm 60\%.$$

The large uncertainties in the above figures resulted from substraction in Eqn. 8 of two quantities of nearly equal magnitude. As a test of our experimental results which would be independent of the probing technique described above, a low-loss optical cavity was placed around the optically-pumped cell, and observations were made of the pressures of the deactivating gases at which laser oscillation

began on the 5461 Å transition. The observed pressures were about 5% below the abscissa-crossing points given above for both nitrogen and carbon monoxide. From this result it was concluded that the actual value of $k'(N_2)$ is likely to be significantly smaller than the value derived above. The uncertainty introduced by the discrepancy in pressures was less severe in the case of deactivation by carbon monoxide and the value given for $k'(CO)$ is felt to be significant. Using the measured cross-section of 41 $Å^2$ for the total deactivation of the 7s $^3S_1$ level by carbon monoxide[9] together with our value of $k'(CO)$, a branching ratio into the 6p $^3P_2$ level of 25% was derived.

In the preceding discussion it has been assumed that terms in Eqn. 8 arising from back-reactions of the type indicated in Eqn. 7 did not contribute significantly to the measured absorption. The best evidence in support of this assumption lies in the quality of the fit of the experimental points in Fig. 3 to straight lines. If the effect of the back-reaction were important it would be most pronounced at pressures at which the measured absorption was near zero. However, no systematic trend away from linearity was found within the limiting sensitivity of 1% in the present experiment. It seems reasonable to conclude then that the effects of the back-reaction at lower pressures of the deactivating

gases where the absorption varied from 10 to 50% were entirely negligible.

An interesting comparison may be made between the cross-sections obtained in the present experiment and those for the total deactivation of the 6p $^3P_1$ and $^3P_0$ levels obtained in earlier studies. In Table 1 are tabulated the relevant cross-sections together with the energy defects in the resonances between the intramultiplet term-value differences in mercury and the energies of the most resonant vibrational "transitions" in each of the molecules. In the case of deactivation of the 6p $^3P_2$ level, the energy defects are given for both the $^3P_2$ - $^3P_1$ and $^3P_2$ - $^3P_0$ term differences. Also included in Table I are the cross-sections for deactivation of the 6p $^3P_0$ level, although the route for relaxation of this level is to the 6s $^1S_0$ ground state. Of note in Table I are the dramatic increases in the cross-sections for deactivation by both molecules as one proceeds from the lowest-lying to the highest-lying of the mercury triplet levels. The enhancement of the cross-sections seems likely to be attributable to the opening of additional channels by which the deactivating reactions can proceed as the energy of the participating triplet state increases.

The first excited electronic states of both nitrogen and carbon monoxide are energetically inaccessible in the collisional deactivation process. It follows then that the

products of the deactivating reactions include only vibrationally excited molecules in the ground electronic states. The result of a recent study[3] also incidates that in deactivation of the 6p $^3P_1$ level by both nitrogen and carbon monoxide the primary reaction route is through intra-multiplet relaxation to the 6p $^3P_0$ level. Under the assumption that the branching ratios to the ground state remain small in the collisional deactivation of the 6p $^3P_2$ level by nitrogen and carbon monoxide, the relatively large cross-sections for deactivation of the above level might be expected to correlate to resonances between electronic and vibrational term differences. Indeed the thirty-fold increase in the cross-section for collisional deactivation of the 6p $^3P_2$ level over that of the 6p $^3P_1$ level by nitrogen corresponds to an almost exact resonance between the 6p($^3P_2$ - $^3P_1$) term difference and the (2-0) vibrational energy difference. In the case of deactivation by carbon monoxide the increase in the cross-section for the 6p $^3P_2$ level over that for the 6p $^3P_1$ level is about a factor of two. This smaller increase might be explained by the smaller difference between the energy defects for the 6p($^3P_2$ - $^3P_1$) and 6p($^3P_1$ - $^3P_0$) deactivation by CO.

While the importance of electronic-vibrational energy resonances cannot be inferred from the present work, this

work does point to the need for an experiment in which the branching ratios in the 6p $^3P_2$ deactivation reaction could be measured. Such a measurement would complete the knowledge of the deactivation routes for all three of the 6p triplet states of mercury and allow meaningful theoretical models for the processes to be developed.

REFERENCES

1. M.D. Sheer and J. Fine, J. Chem. Phys. 36, 1264 (1962).
2. A.C. Viklis, G. Torrie, and D.J. LeRoy, Can. J. Chem. 50, 176 (1972).
3. J. Pitre, K. Hammond, and L. Krause, Phys. Rev. A 6, 2101 (1972).
4. C.H. Bamford and C.F.H. Tipper, Ed., Comprehensive Chemical Kinetics V.3, Elsevier, Amsterdam (1969).
5. F.W. Van Itallie, L.J. Doemeny, and R.M. Martin, J. Chem. Phys. 56, 3689 (1972).
6. H.F. Krause, S. Datz, and S.G. Johnson, J. Chem. Phys. 58, 367 (1973).
7. N. Djeu and R. Burnham, to be published.
8. P. Jean, M. Martin, J.P. Barrat, and J.L. Cojan, Compt. Rend. 264B, 609 (1967).
9. J.P. Barrat, J.L. Cojan, and Y. Lecluse, Compt. Rend. 262B, 609 (1966).
10. J.S. Deech, J. Pitre and L. Krause, Can. J. Phys. 49, 1976 (1971).

TABLE 1

Cross-sections for collisional deactivation of the 6p ^3P levels of mercury by nitrogen and carbon monoxide. The notation following the energy differences in each column indicates the levels participating in the reaction of the form $Hg(^3P_i) + M(v=0) \rightarrow Hg(^3P_f) + M(v=v_f)$ for which the energy defect was determined.

		$^3P_2$ (a)	$^3P_1$ (b)	$^3P_0$ (c)
N_2	$\sigma^2(\mathring{A}^2)$	6.1	0.23	$< 10^{-3}$
	$\Delta E(cm^{-1})$	$1.6(^3P_2,0 \rightarrow {}^3P_1,2)$ $555(^3P_2,0 \rightarrow {}^3P_0,3)$	$563(^3P_1,0 \rightarrow {}^3P_0,1)$	-----
CO	$\sigma^2(\mathring{A}^2)$	12.6	6.9	< 0.1
	$\Delta E(cm^{-1})$	$371(^3P_2,0 \rightarrow {}^3P_1,2)$ $48(^3P_2,0 \rightarrow {}^3P_0,3)$	$376(^3P_1,0 \rightarrow {}^3P_0,1)$	-------

(a) Present work

(b) Reference 10

(c) Reference 4

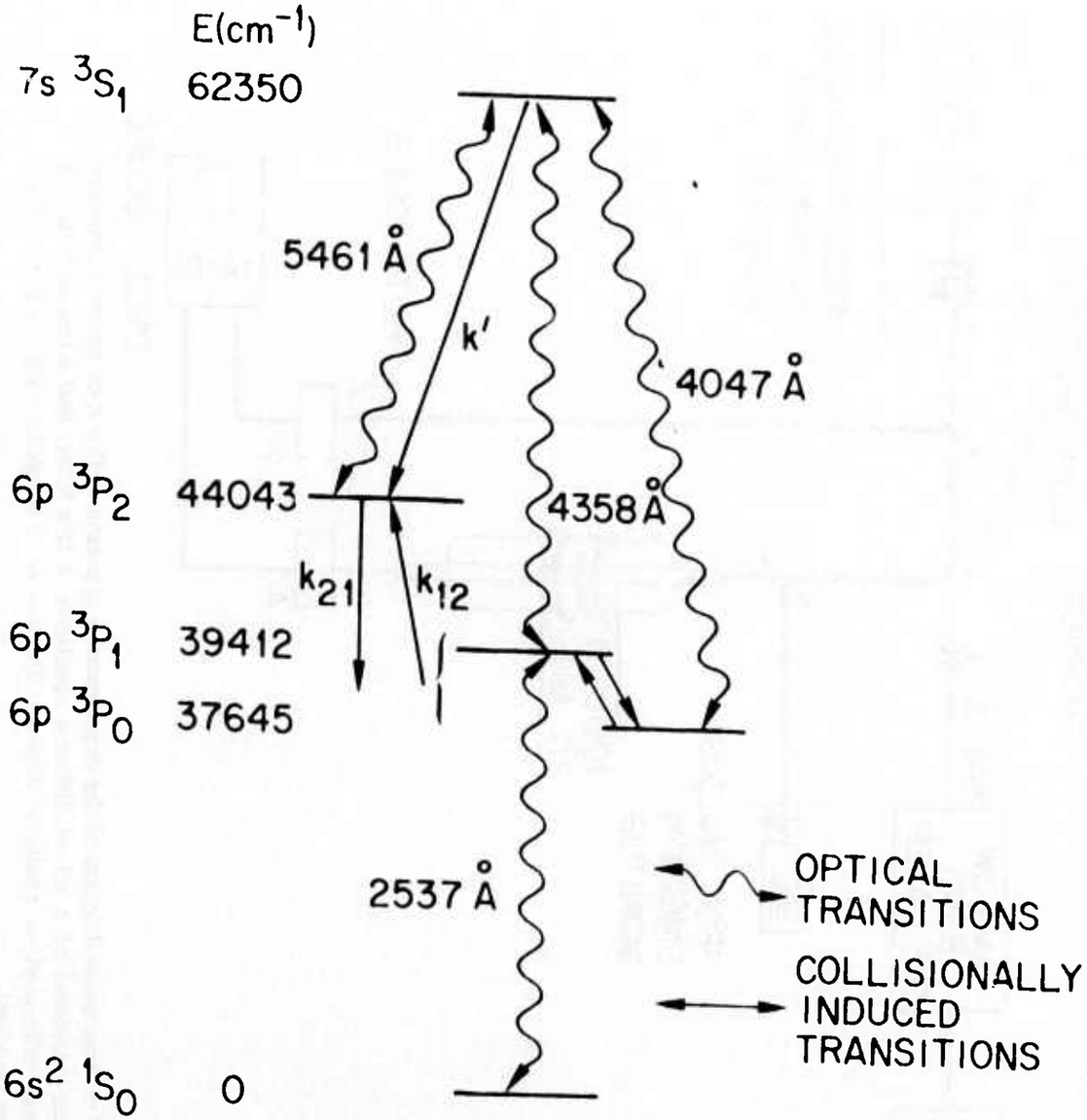

Fig. 1 — Energy level diagram of the relevant states of the mercury atom

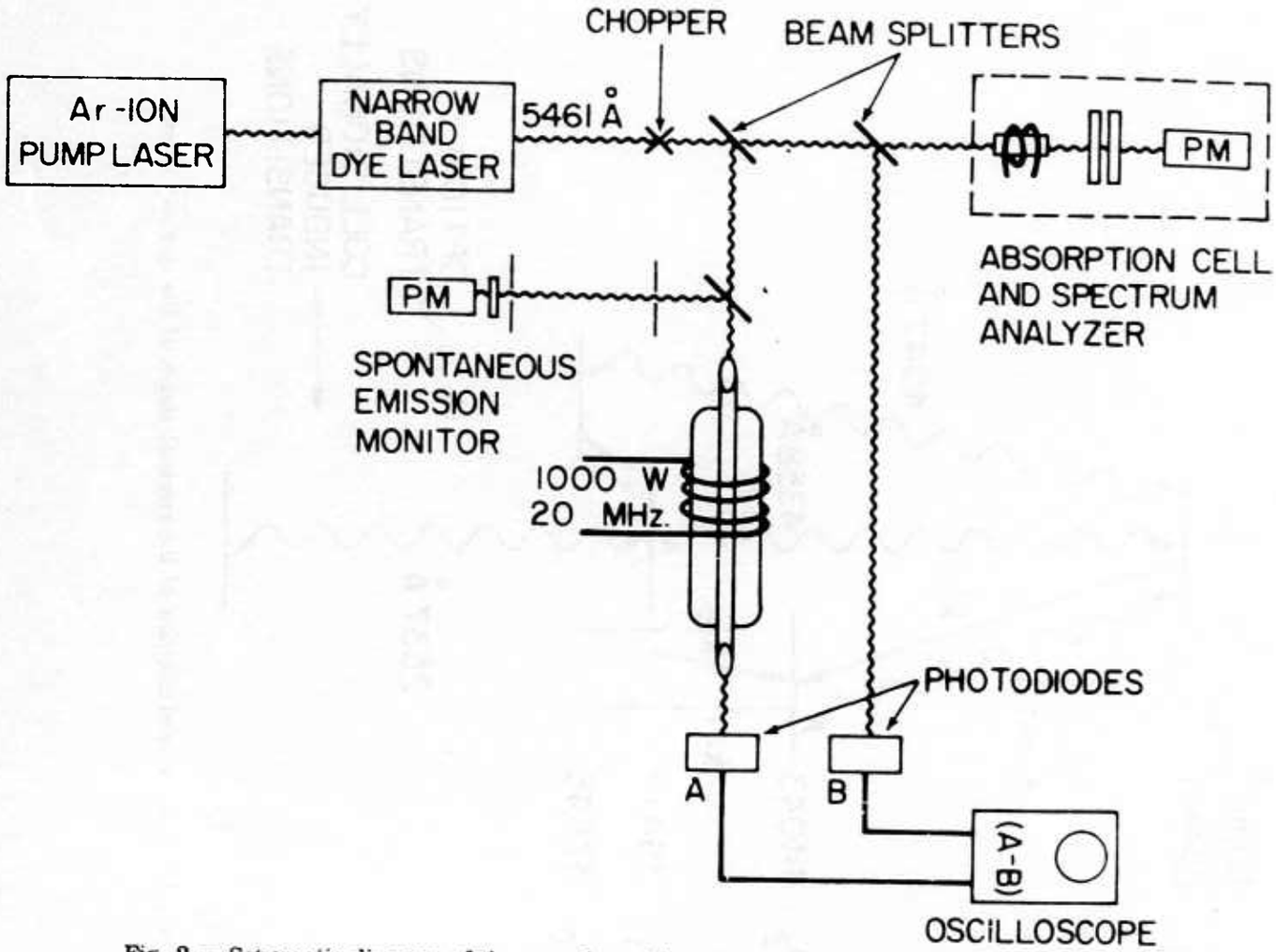

Fig. 2 — Schematic diagram of the experimental apparatus. The spontaneous emission monitor consisted of a set of defining apertures, a line filter, and a photomultiplier and was calibrated in position through the use of a tungsten strip lamp as a comparison standard.

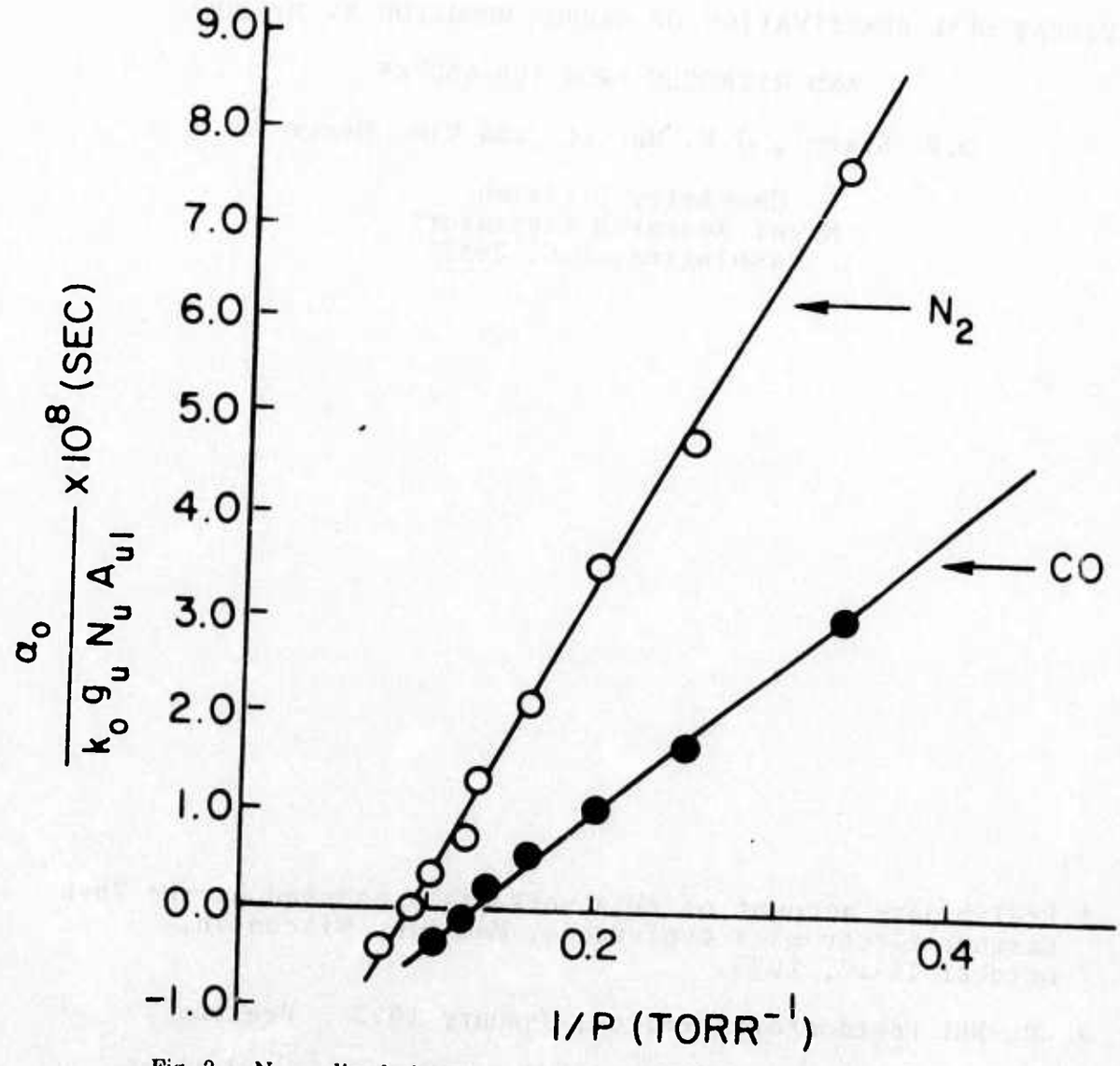

Fig. 3 — Normalized absorption at the center of the 6561 Å line vs the reciprocal of the pressure of the deactivating gases, N_2 and CO

APPENDIX A

VIBRATIONAL DEACTIVATION OF CARBON MONOXIDE BY HYDROGEN AND NITROGEN FROM 100-650°K*

D.F. Starr†, J.K. Hancock and W.H. Green††

Chemistry Division
Naval Research Laboratory
Washington, D.C. 20375

* Preliminary account of this work was presented at the 26th Gaseous Electronics Conference, Madison, Wisconsin, October 16-19, 1973.

† NRC-NRL Postdoctoral Fellow, January 1973 - Present.

††Present Address: Mahoney, Hadlow, Chambers, and Adams, Attorneys-at-Law, 100 Laura Street, Jacksonville, Florida 32201

ABSTRACT

Collisional quenching of carbon monoxide by hydrogen and nitrogen has been studied in the 100 - 650°K temperature range using the laser excited vibrational fluorescence method. The rate constant for CO-H_2 deactivation increases smoothly with temperature from 2.6 ± 0.3 $sec^{-1}torr^{-1}$ at 112°K to 170 ± 15 $sec^{-1}torr^{-1}$ at 623°K. The vibration-to-vibration energy transfer results for CO-N_2 mixtures (exothermic direction) show only a slight temperature dependence from 103 to 651°K with a broad maximum of 420 ± 30 $sec^{-1}torr^{-1}$ in the temperature range 300 to 400°K.

Comparison of our rates with high temperature shock tubes results show excellent agreement for the CO-H_2 V → R,T process and only fair agreement for the CO-N_2 V → V exchange process. This latter discrepancy may be partially due to the uncertainties involved in extracting V → V energy transfer rates from shock tube data.

INTRODUCTION

Several groups of workers have recently reported gas phase vibrational energy transfer rates in the 100 to 300°K temperature region.[1] Such studies are of two-fold interest. First, low temperature rates are relevant to certain gas laser systems, such as CO, which operate more efficiently at tempera-

tures near 100°K. Second, as sample temperatures are lowered and kinetic energy decreases, collisional interactions become more affected by attractive forces. From a mechanistic point of view, this latter effect permits a more detailed study of the intermolecular potential energy between such species. In cases where low-to-intermediate temperature studies and high temperature shock tube studies can be made to overlap (or nearly so), a more complete view of complex collisional processes should be realizable.

In this paper we report the measurement of CO-H_2 and CO-N_2 energy transfer rates from approximately 100 to 650°K using the laser-fluorescence technique. The specific quenching processes under investigation are the following:

$$CO(v=1) + H_2 \xrightarrow{k_{CO-H_2}} CO(v=0) + H_2 + \Delta E = 2143\ cm^{-1}$$

$$CO(v=1) + N_2(v=0) \underset{k'_e}{\overset{k_e}{\rightleftharpoons}} CO(v=0) + N_2(v=1) + \Delta E = -188\ cm^{-1}.$$

Some previous work over the low[1a,1e] and high temperature[2-5] ranges are available for these systems. However the present use of a single technique over a wide temperature range provides a correlation between the two sets of measurements which was previously lacking.

EXPERIMENTAL

Our CO laser excited vibrational fluorescence apparatus has been discussed in detail previously.[6] The only major modification has been the addition of a variable temperature cell with a working range of 100-650°K. Direct excitation of CO(v=0), J = 14 → v = 1, J = 13) is achieved using a coincidental overlap (within 0.003 cm^{-1}) with a frequency doubled CO_2 laser transition. Fluorescence signals were detected with an InSb detector and processed through a Biomation 610B transient recorder which then relayed digitized waveforms to a Nicolet 1072 signal averager. The response time of th- entire detection system is approximately 0.7 microseconds. In most instances, signal-to-noise ratios exceeded one hundred after signal averaging between 256-1024 counts (at 20 cps). All CO-H_2 mixtures exhibited smooth, single exponential fluorescent decay patterns and CO-N_2 mixtures produced double exponential decay, as expected.[6] Only R-branch emission from CO was detected through use of narrow band interference filters. Such filters proved necessary, not only to eliminate scattered laser light, but also to minimize pick up of fluctuations in black body radiation caused by the heater circuit in the temperature cell.

The temperature cell was constructed from oxygen-free copper and was 3 cm in diameter by 6 cm long. Three

Ceramaseal sapphire window assemblies were silver soldered in position to provide an entrance and exit for the laser beam and one fluorescence viewing port at right angles to the beam. The cell was wrapped with 1/8" copper cooling coils (silver soldered in place) through which helium (cooled to liquid nitrogen temperature) was passed. Heat was supplied by a 300 watt nichrome wire heater which was also wrapped around the cell. Thermal isolation was achieved by suspending the cell in an evacuated metal dewar, fitted with CaF_2 windows. A gold coated glass light pipe was used to channel the IR emission to a viewing window in the dewar.

The cell temperature was controlled with an Electronic Control Systems (ECS) Model 6823 three mode temperature controller. This unit proportionately feeds power to the heater coils and can hold and quickly reproduce any dialed temperature setting from 100 to 650°K to within $\pm$ 0.5°K. Temperatures were measured using two copper-constantan thermocouples attached at different locations to the cell. A Doric Model DS-350 digital thermocouple indicator and the ECS controller provided independent methods of measuring temperature. Both units agreed within 2°K over the entire temperature range.

Care was taken to ensure that the thermocouple readings recorded on the outside of the cell corresponded to the gas temperature inside. Simple calibration of thermocouple

junctions at convenient ice, dry ice, and liquid N_2 temperatures proved unsatisfactory in this regard. Precision, fine wire thermocouples (0.005" in diameter, insulated with glass sleeving and wrapped around the cell) were selected to minimize heat transport to and from the junction through the thermocouple lead wires. This problem becomes acute when larger diameter thermocouple wire or insulating sleeving is used. Calibration of the thermocouples was accomplished by measuring the vapor pressure as a function of temperature of selected gases (CO_2, C_3H_8, CF_4, and CH_4) inside the fluorescence cell. This procedure indicated that the recorded temperatures were in error by approximately five percent of the difference between cell temperature and room temperature. This method gave results accurate to $\pm$ 4^{o}K at the temperature extremes.

Gas pressures were measured during sample preparation using Wallace and Tiernan differential pressure gauges (0-20 torr and 0-800 torr). The calibration of these gauges was checked against an MKS Series 144 capacitance manometer equipped with 10 and 1000 torr heads. Agreement between the gauges and the capacitance manometer was better than one percent.

Care was taken in sample preparation to maintain highest possible gas purity. Samples were handled on a greaseless

vacuum line (capable of vacuums to 10^{-6} torr). Matheson Research Grade CO and N_2 and gold label grade H_2 (impurities listed in Ref. 6) were stored under liquid nitrogen for at least three hours prior to use. An initial seasoning of the fluorescence cell was performed by heating a mixture of CO and either H_2 or N_2 to 600°K for 12 hours. Data reported here include only those samples which could be cycled between 100 and 600°K and still maintain, within experimental error, the same initial relaxation time. These samples, when left overnight in the sample cell, did not show signs of degradation.

During experimental runs, the fluorescence cell was detached from the vacuum line, thus its pressure could not be measured. At temperature settings different from the sample preparation temperature, pressures were calculated assuming ideal gas behavior.[7] This assumption is quite good in CO-H_2, N_2 mixtures, even down to 100°K. Calculations based on the virial equation of state showed that in the worst instance for the data presented in Tables I and II the pressure correction due to non-ideality was approximately 0.6%. Confirmation of the reliability of calculating pressures in this manner was provided by filling the fluorescence cell at high temperatures (see Tables I and II) as well as at room temperature. No noticeable

difference was observed in the rate constants measured.

RESULTS AND DISCUSSION

$CO-H_2$ V → R, T Transfer

The data analysis of CO(v=1) quenching by H_2 and N_2 was outlined previously in a room temperature study of these collision partners.[6] The V → R,T quenching rate of CO by H_2 is obtained from observed fluorescent lifetimes using $\tau_{obs}^{-1} = k_{CO-H_2} P_{H_2}$. The CO pressure does not enter into the above calculation because V → V transfer to H_2(v=1) is too endothermic to occur ($\Delta E = -2018$ cm^{-1}) and the CO self-relaxation rate[8] is several orders of magnitude slower than the $CO-H_2$ quenching rates measured.

Table I lists the experimental data and calculated rate constants obtained over the temperature range 112 - 623°K in $CO-H_2$ mixtures. Our results are shown in Figure 1 plotted as Deactivation Probability versus Temperature ($T^{-1/3}$). Also shown are the results of Miller and Millikan[1a] and Stephenson and Mosburg[1e] which cover the temperature range 100 - 300°K, and the shock tube results of Hooker and Millikan.[2] The gap between the existing sets of data has now been smoothly spanned. It is evident that three basically different experimental techniques yield consistent results in overlapping regions.

Deviation from Landau-Teller behavior does not become noticeable in Figure 1 until $T \leq 400$°K. At the lowest

temperatures studied, the CO-H_2 quenching probability is two orders of magnitude larger than predicted by extrapolation of high temperature results. Presumably, attractive forces are at least in part responsible for this discrepancy. Sharma and Kern[9] have shown that long range forces exert an important influence in CO-H_2 encounters due to the near resonant process:

$$CO(v=1) + H_2(v=0,\ j=2) \rightarrow CO(v=0) + H_2(v=0,\ j=6) + \Delta E = 88\ cm^{-1}.$$

Their calculation has successfully accounted for the temperature dependence of the measured rate difference between the two spin states in H_2 in quenching CO.[10] This observation may explain why normal H_2 (1/4 para, 3/4 ortho) is 25-30 times more efficient in quenching CO(v=1) than has been found with D_2 or He.[6,11] Similar near-resonances involving direct coupling of CO(v=1) to the rotational energy levels of D_2 do not exist.

CO-N_2 V → V Transfer

Vibrational relaxation measurements were carried out in CO-N_2 mixtures from 103 - 651°K (see Table II). Each CO-N_2 mixture exhibited two lifetimes as expected. The slower lifetime in CO-N_2 samples reflects a combination of collisional, radiative, and diffusional processes which are not easily separated. Therefore, only the fast relaxation time in the CO-N_2 studies has been reported in

Table II. Rate constants for vibrational energy exchange between CO and N_2 were determined using:

$$\tau_{fast}^{-1} = k_e P_{N_2} + k_e' P_{CO}$$

and

$$k_e / k_e' = e^{\Delta E/kT} (\Delta E = -188 \text{ cm}^{-1}) \quad .$$

The forward and reverse rate constants for V → V transfer between CO and N_2 are shown in Figure 2 as a function of temperature. Also shown are the results of Stephenson and Mosburg[1e] obtained using a technique similar to ours. Exothermic transfer from $N_2(v=1)$ to CO exhibits a broad maximum at 300-400°K with $k_e' = 420 \pm 30$ $\text{sec}^{-1}\text{torr}^{-1}$. The lowest temperature shock tube results are those of vonRosenberg, Bray and Pratt.[3] Their results extend from 960 to 2200°K and suggest a temperature independent rate constant of $500 \leq k_e' \leq 1000$. The overlapping shock tube results of Sato et al[4] (1700 - 2700°K) and McLaren and Appleton[5] (2200-4000°K) suggest rates increasing with temperature with values extending from 1500 to 25,000 $\text{sec}^{-1}\text{torr}^{-1}$.

In contrast to the situation for V → R,T transfer, measurement of V → V processes by shock tube methods is quite difficult. The first rigorous analysis of the

phenomenological equations covering V → V processes in shock tubes was provided by Sato et al[4] in 1969.[12] The accuracy of these measurements depends to a large degree upon the extent of vibrational coupling between the two molecular species as both are being shock heated (undergoing T → V energy transfer). Laser fluorescence studies do not have this added complication as only one species is initially excited.

The probability of V → V energy exchange between N_2 and CO versus $T^{-1/3}$ is shown in Figure 3. There is some discontinuity between the laser fluorescence studies and the lowest temperature shock tube results. Our highest temperature data (near 650°K) show a leveling of the exchange probability at 5×10^{-5} which does not extrapolate to the shock tube measurements. Near 1000°K, this probability is $(1\text{-}2) \times 10^{-4}$.

Theoretical calculations of vibrational energy transfer fall into two distinct limiting situations. In the case of near resonant V → V transfer and at low temperatures, long range forces dominate and a linear log P_{10}^{01} vs T^{-1} behavior is expected.[13] For large energy defects (V → R,T transfer) and high temperatures, short range interactions are most important and $T^{-1/3}$ temperature dependence is observed.[14] N_2-CO V → V energy transfer represents an intermediate case. At least three separate theoretical approaches towards calculating N_2-CO V → V transfer rates have been undertaken.[15,17]

Shown in Figure 3 are the classifical trajectory calculations of Berend and Benson[15] and the recent semi-classical calculations of Shin.[16] Both repulsive and attractive terms are included in the intermolecular potential function in these investigations. Standard SSH calculations[18] predict an extremely rapid fall off in transfer probability near room temperature, contrary to experimental observations, and these computations have not been included in Figure 3. None of the published theoretical calculations[15,16,19] satisfactorily accounts for the order of magnitude increase in N_2-CO V → V transfer probability between 2000 - 4000°K reported by McLaren and Appleton. However Shin's results are in accord with the measured probabilities below 2000°K.

CONCLUSIONS

We have measured the temperature dependence of CO(v=1) quenching rates in collisions with H_2 and N_2 from 100-650°K. The V → R,T deactivation of CO by H_1 begins to deviate from Landau Teller behavior near 400°K and at 100°K is about two orders of magnitude faster than extrapolated high temperature results. Direct transfer from CO(v=1) into rotation in H_2(j=2 → 6) is one possible explanation.

It was not possible to overlap the present laser fluorescence studies in CO-N_2 V → V transfer with the shock tube results which start near 1000°K. The shock tube results, taken as

a whole suggest a moderately rapid decrease in deactivation probability with $T^{-1/3}$. Our results indicate a leveling off of this rate at higher temperatures (650°K). The lowest temperature shock tube results yield exchange probabilities approximately two to four times larger than the value we measured at 650°K.

ACKNOWLEDGEMENTS

The authors would like to thank Professor R.C. Millikan and Dr. J.C. Stephenson for communicating results prior to publication. This project was supported in part by the Defense Advanced Research Projects Agency under ARPA Order No. 2062.

REFERENCES

1. (a) D.J. Miller and R.C. Millikan, J. Chem. Phys. 53, 3384 (1970).
   (b) B.M. Jopkins, Hao-Lin Chin and R.D. Sharma, J. Chem. Phys. 59, 5758 (1973).
   (c) P.F. Zittel and C.B. Moore, J. Chem. Phys. 59, 6636 (1973).
   (d) M.M. Audibert, C. Joffrin, and J. Ducuing, Chem. Phys. Lett. 25, 158 (1974).
   (e) J.C. Stephenson and E.R. Mosburg, Jr., J. Chem. Phys. 60, 3562 (1974).
   (f) J.C. Stephenson, J. Chem. Phys. 60, 4289 (1974).
   (g) D.J. Miller and R.C. Millikan, Chem. Phys. Lett. 27, 10 (1974); J. Lubasik and J. Ducuing, Chem. Phys. Lett. 27, 203 (1974).

2. W.J. Hooker and R.C. Millikan, J. Chem. Phys. 38, 214 (1963); R.C. Millikan, (unpublished results).

3. C.W. vonRosenberg, Jr., K.C.N. Bray and N.H. Pratt, J. Chem. Phys. 56, 3230 (1972).

4. Y. Sato, S. Tsuchiya, and K. Kwiatani, J. Chem. Phys. 50, 1911 (1969).

5. T.I. McLaren and J.P. Appleton, Proc. 8th Int. Shock Tube Symp., J.L. Stollery, A.G. Gaydon, and P.R. Owen, Eds., London, Chapman and Hall, 1971.

6. W.H. Green and J.K. Hancock, J. Chem. Phys. 59, 4326 (1973).

7. A small correction factor was applied to the pressure calculations to account for the fact that a relatively small volume of gas in the connection tubing was not at the cell temperature. By this method a pressure error of approximately seven percent was avoided at the temperature extremes.

8. M.A. Kovacs and M.E. Mack, Appl. Phys. Lett. 20, 487 (1972).

9. R.D. Sharma and C.W. Kern, J. Chem. Phys. 55, 1171 (1971).

10. R.C. Millikan and L.A. Osburg, J. Chem. Phys. 41, 2196 (1964); R.C. Millikan and E. Switkes (unpublished results).

11. R.C. Millikan, J. Chem. Phys. 38, 2855 (1963).

12. Semi-empirical equations describing analysis of V → V data with shock tubes were first provided by T.L. Taylor, M. Camac, and R.M. Feinberg, Eleventh Symposium (International) on Combustion. The Combustion Institute, Pittsburg, Penn. (1965), p. 49.

13. B.H. Mahan, J. Chem. Phys. 46, 98 (1967); R.D. Sharma and C.A. Brau, J. Chem. Phys. 50, 924 (1969).

14. R.C. Millikan and D.R. White, J. Chem. Phys. 39, 3209 (1963).

15. G.C. Berend and S.W. Benson, J. Chem. Phys. 51, 1480 (1969).

16. H.K. Shin, J. Chem. Phys. 60, 1064 (1974).

17. R.D. Sharma (unpublished results).

18. W.H. Green and J.K. Hancock, IEEE J. Quant. Elec. QE-9, 50 (1973).

19. D. Rapp, J. Chem. Phys. 43, 316 (1965).

TABLE I

VIBRATIONAL ENERGY TRANSFER RESULTS FOR CO-H_2 MIXTURES

PRESSURE CO(torr)	PRESSURE H_2(torr)	TEMPERATURE (^oK)	RELAXATION TIME τ(μsec)	RATE CONSTANT[b] $k(sec^{-1}torr^{-1})$	DEACTIVATION PROBABILITY[c] $P_{10} \times 10^7$
8.28	789	297[a]	86.6	14.6	7.36
		112	1200	2.63	.82
		124	885	3.23	1.05
		137	644	4.05	1.39
		151	462	5.16	1.86
		169	344	6.20	2.36
		197	233	7.96	3.27
		223	178	9.27	4.05
		250	139	10.7	4.95
		277	104	13.0	6.33
		300	84.0	14.9	7.55
		356	51.5	20.9	11.5
3.71	428	297[a]	157	14.9	7.51
		406	57	30.9	18.2
		516	20	71.1	47.3
		623	7.1	170	124
		295	162	14.5	7.29
5.93	569	614[a]	12.3	144	104
		353	134	21.7	11.9
		406	84	30.5	18.0
		454	53	43.7	27.3
		511	31.5	66.2	43.8
		562	20	95.9	66.5

(a) Temperature at which gas sample was prepared. Pressures varied with temperature during experimental runs (see text).

(b) Collision cross sections for CO-H_2 encounters can be calculated from the measured rate constant k using $\sigma(\text{Å}^2) = (9.92 \times 10^{-8})kT^{\frac{1}{2}}$.

(c) Deactivation probabilities were calculated using $P_{10} = k/Z$ where the collision frequency is in units $sec^{-1}torr^{-1}$ and the hard sphere diameters for CO and H_2 are 3.7 and 2.9 respectively.

TABLE II

VIBRATIONAL ENERGY TRANSFER RESULTS FOR CO-N_2 MIXTURES

PRESSURE CO(torr)	PRESSURE N_2(torr)	TEMPERATURE °K	RELAXATION TIME τ(μsec)	RATE CONSTANT[b] k_e($sec^{-1}torr^{-1}$)	EXOTHERMIC RATE k_e'($sec^{-1}torr^{-1}$)	DEACTIVATION[c] Probability x 10
4.18	686	297[a]	8.64	166	413	4.50
		238	14.0	125	390	3.81
		201	22.8	90.0	345	3.09
		169	39.5	60.3	298	2.45
		144	68.0	40.4	264	2.00
		103	193	18.8	260	1.67
2.46	51.6	297[a]	105	165	410	4.47
		271	126	148	403	4.20
		218	202	110	379	3.54
		366	74	197	413	5.00
		428	59	217	407	5.33
		480	54.0	215	378	5.24
		544	45.7	228	375	5.53
		596	45.5	212	334	5.16
		651	41.3	217	329	5.31
7.86	549	304[a]	10.0	174	425	4.69
		112	218	18.1	204	1.37
		125	133	27.7	242	1.71
		138	83	41.1	292	2.17
		150	63	50.7	307	2.38
		179	35.5	77.7	351	2.97
		196	28.0	91.4	364	3.22
		224	18.8	121	407	3.85
		249	14.3	145	431	4.30
		277	11.8	160	426	4.49
9.83	118.4	561[a]	32.5	236	382	5.72
		613	31.0	230	358	5.61
		510	35.5	234	398	5.69
		453	40	229	415	5.59
		408	45	222	430	5.50
		354	55	203	435	5.18
		304	72	175	426	4.70
		250	109	133	394	3.94
		196	183	93.1	370	3.28
		143	430	45.7	303	2.29
		614	30.5	234	363	5.69

(a) Temperature at which gas sample was prepared and to which listed gas pressures correspond.

(b) Collision cross sections for CO-N_2 encounters can be calculated using $\sigma(\text{Å}^2) = (2.72 \times 10^{-7})\, k_e' T^{\frac{1}{2}}$.

(c) Deactivation probabilities were calculated using a hard sphere collision diameter of 3.7 for both CO and N_2. (Values listed are in the exothermic direction).

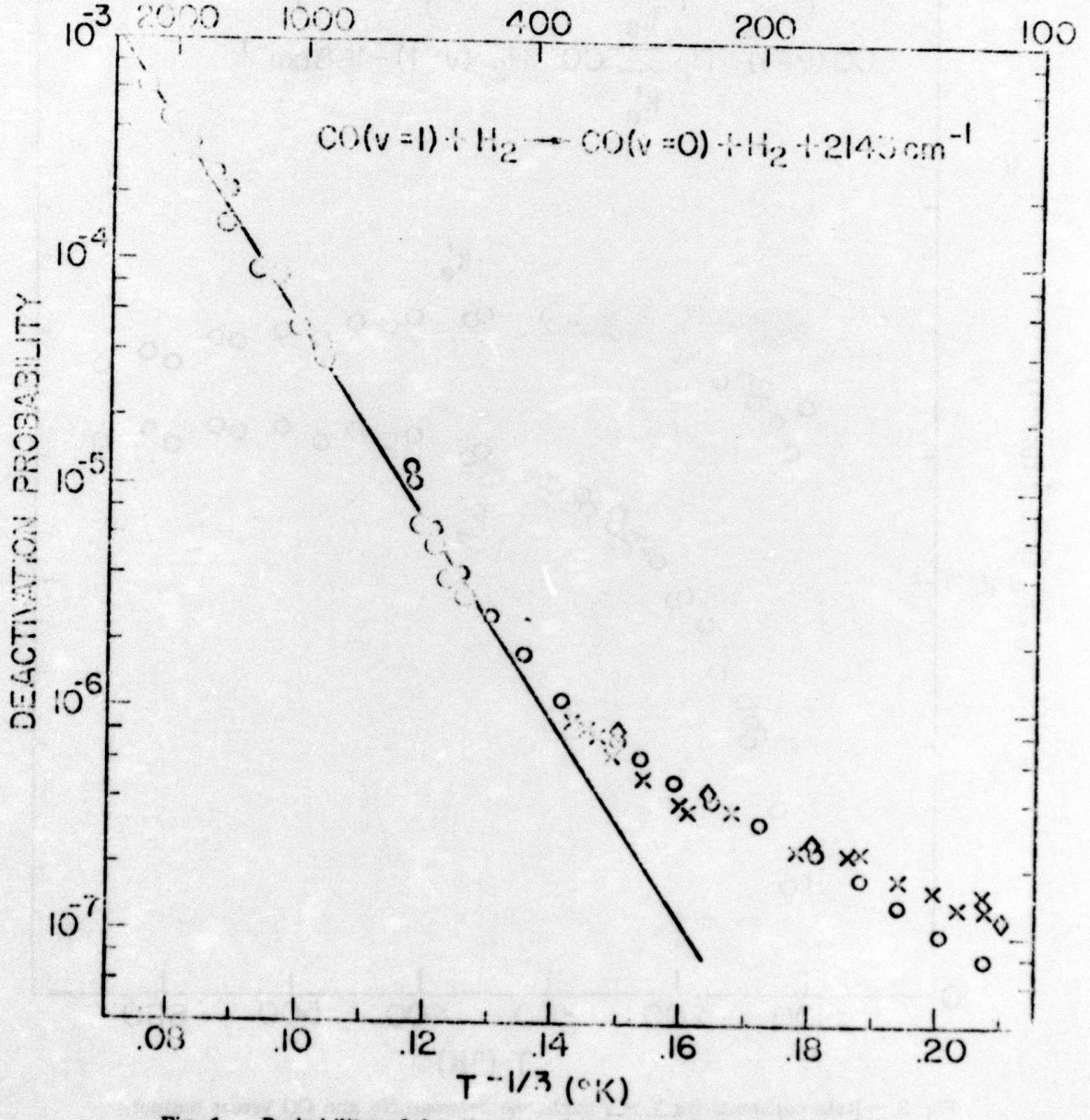

Fig. 1 — Probability of deactivation of CO(v=1) by H_2 versus $T^{-1/3}$;
o present results;
● Hooker and Millikan (Ref. 2);
x Miller and Millikan (Ref. 1a);
◇ Stephenson and Mosburg (Ref. 1e).

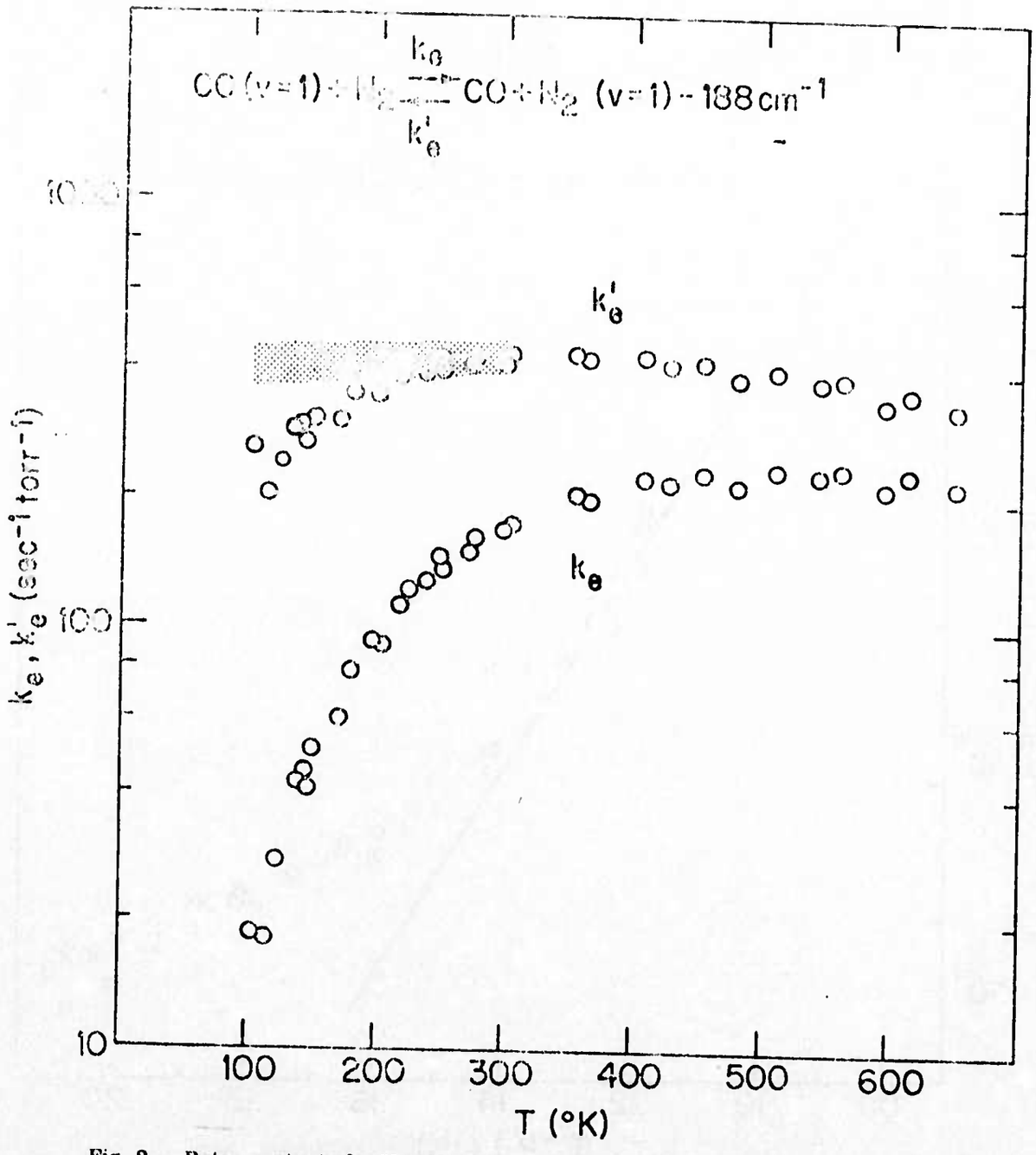

Fig. 2 — Rate constants for V → V exchange between N_2 and CO versus temperature; k_e and k'_e are related through microscopic reversibility $k_e/k'_e = \exp(-188\ cm^{-1}/kT)$. Present results are shown by circles. The shaded area represents the results of Stephenson and Mosburg (Ref. 1e).

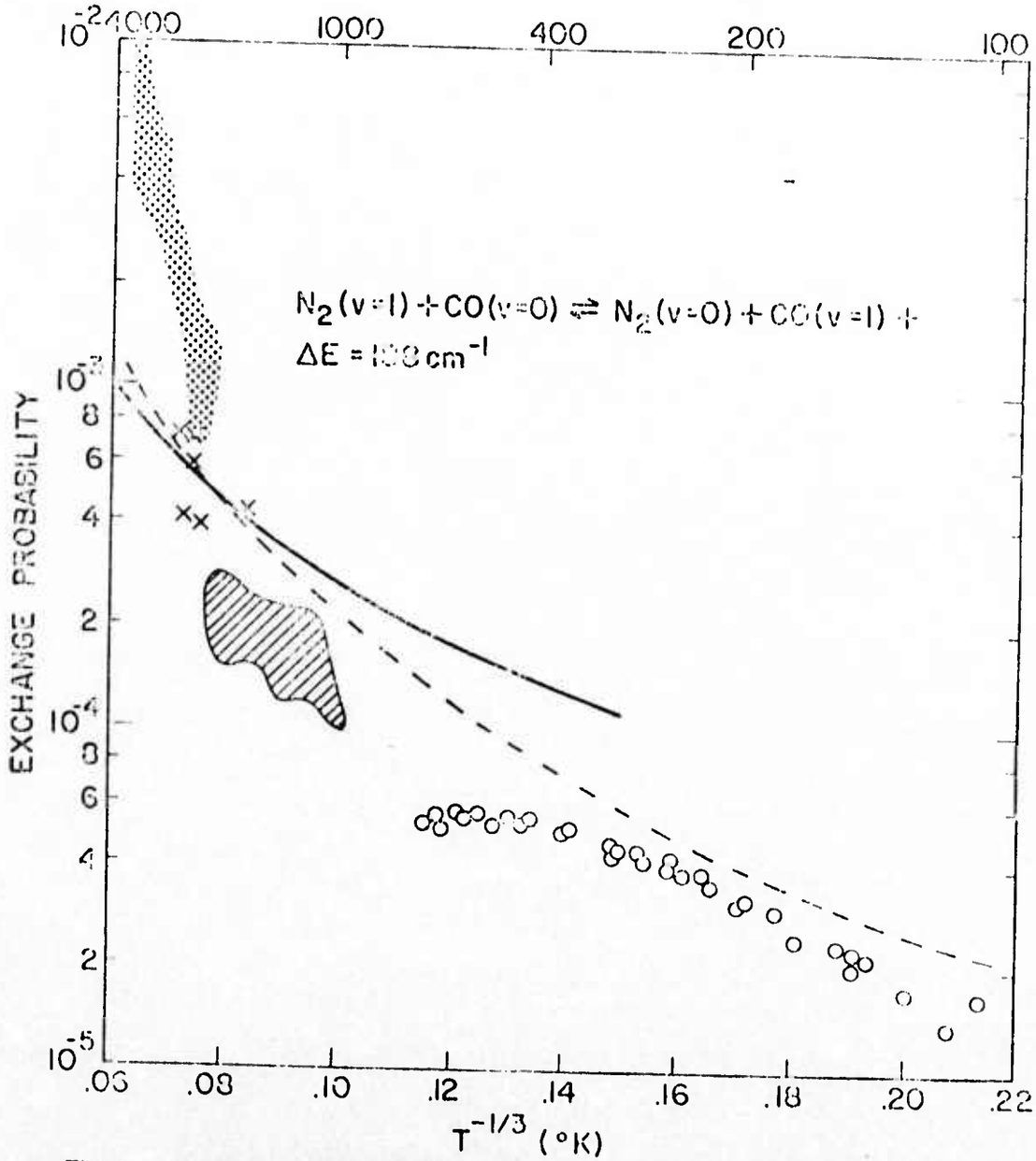

Fig. 3 — Theoretical and experimental V → V exchange probabilities for N_2(v=1) + CO(v=0) ⇄ N_2(v=0) + CO(v=1) versus $T^{-1/3}$. Experimental results are:

- ○ present study;
- X Sato et al (Ref. 4);
- ::::::: vonRosenberg et al (Ref. 3);
- //// McLaren and Appleton (Ref. 5).

Theoretical results are:

- —— Berend and Benson (Ref. 15);
- - - Shin (Ref. 16).